Assessment of starch branching and lamellar structure in rice flours

Matthew Paul van Leeuwen, Michelle Rosemarie Toutounji, Jitendra Mata, Rachelle Ward, Elliot Paul Gilbert, Patrice Castignolles, Marianne Gaborieau

Assessment of starch branching and lamellar structure in rice flours

Matthew Paul Van Leeuwen[a], Michelle Rosemarie Toutounji[a], Jitendra Mata[b], Rachelle Ward[c], Elliot Paul Gilbert[b,d], Patrice Castignolles[a], Marianne Gaborieau[a,e]*

[a] Western Sydney University, Australian Centre for Research On Separation Science (ACROSS), School of Science, Parramatta, NSW 2150, Australia

[b] Australian Centre for Neutron Scattering, Australian Nuclear Science and Technology Organisation (ANSTO), Lucas Heights, NSW 2234, Australia

[c] Yanco Agricultural Institute, NSW Department of Primary Industries, Yanco, NSW 2703, Australia

[d] The Australian Institute for Bioengineering and Nanotechnology and Queensland Alliance for Agriculture and Food Innovation, The University of Queensland, Brisbane, QLD 4072, Australia

[e] The University of Queensland, Centre for Nutrition and Food Sciences, St Lucia, QLD 4072, Australia

E-mail addresses: matt211092@gmail.com, mtoutounji@csu.edu.au, jtm@ansto.gov.au, rachelle.ward@dpi.nsw.gov.au, epg@ansto.gov.au, p.castignolles@westernsydney.edu.au, m.gaborieau@westernsydney.edu.au

* corresponding author: m.gaborieau@westernsydney.edu.au

Abstract

Apparent amylose content is used to describe milled rice flour composition. This spectrophotometric method is often the only direct measurement of starch structure in routine quality analysis. However, starch exhibits 6 levels of structure. The (supra)molecular starch structure in rice flours was measured: average degree of branching by ^{1}H NMR spectroscopy and semi-crystalline lamellar structure by small

angle X-ray scattering (SAXS). The suitability of these methods in routine quality analysis for breeding programs or the food industry was assessed in terms of precision and accuracy. Determination of apparent amylose content exhibits high precision (ca 5 % error) but low accuracy. Determination of average degree of branching exhibits a similar precision but good accuracy. Sample preparation (dissolution) is the first source of error in ^{1}H NMR spectroscopy and presumably also in spectrophotometry. Within narrow ranges of apparent amylose content (less than 2.5 % absolute difference) differences in average degree of branching and lamellar structure could be observed. The difference between chemical structures of different amyloses/amylopectins within a given sample is not negligible. This opens a way to explore how finer details of molecular and supramolecular starch structure can play a role in understanding rice quality.

Keywords

Rice, starch, amylose, branching, SAXS, NMR

1. Introduction

Rice is an important crop providing the main nutritional intake of two-thirds of the global population (Juliano, 2016). Milled rice grains primarily comprise starch along with water, proteins and lipids (Juliano, 2016). Many commercial rice varieties are the result of rice breeding to maximise production efficiency, convey pest and disease resistance and to ensure the grain traits used to describe grain quality meet domestic and international market preferences (Ward, 2017). Descriptors of rice quality include physical, compositional and functional properties such as chalkiness, colour, gelatinisation temperature, apparent amylose content (*AAC*), texture and digestibility (Ward, 2017). Variation in some traits can primarily be explained by molecular markers (Ayres et al., 1997; Waters et al., 2006) and these are used in early generation breeding selections. Other traits are interdependent, for example, digestibility has generally been observed to decrease when *AAC* increases (Fitzgerald et al., 2011), but *AAC* values by themselves do not allow an accurate prediction of rice digestibility. Different

factors can impact grain quality, for example growing conditions have been observed to affect *AAC*, gelatinisation and chalkiness (Jiang et al., 2003; Krishnan et al., 2011; Misra et al., 2015). Post-harvest processing of starch into foods can also strongly affect starch structure in some cases but not others, which in turn impacts nutritional and sensory properties (e.g. texture, visual aspect and flavour) (Blazek & Gilbert, 2011). From rice breeding to processing, there is a common need for a deeper understanding of drivers of rice quality traits (Concepcion et al., 2015), and characterising starch structure at each level of organisation is a novel approach to do that.

The properties measured in describing grain quality often do not include any direct measures of starch structure outside of *AAC* (Pallas, 2016; Ward, 2017). Native starch structure is complex, exhibiting a multi-level hierarchical structure (Figure 1). Starch macromolecules consist of glucose monomer units connected by α(1, 4) glycosidic bonds with branch points involving α(1, 6) linkages. Branched chains are regularly arranged into tightly packed clusters of double helices that are the building blocks of crystalline regions within the repeating semi-crystalline lamellar structure of each starch granule (Buléon et al., 1998).

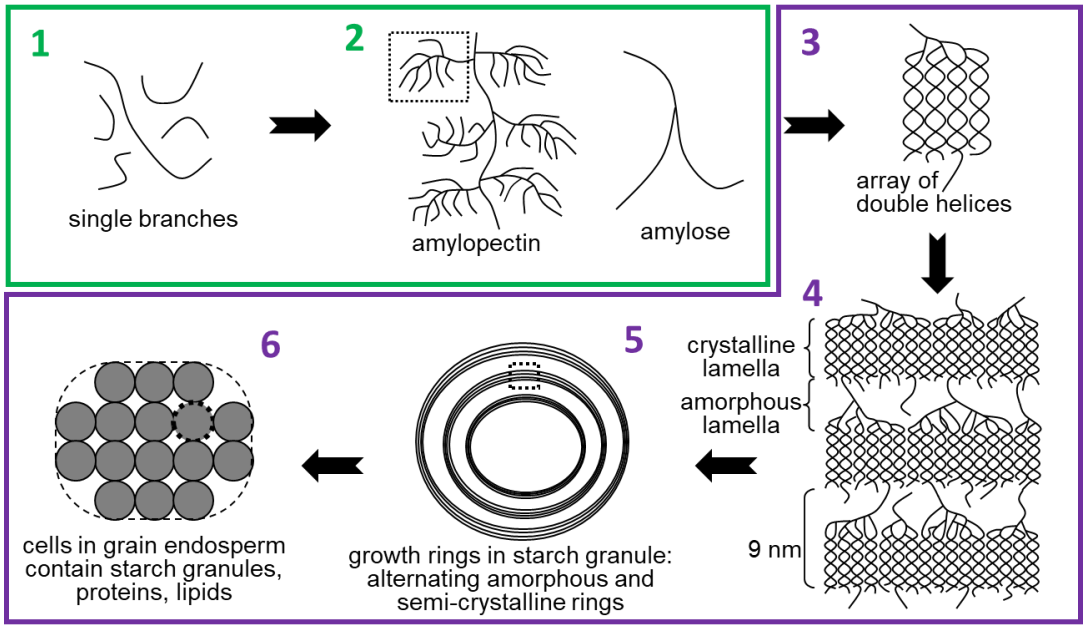

Fig. 1. Hierarchical structural levels of starch showing the molecular (levels 1 and 2) and supramolecular (levels 3-6) structures.. Adapted from (Gaborieau & Castignolles, 2009)

Native and modified starch structures have been characterised by a range of analytical techniques (Blazek & Gilbert, 2011; De Bruyn et al., 2006; Pérez & Bertoft, 2010). The molecular level of structure refers to the individual starch molecules and their branching structure (Figure 1, Levels 1 and 2). Amylose and amylopectin are respectively linear/slightly branched and highly branched starch. Starch has no chromophores, but *AAC* is most commonly determined by spectrophotometric methods after binding to iodine (AACC International, 2011; Fitzgerald et al., 2009). Nuclear magnetic resonance (NMR) spectroscopy is one of the most versatile and informative spectroscopic techniques available for elucidation of molecular and supramolecular structure and dynamics (Figure 1, Levels 2 to 4) (Claridge, 2009; Gartner et al., 2011). ^{1}H NMR spectroscopy can differentiate between anomeric protons involved in α(1, 4) and α(1, 6) linkages and has been used to estimate the average degree of branching (*DB*) of D-glucans (Usui et al., 1974), oligosaccharides (Gaborieau & Castignolles, 2009; Gaborieau et al., 2009; Hernández et al., 2008) and starches (Gidley, 1985). NMR is the preferred choice to determine the average *DB* (Ward, 2017) (Figure 1, Level 2). The measurement of average *DB* by ^{1}H NMR spectroscopy is one of the few established methods available for probing the branching structure of starch, with separation methods such as HPAEC (high-performance anion-exchange chromatography), SEC (size-exclusion chromatography), or CE (capillary electrophoresis) also available to probe other aspects of the branching structure such as the molar mass distribution of enzymatically debranched starch, commonly named "chain length distributions" (Castro et al., 2005; Kazarian et al., 2010; Koch et al., 1998; Witt et al., 2012).

Characterisation of the multiple levels of crystalline structure in starch can be explored through a variety of techniques (Figure 1, Levels 3 to 5). X-ray diffraction (XRD) is capable of identifying and quantifying underlying A, B and C-type crystalline structures in starch (Buléon et al., 1998; Lopez-Rubio et al., 2008). The proportions of single and double helices relative to the amorphous structure of starch can also be measured by ^{13}C solid-state NMR spectroscopy, allowing for insight into the short-range molecular order (Lopez-Rubio et al., 2008). Fourier transform infrared spectroscopy (FTIR) has been extensively used to characterise starch crystallinity, particularly in the range 1300-800 cm^{-1} where a

crystalline index is often referenced. Crystalline index is defined as the ratio of 'crystalline' and 'amorphous' absorbance band intensities (Capron et al., 2007; van Soest et al., 1995). However, strong overlap in absorbance bands and sensitivity to moisture limit the ability to obtain accurate data (Warren et al., 2016).

Lamellar starch structure can be measured by small angle X-ray scattering (SAXS) (Figure 1, Level 4 to 5) (Blazek & Gilbert, 2011). Chain length distribution (i.e., distribution of degrees of polymerisation of the branches) and proportion of crystallinity correlate with the size and distribution of the lamellar structures in extracted starch (Witt et al., 2012). This has important implications for understanding the activity of branching enzymes in starch synthesis, the resulting dynamic composition of amylose and amylopectin, and their unique branching characteristics (Liu et al., 2012). These structural changes can consequently have significant impacts on the functional properties of the starch (Aravind et al., 2013; Shrestha et al., 2012). SAXS can also monitor starch processes including starch swelling (Salman et al., 2009), gelatinisation (Vermeylen et al., 2005), retrogradation (Bayer & Baltá-Calleja, 2006) and annealing (Vermeylen et al., 2006).

AAC is known to be a valuable parameter in describing grain quality traits relevant to key consumer preferences such as texture. However, there is scope to explore other structural features of starch. Rice flours were chosen rather than purified starches for their relevance to rice breeding programs or the food industry. Here, the suitability of characterisation methods in differentiating rice flour samples based on starch structure is assessed. This is achieved by investigating *AAC* by the iodine binding spectrophotometric method, average *DB* by ^{1}H solution-state NMR spectroscopy and semi-crystalline lamellar structure by SAXS. It is preceded by an in-depth, comparative assessment of the performance of *AAC* and *DB* measurements in terms of precision and accuracy.

2. Materials and Methods

2.1 Materials

Seven varieties of rice were grown at the NSW Department of Primary Industries at Yanco, NSW, Australia. These varieties are examples of rice with different end-quality attributes and different genetic backgrounds. Details of the rice growing in different temperature treatments, harvesting and preparation to flours are given in section S1.1 in supporting formation.

Hot-water soluble (HWS) and hot-water insoluble (HWI) fractions from flours of the waxy rice varieties Hom, Makfay, Med Gnay, Laboun and Phae Savan were provided as freeze-dried powders by the International Rice Research Institute (Los Baños, Philippines). HWS and HWI fractions are specified as waxy varieties in the text.

Other materials are described in section S1.2 in supporting information.

2.2 Methods

2.2.1 Apparent amylose content

AAC was determined using a modified AACCI approved method 61-03.01 (AACC International, 2011).

Rice flour was weighed (100 mg) and transferred quantitatively to 100 mL volumetric flasks. To this, 1 mL of 95 % ethanol (5 % H_2O) was added to wet the sample followed by vortexing, then 9 mL of 1 M aqueous NaOH added. Samples were then left at room temperature for 15-25 h to disperse. After dispersion, samples were made up to 100 mL with distilled water and vortexed.

For iodine colour measurements, 1 mL of dispersion was quantitatively transferred to a 20 mL test tube. To this, 2 mL of 0.1 M citric acid in water was added with mixing, followed by 1 mL of iodine solution (0.2 wt% aqueous I_2 and 2.0 wt% aqueous KI) then made up to 20 mL with distilled water. The dispersion was then mixed and left to stand for 20 min. Colour absorbance was recorded for 2 aliquots of each sample solution at 620 nm. Measurements were made on a Beckman Coulter DU800 Spec (Beckman Coulter Life Sciences, Indianapolis, United States).

Standard curve samples were prepared daily using water plus two in-house calibrated rice samples from NSW DPI. The absorbance at 620 nm was plotted against amylose content for each standard solution. The resulting standard curve was used to read *AAC* values for test samples.

The *AAC* of each variety and temperature is reported as the average of the replicate measurements and replicate glasshouse samples (n=4). Error bars are the standard error of the mean. Groupings of *AAC* were based on a range of *AAC* independent of error bars (<2.5 % absolute difference).

2.2.2 Average DB

Rice flours (10 mg) were suspended in 2.24 g D_2O (5 g·L^{-1}) in round bottom flasks (50-250 mL), rinsed with D_2O prior to use. The flasks were sealed with Parafilm M®, mounted on an orbital shaker. Samples were continuously shaken (200 rpm) for 8 to 17 h at room temperature. Samples were then freeze-dried. This process was repeated once to ensure complete exchange of hydroxylic protons and minimise any resonance interference from residual solvent. The dried, selectively deuterated sample (4.5 mg) was dissolved in 0.45 mL of a 5 wt% LiBr DMSO-d_6 solution (made fresh from DMSO-d_6 with molecular sieves and LiBr powder stored in a desiccator) and heated in sealed glass vials at 80 °C overnight (approximately 15 h). 0.15 mL of D_2O was subsequently added to give a final sample concentration of 7.5 g·L^{-1} in DMSO-d_6/D_2O (75/25). Samples were kept at 80 °C and measured immediately (less than 2 min later).

The solution state ^{1}H NMR spectroscopy measurements were performed with a Bruker DRX300 spectrometer (Bruker BioSpin Ltd, Sydney) equipped with a 5 mm dual ^{1}H/^{13}C probe, at a Larmor frequency of 300.15 MHz. For older measurements in the reproducibility experiment (see Figure S4 in section S2.7, and accompanying text), experiments were performed with the same setup but at a Larmor frequency of 300.13 MHz (due to decommissioning and recommissioning of spectrometer to new location). ^{1}H NMR spectra were recorded using a 10 000 Hz spectral width, 90° flip angle, and acquired at 90 °C (see section S2.1 for temperature calibration).

The probe was tuned and the spectrometer was shimmed for each sample to ensure optimal signal-to-noise and resolution, respectively. Spectra were recorded and treated using Topspin software. Longitudinal relaxation times (T_1) of the signals of interest were estimated using the one-dimensional inversion recovery pulse sequence (see supporting information, Figure S1 in section S2.3 and accompanying text). Quantitative spectra were recorded with a 7.5 s repetition delay, which is longer than 5 times T_1 for the signals of interest. The chemical shift scales were calibrated with respect to the signal of DMSO at 90 °C (2.526 ppm) (Hoffman, 2006).

Average *DB* was calculated with equation 1 (Manelius et al., 2002),

$$DB\ (\%) = \frac{I_{\alpha(1,6)} \times 100}{I_{\alpha(1,4)} + I_{\alpha\ \text{reducing}} + I_{\alpha(1,6)} + I_{\beta\ \text{reducing}}} \qquad \text{Equation 1}$$

where I_y is the integral of the ^{1}H NMR signal of the anomeric proton of type y, with observed y signals being α(1, 4) (5.13 ppm), α reducing end (5.00 ppm), α(1, 6) (4.80 ppm) and β reducing end (4.45 to 4.35 ppm) (Gidley, 1985; Hernández et al., 2008; Manelius et al., 2002; Nilsson et al., 1996). An example of the partial spectra and integration regions is shown in Figure S6. Reported values are the average of glasshouse replicates (n=2). Error is reported as the standard error of the mean, and groupings of similar *DB* based on error bars.

For waxy rice flour fractions, the protocol above was slightly modified as detailed in section S2.2.

2.2.3 Semi crystalline lamellar structure

Samples were packed into 2 mm quartz glass capillaries. Packed samples were hydrated with excess Milli-Q® quality water for at least 12 h prior to analysis and tubes sealed using paraffin wax.

Small–angle X-ray scattering experiments were performed on a Bruker NANOSTAR SAXS system, employing 3 pinhole collimation for focussing, Cu *K*α radiation with a wavelength of 1.541 Å and a VANTEC1000 2D detector (resolution 68 μm). The scattering vector, ***q***, in the range of 0.01 to 0.35 Å^{-1} was used with optics and sample chamber under vacuum.

Scattering files were radially averaged using Bruker NANOSTAR software package, appropriately water background subtracted and scaled relative to a water filled capillary using the ATSAS software package (Petoukhov et al., 2012). Scattering curves were fitted using a power law function to represent large-scale structure combined with a combined Gaussian/Lorentzian function for the main starch peak ($\boldsymbol{q}$ ≈ 0.067 $Å^{-1}$) and a Gaussian function for the secondary peak ($\boldsymbol{q}$ ≈ 0.13 $Å^{-1}$) (Equation S2). Fitting parameters were iteratively calculated to minimise chi-square using WaveMetrics Igor Pro software (WaveMetrics Inc.) and National Institute of Standards and Technology (NIST) Centre for Neutron Research macros (Kline, 2006). An example curve and fit is shown in Figure S37.

Reported values are the average of triplicate measurements of glasshouse duplicates (n=6). Error bars are reported as the standard error of the mean, and groupings of similar values based on error bars.

3. Results and discussion

3.1 Performance of determination of AAC by spectrophotometry and average DB by NMR spectroscopy in characterising molecular structure

To allow a meaningful comparison of *AAC* and *DB* values measured on different samples, the performance of both methods first needs to be assessed. The precision and accuracy of the determination of *AAC* and average *DB* are compared below. The reproducibility was also assessed through the measurement of the same samples by different operators on different instruments. Here a comparison between the two methods to characterise level 2 of the starch structure is provided, assessing three major points: 1) sample preparation, 2) the measurement itself and 3) the results obtained.

3.1.1 Sample preparation

In the first point, the sample preparation is an important aspect of both methods, both sensitive only to starch that is solubilised from flour at the molecular level. Full dissolution is sometimes assumed

when a transparent liquid is obtained or when no precipitation occurs upon centrifugation. Quantitative solution-state NMR spectroscopy showed that a transparent liquid, even upon centrifugation, can be obtained even if starch is not fully dissolved.(Schmitz et al., 2009)The NMR methodology published initially (Gidley, 1985) was modified in this work using dry DMSO-d_6 with the addition of 5 wt% LiBr instead of D_2O for dissolution of the samples (Hoang et al., 2008; Schmitz et al., 2009) to ensure complete dissolution at the molecular level. This high LiBr concentration was used (130:1 LiBr to glucose stoichiometry) since lower LiBr concentrations (12.4:1 LiBr to glucose stoichiometry) lowered the precision of average *DB* (see Figure S3 in section S2S2.5, and accompanying text). This large molar excess of LiBr compared to glucose units is needed not only to interact with the starch hydroxyl groups (inhibiting hydrogen bonds) but also to interact with and modify DMSO as a solvent (Striegel, 2003). Dry DMSO was used since even minute amounts of water in DMSO slow down the dissolution (Dona et al., 2007). D_2O was added after dissolution to shift the residual H_2O solvent peak, yielding further improved resolution of starch signals (Hernández et al., 2008). The error associated with sample preparation was determined through 4 repeat preparations, yielding a relative standard deviation (*RSD*) of 2.6 % on the average *DB* of Doongara (see Table S1 in section S2sS2.6, and accompanying text).

In the spectrophotometric determination of *AAC,* the sample preparation requires quantitative solubilisation of the starch at the molecular level but also iodine binding to occur. Suspension of starch in 90 % DMSO/10 % water before iodine binding has been attempted a few times.(Knutson, 1999; Singh et al., 2006) Dissolution of starch with DMSO and LiBr has never been attempted for *AAC* determination. The AACCI method for *AAC* determination prescribes the use of aqueous sodium hydroxide for solubilisation, a protocol that is typically maintained even in modified *AAC* determination methods. However, the solubility of starch in aqueous sodium hydroxide at the molecular level has yet to be determined. The sample preparation in the accepted *AAC* determination methods could thus lead to low accuracy with especially some systematic errors.

234 3.1.2 Precision and accuracy of average *DB*

235 The measurements clearly differ between NMR spectroscopy and spectrophotometry, with
236 differences in precision and accuracy. A typical limitation of NMR spectroscopy is its sensitivity. The
237 error related the signal-to-noise ratio (*SNR*) can be determined from an empirical relation (Castignolles
238 et al., 2009; Maniego et al., 2017). In this work, spectra were collected until an *SNR* of at least 60 was
239 obtained for the α(1, 6) signal (about 700 scans, in about 90 min, yielding a *RSD* lower than 1 %. The
240 error due to data processing (phasing, baseline correction) was deemed negligible in the case of
241 determination of chitosan composition by NMR when *SNR* was above 50 for the least intense signal
242 of interest.(Thevarajah, Bulanadi, et al., 2016) The resolution of the signals of interest in NMR of
243 chitosan is similar to that observed in this work (see Figure S5 in section S2.8 for a typical ^{1}H NMR
244 spectrum of rice flour). The error due to processing is thus likely negligible for average *DB* in this work.

245 Measurements by ^{1}H NMR spectroscopy are not intrinsically quantitative contrary to common belief.
246 To determine quantitative conditions in which signal intensities reflect the quantities of species
247 dissolved in the sample, appropriate estimation of T_1 relaxation times was performed in this work for
248 all signals of interest(section S2.3). This T_1 assessment will apply to other instruments at the same
249 magnetic field (300 MHz ^{1}H Larmor frequency). To ensure accurate integration of the signals of
250 interest, the resolution was improved by high probe temperature (90 °C) on top of the addition of D_2O
251 after dissolution (Hernández et al., 2008) (see Figure S2 in section S2.4, and accompanying text). In
252 addition, the presence of lipids and proteins in rice flours did not affect the accuracy of DB
253 quantification; their presence does not affect the quantification of starch solubility with ^{1}H NMR
254 spectroscopy, and no significant ^{1}H NMR signals from proteins and lipids in rice flours are detected in
255 the range of the signals of the anomeric hydrogen used in the quantification of the degree of branching
256 (Schmitz et al., 2009).

257 These conditions were then used to test long- and short-term sample aging. A negligible effect of long-
258 term aging (of the flour) was confirmed through repeat measurements 4 years after their initial

measurement and storage at 4 °C in a refrigerator, with a change in operator and instrument giving an indication of the good reproducibility of the method (see Figure S4 in section S2.7, and accompanying text). In contrast, short term aging (of the dispersion) was found to occur, with slow degradation after the addition of D_2O if the sample was left to evolve over several hours (see Figure S22 in section S2.10, and accompanying text), therefore measurements were consistently performed immediately after addition of D_2O.

Calculations of average *DB* in the literature differ in the inclusion or exclusion of α and β reducing ends (Gidley, 1985; Manelius et al., 2002; Nilsson et al., 1996). For non-waxy rice flours α and β reducing ends were detected and included in the average *DB* calculation as previously reported (Manelius et al., 2002). For the waxy HWS and HWI fractions, α and β reducing ends were considered negligible and not included In the rest of the work, the error bars are based on precision values, likely a reasonable estimate of the accuracy in this case.

3.1.3 Precision and accuracy of *ACC*

For *AAC* determination using spectrophotometry, sensitivity is not an issue. However, resolution is a limitation: amylose and amylopectin's UV absorption spectra are not fully resolved after iodine binding. Their bands are particularly broad due to branching affecting iodine binding. The absorbance assumed to be from amylose includes some absorbance due to amylopectin (Fitzgerald et al., 2009) introducing some systematic error. Therefore, without corrective procedures, *AAC* determination is inherently semi-quantitative. The variability present in the methods of *AAC* determination has been assessed in a broad interlaboratory round-robin test (17 rice cultivars and 27 laboratories) (Fitzgerald et al., 2009). The repeatability was found to be high a result consistent with this work (5 % *RSD*), and similar to that of the determination of average *DB* by NMR (6 % *RSD*).

Reproducibility was however found to be low for *AAC* determination, identifying differences in standards and methodology as major sources of error (Fitzgerald et al., 2009). However, the use of

283 rice cultivar standards instead of potato ones improved reproducibility. Here, an average relative
284 difference in *AAC* of 6.8 % for this sample set was observed in reproducing measurements 4 years
285 apart with different operators, instruments and methods (see Table S4 in section S3, and
286 accompanying text). In the rest of the work, the error bars are based on precision values, likely an
287 underestimate of accuracy in this case.

288 3.1.4 Comparison of average DB and AAC

289 The results of the two methods were compared to assess the consistency of the data between them
290 (Figure 2). An apparent linear relationship between the average *DB* and *AAC* indicates, as expected, a
291 decrease in average *DB* with increasing *AAC*; it is due to amylose being substantially more sparsely
292 branched than amylopectin. Boundary conditions were plotted to detect any potential variations in
293 the linear relation for either measurement. These boundary conditions were created by taking the
294 extreme values measured for average *DB* of waxy HWS and HWI rice flour fractions (assuming 0 %
295 *AAC,* see Table S2 in section S2.11 for DB values) and linearly extrapolating to 100 % *AAC* and 0 %
296 average *DB* (assuming negligible branching in amylose), shown as dashed lines. Boundaries were also
297 plotted based on the highest and lowest average *DB* reported in literature for waxy starches in general,
298 irrespective of botanical origin (see Table S3 in section S2.11 for *DB* values), shown as dotted line. The
299 linear correlation between the average *DB* and *AAC*, as well as their confinement within the boundary
300 conditions indicates that the data are consistent. However, with the adjusted r^2 of 0.93, it is possible
301 that deviations are occurring as a result of different branching structures.

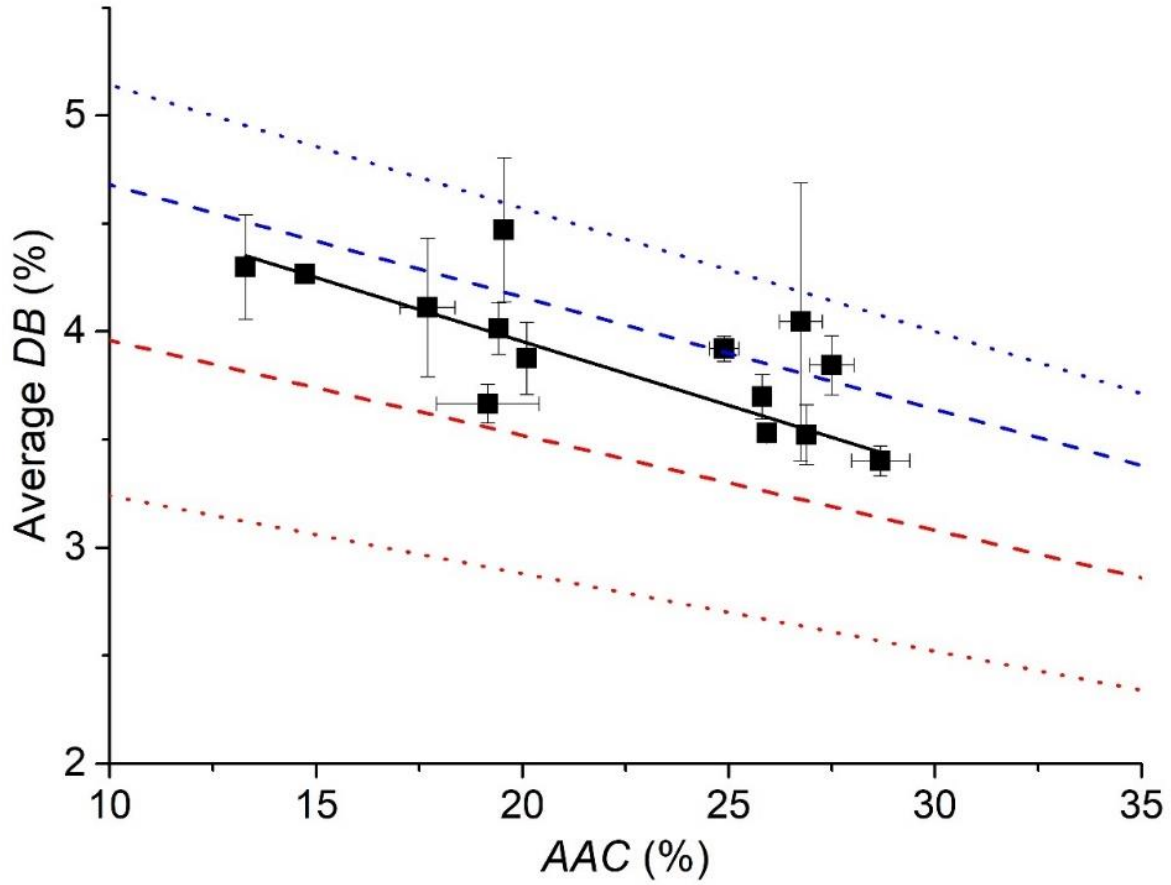

Fig. 2. Average *DB* by ^{1}H NMR plotted against *AAC* for rice flours of different varieties grown at lower and higher temperature (black squares) showing a linear correlation (black line, adjusted r^2 = 0.93). Dashed lines are linear extrapolations of extreme values of average *DB* measured for HWS (blue) and HWI (red) fractions of waxy rice flours (Table S2). Dotted lines are linear extrapolations from the highest (blue) and lowest (red) average *DB* values for waxy starches from literature (Table S3). Boundary conditions were extrapolated linearly between the measured waxy sample (measured *DB* listed in Tables S2-S3 in section S2.11, assumed *AAC* = 0 %) and an assumed point (*DB* = 0 %, *AAC* = 100%) at the other end of the AAC scale. *AAC* error bars represent the standard error of 4 values (2 independent replicates of temperature and 2 instrument readings for each replicate). Average *DB* error bars represent the standard error of 2 values (2 independent replicates of temperature). See Table S5 for individual *AAC* and average *DB* values.

As a tool for rice quality assessment, the determination of *AAC* by iodine binding is a high-throughput, cost-effective method with standard methods strengthening its deployment (AACC International, 2011; The International Organization for Standardization, 2015). Spectrophotometry and NMR spectroscopy provide valuable data with which to assess the molecular structure of starch, both exhibiting a similar precision, with average *DB* expected to provide more accurate information. In contrast, while *AAC* and average *DB* methods are impacted by dissolution and branching structures, the measurement of the semi-crystalline lamellar structure by SAXS is impacted primarily by the availability of, and competency in use of, instrumentation and the application of appropriate models.

Given SAXS analysis is on solid samples, with excess hydration the only modification, sample preparation is simple and consistent. One exception is in the influence of sample packing density on relative intensity; however, this was observed to be adequately controlled in this work (see section 3.4).

3.2 Assessing molecular structure through AAC and average DB

AAC is known to be influenced by variety and temperature during the grain-filling period, with higher temperatures leading to a decrease in amylose synthesis for some varietals (Hirano et al., 1998; Larkin & Park, 1999). In this work seven rice varieties were grown in two different temperature treatments. At lower growing temperatures, Quest and Kyeema recorded an *AAC* of 19-20 % that reduced to 13-15 % at higher growing temperatures. The remaining varieties recorded an *AAC* above 25 % at lower growth temperatures, with only Cocodrie and I-Geo-Tze maintaining a high *AAC* at higher growing temperatures (Figure 3). These observations have been explained by the expression of granule bound starch synthase (GBSSI) and the Waxy gene (Chen et al., 2008; Hirano et al., 1998; Larkin & Park, 1999; Sano et al., 1991). Thus, the determination of additional structural features such as average *DB* will serve to identify how the starch structure differs between temperature treatments and varieties.

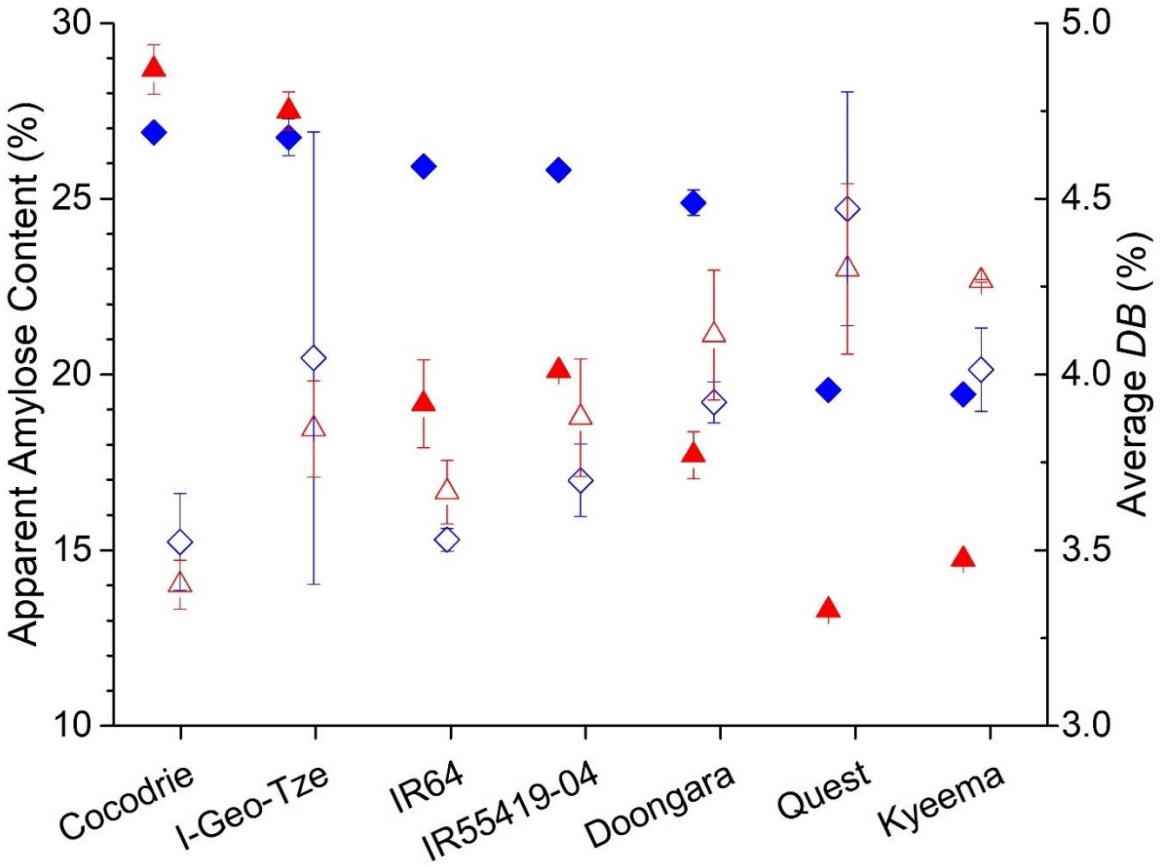

Fig. 3. *AAC* measured by iodine binding (left axis, solid shapes) and average *DB* measured by ^{1}H NMR spectroscopy (right axis, hollow shapes) for rice flours of different varieties grown at lower (blue diamonds) and higher (red triangles) temperature. Error bars for *AAC* represent the standard error of 4 values (2 independent replicates of temperature, 2 instrument readings for each). Error bars for average *DB* represent the standard error of 2 values (2 independent replicates of temperature). See Figures S7 to S20 for partial ^{1}H NMR spectra. See Figure 2 for data consistency check. See Table S5 for individual values.

Average *DB* is a metric related to *AAC*, with increasing proportions of less branched molecules generally expected to result in a decrease in the average *DB* (Figure 2). The average *DB* within the rice varieties grown at different temperatures is also shown in Figure 3. Average *DB* ranged from 3.4 to 4.5 % for all varieties and growing temperatures. Growing temperature did not influence average *DB* in any variety except Kyeema, where error bars indicated an apparent increase in average *DB* potentially arising from the coinciding decrease in *AAC* rather than a change in branching structure. All other varieties but Cocodrie and I-Geo-Tze displayed a reduction in *AAC* at the higher temperatures, but no

significant change in average *DB*, counter to the observation in Kyeema and suggesting no direct association between *AAC* and average *DB* in these varieties. This is despite the general trend of decreasing average *DB* with increasing *AAC*, highlighting the need to report on a varietal basis (Figure 2). It is hypothesised that the reduction in the less branched amylose component had been counteracted by a decrease in *DB* primarily in the amylopectin component as a result of the higher growing temperature.

Differences in average *DB* could be noted between some varieties. At lower growing temperature, for the first grouping of varieties by *AAC* (24.9 to 26.9 %), the average *DB* was within the error bars, except for Doongara. For the second grouping (*AAC* of 19.4 to 19.6 %), a difference in their average *DB* was observed. At higher growing temperatures, two of the groupings by *AAC* (27.5 to 28.7 %, and 17.7 to 20.1 %) displayed a different average *DB* between varieties. For the third grouping, Kyeema and Quest (13.3 to 13.7 %), the average *DB* was within error.

While differences in average *DB* were observed between varieties, the average *DB* alone masks the distribution of α(1, 6) bonds between amylose and amylopectin. For example, the fine details of the branching structure such as short chain and long chain branches or the position of the branches, cannot be assessed. Given the multitude of possible combinations in branching and amylose content, it is expected that many of these can yield the same average *DB* despite displaying different branching distributions. Therefore, while the average *DB* may be a useful tool for general assessment of branching characteristics in some cases, it does not yield the fine details necessary to assess the potential relationships between branching structures and rice quality traits.

3.4 Assessing semi-crystalline lamellae with SAXS

The semi-crystalline lamellar structure of starch is packing of amylose and amylopectin as a function of their branching and size within each starch granule (Figure 1, Levels 3 to 5). The characteristic lamellar peak of starch ($\boldsymbol{q} \approx 0.06\text{-}0.07$ Å^{-1}, d-spacing ≈ 9-10.5 nm) has been well studied with SAXS in a

diverse array of starches including rice starch (H. Wang et al., 2018; Witt et al., 2012); however, to the best of our knowledge this is the first time it has been studied on milled rice flour. This and a second higher $\boldsymbol{q}$ peak ($\boldsymbol{q} \approx 0.13$ Å^{-1}) were observed here for all varieties (Figure S37). This second peak is rarely reported in the literature and likely to have its origin as a second order reflection from the lamellar peak. The extracted parameters of the primary lamellar peak are related to the features of the semi-crystalline lamellar structure of starch (Blazek & Gilbert, 2011), providing an additional avenue in assessing the subtle differences in starch nanostructure beyond information on *AAC* and average *DB*.

3.4.1 Extent of semi-crystalline order

The relative intensity of the primary lamellar peak ($\boldsymbol{q} \approx 0.067$ Å^{-1}) relates to the extent of semi-crystalline order present in the sample. The peak intensity of rice grown in two temperature treatments is shown in Figure 4. It is important to note that the relative intensity in SAXS is sensitive to sample thickness and packing density, and that care must be taken to minimise differences when comparing scattering intensity from different samples (Blazek & Gilbert, 2011). In this work, the sample thickness and packing density in preparation were not specifically controlled, so bias in relative scattering intensities may be introduced. However, a general decrease in relative intensity with increasing amylose content has been reported in the literature (Blazek & Gilbert, 2011) and has also been observed in this study (Figure S38). This trend indicates that packing densities were adequately controlled. This apparent relationship of *AAC* with relative peak intensity has been explained by the accumulation of defects within the lamellar architecture (Blazek & Gilbert, 2011).

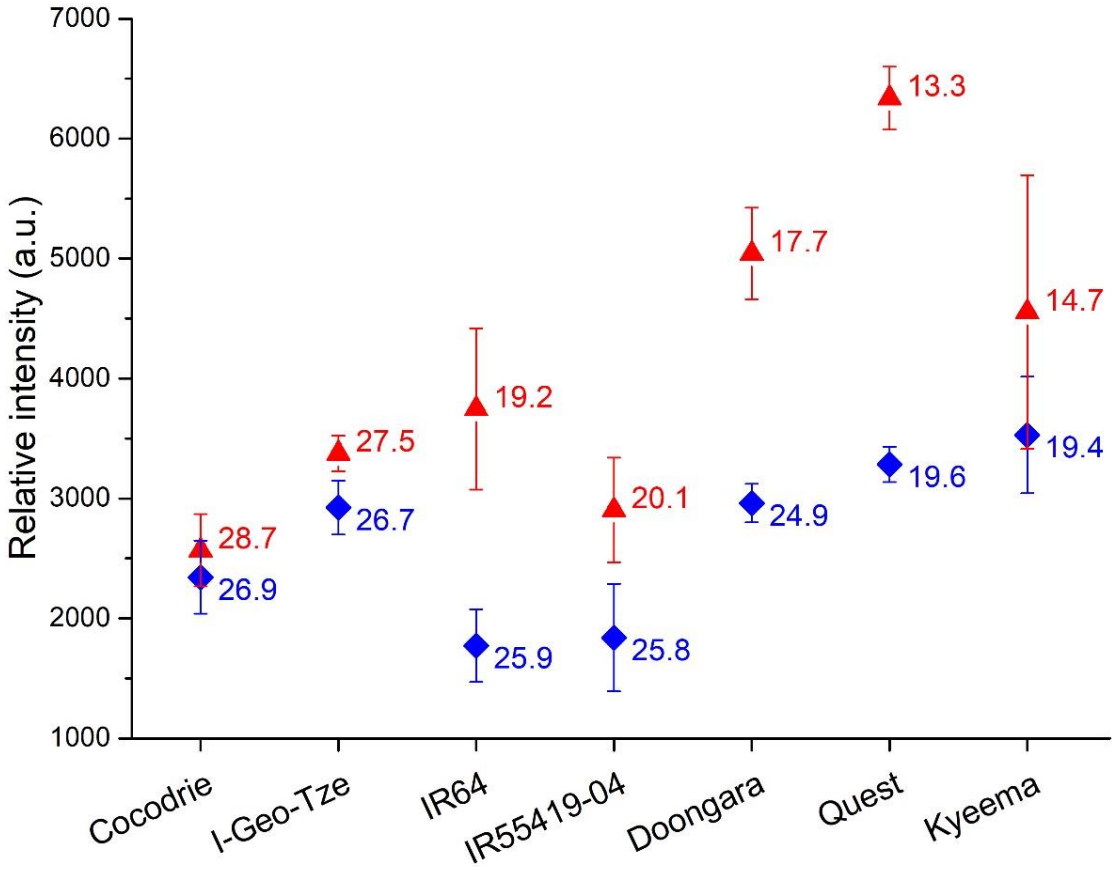

393

394 **Fig. 4. Relative peak intensity of main lamellar peak observed in SAXS for rice flours of different varieties**
395 **grown at lower (blue diamonds) and higher (red triangles) temperature for each variety and temperature.**
396 **Average *AAC* of samples is shown adjacent to data point. Error bars represent the standard error of 6 values**
397 **(2 independent replicates of temperature, 3 preparations for each). See Figures S23 to S36 for SAXS curves.**
398 **See Table S5 for individual mean peak intensity values.**

399 Differences in relative intensity between temperature treatments were within the error bars for
400 Cocodrie and I-Geo-Tze, and given *AAC* and average *DB* were unchanged, this suggests no change in
401 the extent of semi-crystalline order. IR64, IR55419-04, Doongara and Quest varieties exhibited a
402 measurable increase in the relative intensity, a decrease in *AAC* and similar average *DB* at the higher
403 growing temperature. These results agree with the consideration that amylose contributes mainly to
404 the amorphous regions of the semi-crystalline structure (T. L. Wang et al., 1998). The extent of semi-
405 crystalline order is thus expected to increase as a result of a decrease in the amorphous component.
406 The consistency in average *DB* for all varieties except Kyeema indicates that the extent of semi-

crystalline order is independent of a change in branching frequency, reflected in the relationship of strongly increasing relative intensity (by 110 %) with weakly increasing average *DB* (by 25 %, see Figure S39). At higher growing temperatures, Kyeema displayed no measurable increase in relative intensity despite an apparent decrease in *AAC* and increase in average *DB*. This suggests the formation of crystalline structure has not been influenced by the reduced *AAC* or changes to branching structure. The large error in the relative intensity for Kyeema may indicate that intragranular packing density was significantly interrupted, especially at the higher temperature.

Differences in relative intensities could also distinguish varieties within each temperature treatment. The two groupings of varieties by *AAC* at lower growing temperatures (24.9 to 26.9 %, and 19.4 to 19.6 %), could be distinguished into three groups by their relative intensities. Of the higher *AAC* varieties, I-Geo-Tze and Doongara displayed the highest relative intensities and IR55419-04 and IR64 the lowest, while Cocodrie overlapped both. This highlights the difference in extent of semi-crystalline order that can occur between varieties despite a relatively narrow range of *AAC.* In contrast, the lower *AAC* Kyeema and Quest had both similar *AAC* and similar relative intensities. Interestingly, despite much lower *AAC*, the relative intensity of these varieties was similar to some of the higher AAC varieties at the lower growing temperature. At higher growing temperatures, the three groupings of varieties by *AAC* all displayed differences in relative intensity within the groupings, highlighting again how differences in the extent of semi-crystalline order can manifest independent of *AAC*. However, intergroup overlap of relative intensities was noted for the higher and intermediate *AAC* groupings, counter to the general observation of decreasing relative intensity with increasing *AAC* (Figure S38).

At both lower and higher temperatures, varieties exhibiting similar average *DB* could not be further discriminated by their relative intensity. One exception was Doongara, displaying a substantially higher relative intensity at higher growing temperature than I-Geo-Tze and IR55419-04 despite similar average *DB;* however, due to the large error no conclusions can be drawn.

3.4.2 Thickness of semi-crystalline lamellae

The position of the primary lamellar peak relates to the thickness of the lamellar repeat unit, one crystalline plus one amorphous lamella, in real space (Figures 1 and 5). The lamellar repeat thickness was typical of what has been reported for starch (Donald et al., 2001), with varieties exhibiting sizes between 8.9 and 9.7 nm.

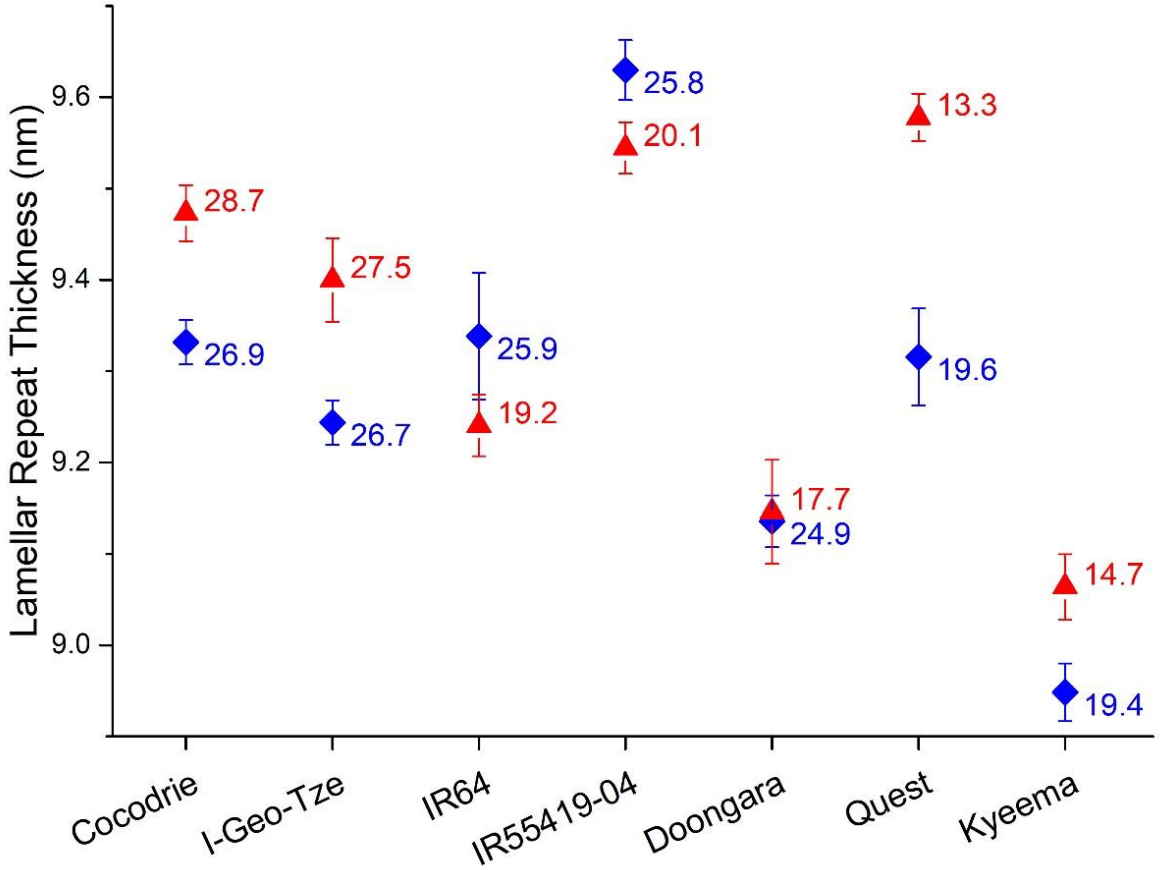

Fig. 5. Lamellar repeat thickness measured with SAXS for rice flours of different varieties grown at lower (blue diamonds) and higher (red triangles) temperatures (Equation S6). Average *AAC* of samples is shown adjacent to data point. Error bars represent the standard error of 6 values (2 independent replicates of temperature, 3 preparations for each). See Figures S23 to S36 for SAXS curves. See Table S5 for individual mean thickness values.

All varieties displayed a change in the lamellar repeat thickness, within error, between temperature treatments except for IR64 and Doongara (Figure 5). Both IR64 and Doongara also displayed a

445 decrease in *AAC*, similar average *DB* and an increase in extent of semi-crystalline order with the higher
446 temperature treatment. This similarity in lamellar repeat thickness strongly indicates that the
447 decrease in *AAC* is linked primarily with a decrease in the fraction of bulk amorphous regions (Figure
448 1, level 5) rather than in the amorphous lamellae of the semi-crystalline regions (Figure 1, level 4). Of
449 the varieties in which higher temperature treatment impacted the lamellar repeat thickness, Cocodrie
450 and I-Geo-Tze had displayed no large difference in *AAC*, indicating again that *AAC* itself is not a primary
451 driver of the lamellar repeat thickness, but may play a role. Variations in lamellar repeat thickness
452 have indeed been reported to coincide with increased concentration of longer chain lengths of
453 debranched starch (degree of polymerisation higher than 13), with either increased disordered chain
454 ends contributing to amorphous regions or production of larger crystalline lamellae (Witt et al., 2012).
455 Kyeema was the only variety with a change in both lamellar repeat thickness and average *DB* between
456 temperature treatments, potentially indicating a change in concentration of longer chain lengths.
457 However, these suggestions cannot be confirmed by the average *DB* as it does not inform on such
458 aspects of the branching structure.

459 The lamellar repeat thickness appeared to be independent of *AAC* between varieties within each
460 temperature treatment. An exception to this was Cocodrie and I-Geo-Tze which displayed similar
461 lamellar repeat thicknesses at the higher growing temperature, reflecting the consistency in other
462 measured parameters. For the remaining varieties, grouped by *AAC* and exhibiting similar average *DB*,
463 differences in lamellar repeat thickness were noted within groupings. At lower temperature
464 treatment, this was observed for the grouping of Kyeema and Quest varieties, as well as for the
465 grouping of IR55419-04 and Doongara varieties. At higher growing temperatures this was observed
466 for the grouping of IR55419-04, IR64 and Doongara varieties. These observations confirm that *AAC* or
467 average *DB* are not in themselves the primary drivers of the lamellar repeat thickness, though it is
468 possible these differences arise from varietal differences in chain length distribution, similar to
469 observations of the temperature treatments (Witt et al., 2012).

3.4.3 Heterogeneity of lamellae

The half width half maximum (HWHM) of the observed scattering peak for starch is related to the uniformity of the lamellar repeat thickness, with an increase in HWHM corresponding to a greater variation between the thickness of lamellae (Figures 1 and 6). There is a positive relationship between HWHM and average lamellar repeat thickness (see Figure S40 in section S4.3). This previously reported observation was explained by a minimum number of glucose units (degree of polymerisation of 10-12) required to form a helix (Witt et al., 2012).

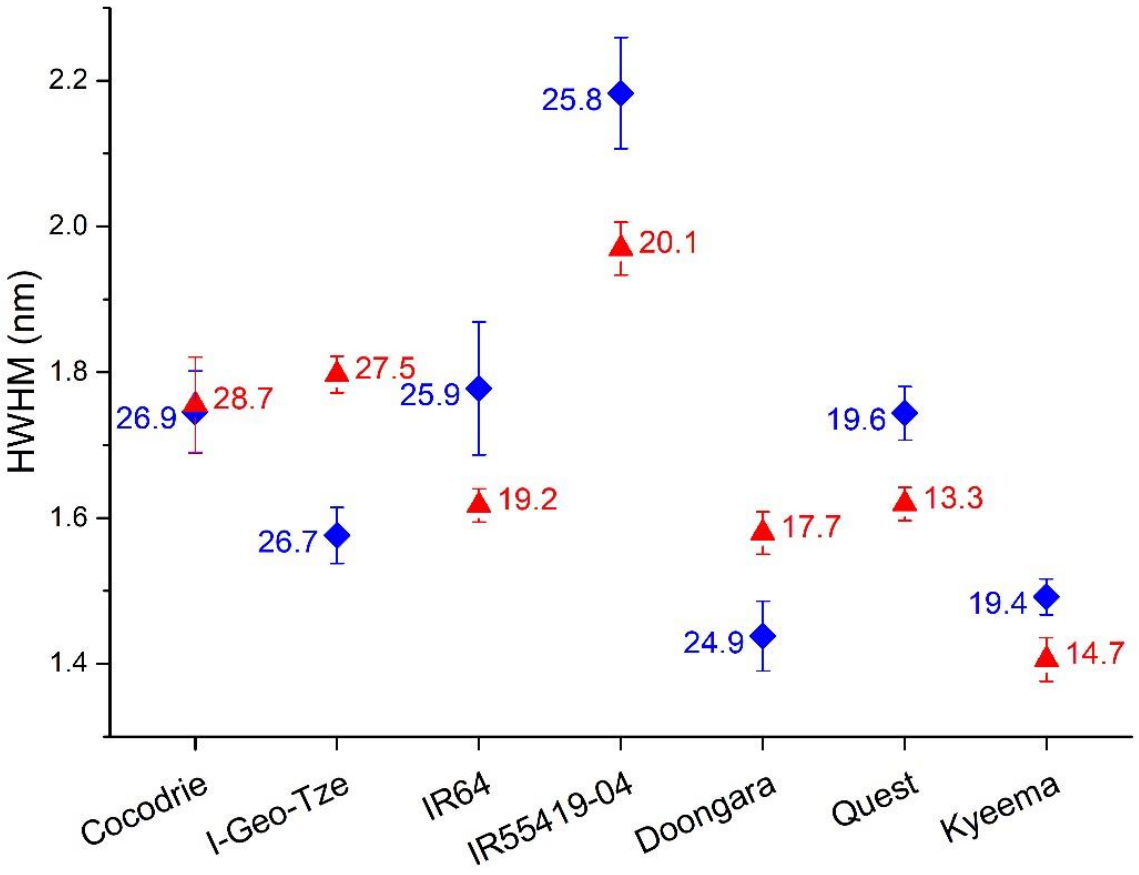

Fig. 6. HWHM of the lamellar peak measured with SAXS for rice flours of different varieties grown at lower (blue diamonds) and higher (red triangles) temperatures (Equation S7). Average *AAC* of samples is shown adjacent to data point. Error bars represent the standard error of 6 values (2 independent replicates of temperature, 3 preparations for each). See Figures S23 to S36 for SAXS curves. See Table S5 for individual mean HWHM values.

All varieties displayed a change in lamellar heterogeneity between temperature treatments, except for Cocodrie (Figure 6). For Cocodrie this indicates a consistency in the lamellar repeat thickness between the lamellae, reflected in both the unchanged *AAC* and average *DB*, though an increase in the lamellar repeat thickness in the higher temperature treatment (Figure 5) indicates that some structural changes are still occurring. Of the other varieties where lamellar heterogeneity was different between temperature treatments, all except I-Geo-Tze recorded a decrease in *AAC* at higher growing temperature. Varieties displaying both positive and negative changes in HWHM were observed indicating an independence of lamellar heterogeneity from *AAC*. Kyeema was the only variety that exhibited a change in both the average *DB* between temperature treatments and in HWHM, which may again hint at some aspect of the branching structures playing a role; however, this cannot be confirmed.

Differences in lamellar heterogeneity were also observed between varieties within each temperature treatment. At lower growing temperature, the grouping of higher *AAC* varieties (24.9 to 26.9 %) exhibited a range of different HWHM values, indicating large differences in the lamellar heterogeneity between them. An exception to this was Cocodrie and IR64, for which along with HWHM both average *DB* and lamellar repeat thickness were similar. This could suggest that these varieties exhibit similar branching structures that account for the similarities observed, though similar HWHM of the lower *AAC* suggests that *AAC* is not a major factor in HWHM. This is further highlighted by the difference in HWHM between Kyeema and Quest at lower growing temperature despite similar *AAC* and average *DB*. At higher growing temperatures, similar observations were made for the three groupings of varieties with similar *AAC* exhibiting differences in lamellar heterogeneity. Where varieties also exhibited similar average *DB*, HWHM distinguished between them (e.g., Quest and Kyeema). An exception was Cocodrie and I-Geo-Tze, displaying similar HWHM and a narrow range of *AAC* (27.5 to 28.7 %), but an apparent difference in average *DB* suggests some similarity in branching structure that is independent of branching frequency.

3.4.4 General statements on semi-crystalline structure

When comparing groupings of varieties by *AAC*, features of the semi-crystalline lamellar structure could be used to differentiate between varieties and the impact of growing temperature. Similarly, when comparing varieties of similar average *DB*, the lamellar features could be used to further differentiate samples. Drivers of such changes in the semi-crystalline structure could be explored at the molecular level, for example in terms of chain length distribution of debranched starch (Witt et al., 2012) or of distribution of branching structures (Thevarajah, Sutton, et al., 2016). FTIR may provide a more accessible approach to explore the crystalline structure. However, the complex non-linear relationship of the crystallinity index determined from FTIR with crystallinity measured by NMR or XRD (Warren et al., 2016) indicates that such an approach is not straightforward; this is principally associated with the deconvolution of strongly overlapping signals biasing the intensity of the peaks of interest. Cryogenic temperatures have been suggested to improve resolution (Hermann & Harvey, 1969); however, an adequate resolution could still not be obtained for starch in this work even at cryogenic temperatures (see Figure S41 in section S6.2).

Tentative conclusions could be drawn from the SAXS peak intensity data. The lamellar repeat thickness and HWHM offer valuable information to characterise differences between samples. As far as its association with *AAC* and average *DB* is concerned, it is apparent that the lamellar structure is influenced by the *AAC*; however, within the range of samples studied, the average *DB* does not offer any more depth than *AAC* when examining the lamellar structure.

4. Conclusions

Determination of *AAC* by spectrophotometry is a standard and valuable measurement conducted on rice grains as part of grain quality assessment . However, there is a range of characteristics in starch structure that could also play a role in grain quality. Whereas *AAC* has high precision and low accuracy, determination of the degree of branching using NMR offers a similar precision but the accuracy may

be higher. There are intrinsic errors in NMR due to sampling and dissolution; however, this can be largely addressed by dissolving the starch in dry DMSO and then measuring the sample as soon as D_2O has been added. The accuracy of *AAC* may be investigated by adopting similar dissolution protocols shown to effectively solubilise starch; however, this would also require determination of the impact on the iodine binding. In terms of NMR, a round-robin test would give an important assessment of the accuracy of the average *DB*.

Average *DB* could distinguish varieties, showing groupings despite differences in other structural features. However, the subtle changes caused by a stressor to a single variety, in the current case temperature, are more challenging to detect if present. Varieties with similar *AAC* could be distinguished by their average *DB* within an *AAC* grouping. However, the contributions of different branching structures and their distributions are averaged into this single value. As an alternative approach in the characterisation of molecular structure in starch, the separation of different branching structures using free-solution capillary electrophoresis shows promise as a complementary technique (Herrero-Martínez et al., 2004). Evaluation of the lamellar structure similarly was able to distinguish different varieties and could also indicate differences in structure as a result of growing temperature. The ability of SAXS to investigate the semi-crystalline lamellar structure yields unique insights into the crystalline structure compared to the lateral long-range crystalline information that can be obtained by XRD; however, SAXS instrumentation is generally less accessible to food materials scientists.

Ultimately, features of starch structure other than *AAC* in rice flour are also capable of distinguishing samples, even in some cases where *AAC* was unchanged. However, the relevance of *AAC* to other quality parameters such as gelatinisation temperature, texture and digestibility is a major reason that it has cemented its importance as a quality parameter of rice flour. The use of more robust statistical approaches to explore the value of different measurements of starch structure in distinguishing between rice varieties or rice qualities would be a valuable approach.

While the focus of this study was on starch characteristics, it must also be acknowledged that proteins, lipids and other polysaccharides will contribute to rice grain quality. However, there is still an opportunity to explore how finer details of starch structure, including molecular (branching structures) and supramolecular (lamellar) structure, are linked to or can define other important quality traits of rice grains. Such a link would strengthen the case for inclusion of these alternative and complementary features of starch structure within routine rice quality analysis. Considering costs and accessibility, the characterisation of the lamellar structure (by SAXS) would be limited to selected samples, the measurement of average *DB* (by NMR) would be applicable to a larger range of samples to select the more promising ones, and the determination of the distribution of branching structures (with capillary electrophoresis) would be applicable as a high-throughput tool for the initial pre-selection.

Acknowledgements

This work was supported by the Australian Government [Research Training Program scholarship to MVL], AgriFutures [PRJ-010712 to MVL, MG, PC, RW, EG], the Australian Institute of Nuclear Science and Engineering (AINSE) [Post-Graduate Research Award to MVL], Western Sydney University [Academic Development Plan to MG], and the Molecular Medicine Research Group at WSU [travel grant to MVL]. The Australian Nuclear Science and Technology Organisation (ANSTO) is acknowledged for granting access to the SAXS instrument (X4647 and P6398) and Robert Knott for training and technical assistance with the SAXS instrument. Tim Murphy and Richard Wuhrer (Advanced Materials Characterisation Facility, WSU) are thanked for training and general discussion. NSW DPI cereal chemistry team are thanked for rice samples, data and general discussion, IRRI for providing samples and Lorraine Spohr (NSW DPI) for biometric advice.

Declaration of interest

None.

References

AACC International. (2011). Amylose content of milled rice (Method 61-03.01). *Approved Methods of Analysis 11th ed.* St. Paul (MN, USA): Cereals & Grains Association.

Aravind, N., Sissons, M., Fellows, C. M., Blazek, J., & Gilbert, E. P. (2013). Optimisation of resistant starch II and III levels in durum wheat pasta to reduce in vitro digestibility while maintaining processing and sensory characteristics. *Food Chemistry, 136*, 1100-1109. https://doi.org/10.1016/j.foodchem.2012.08.035

Ayres, N. M., McClung, A. M., Larkin, P. D., Bligh, H. F. J., Jones, C. A., & Park, W. D. (1997). Microsatellites and a single-nucleotide polymorphism differentiate apparentamylose classes in an extended pedigree of US rice germ plasm. *Theoretical and Applied Genetics, 94*, 773-781. https://doi.org/10.1007/s001220050477

Bayer, R. K., & Baltá-Calleja, F. J. (2006). Nanostructure of potato starch, part I: Early stages of retrogradation of amorphous starch in humid atmosphere as revealed by simultaneous SAXS and WAXS. *International Journal of Polymeric Materials and Polymeric Biomaterials, 55*, 773-788. https://doi.org/10.1080/00914030500440229

Blazek, J., & Gilbert, E. P. (2011). Application of small-angle X-ray and neutron scattering techniques to the characterisation of starch structure: A review. *Carbohydrate Polymers, 85*, 281-293. https://doi.org/10.1016/j.carbpol.2011.02.041

Buléon, A., Colonna, P., Planchot, V., & Ball, S. (1998). Starch granules: structure and biosynthesis. *International Journal of Biological Macromolecules, 23*, 85-112. https://doi.org/10.1016/S0141-8130(98)00040-3

Capron, I., Robert, P., Colonna, P., Brogly, M., & Planchot, V. (2007). Starch in rubbery and glassy states by FTIR spectroscopy. *Carbohydrate Polymers, 68*, 249-259. https://doi.org/10.1016/j.carbpol.2006.12.015

Castignolles, P., Graf, R., Parkinson, M., Wilhelm, M., & Gaborieau, M. (2009). Detection and quantification of branching in polyacrylates by size-exclusion chromatography (SEC) and melt-state 13C NMR spectroscopy. *Polymer, 50*, 2373-2383. https://doi.org/10.1016/j.polymer.2009.03.021

Castro, J. V., Ward, R. M., Gilbert, R. G., & Fitzgerald, M. A. (2005). Measurement of the molecular weight distribution of debranched starch. *Biomacromolecules, 6*, 2260-2270. https://doi.org/10.1021/bm050041t

Chen, M.-H., Bergman, C., Pinson, S., & Fjellstrom, R. (2008). Waxy gene haplotypes: Associations with apparent amylose content and the effect by the environment in an international rice germplasm collection. *Journal of Cereal Science, 47*, 536-545. https://doi.org/10.1016/j.jcs.2007.06.013

Claridge, T. D. W. (2009). Chapter 2 - Introducing high-resolution NMR. *High-Resolution NMR Techniques in Organic Chemistry* (pp. 11-34). Oxford (UK): Elsevier.

Concepcion, J. C. T., Ouk, M., Zhao, D., & Fitzgerald, M. A. (2015). The need for new tools and investment to improve the accuracy of selecting for grain quality in rice. *Field Crops Research, 182*, 60-67. https://doi.org/10.1016/j.fcr.2015.05.003

De Bruyn, H., Sprong, E., Gaborieau, M., David, G., Roper III, J. A., & Gilbert, R. G. (2006). Starch-graft-copolymer latexes initiated and stabilized by ozonolyzed amylopectin. *Journal of Polymer Science A Polymer Chemistry, 44*, 5832-5845. https://doi.org/10.1002/pola.21703

Dona, A., Yuen, C.-W. W., Peate, J., Gilbert, R. G., Castignolles, P., & Gaborieau, M. (2007). A new NMR method for directly monitoring and quantifying the dissolution kinetics of starch in DMSO. *Carbohydrate Research, 342*, 2604-2610. https://doi.org/10.1016/j.carres.2007.08.010

Donald, A. M., Kato, K. L., Perry, P. A., & Waigh, T. A. (2001). Scattering studies of the internal structure of starch granules. *Starch - Stärke, 53*, 504-512. https://doi.org/10.1002/1521-379X(200110)53:10<504::AID-STAR504>3.0.CO;2-5

Fitzgerald, M. A., Bergman, C. J., Resurreccion, A. P., Möller, J., Jimenez, R., Reinke, R. F., Martin, M., Blanco, P., Molina, F., Chen, M.-H., Kuri, V., Romero, M. V., Habibi, F., Umemoto, T., Jongdee, S., Graterol, E., Reddy, K. R., Bassinello, P. Z., Sivakami, R., Rani, N. S., Das, S., Wang, Y. J., Indrasari, S.

D., Ramli, A., Ahmad, R., Dipti, S. S., Xie, L., Lang, N. T., Singh, P., Toro, D. C., Tavasoli, F., & Mestres, C. (2009). Addressing the dilemmas of measuring amylose in rice. *Cereal Chemistry, 86*, 492-498. https://doi.org/10.1094/cchem-86-5-0492

Fitzgerald, M. A., Rahman, S., Resurreccion, A. P., Concepcion, J., Daygon, V. D., Dipti, S. S., Kabir, K. A., Klingner, B., Morell, M. K., & Bird, A. R. (2011). Identification of a Major Genetic Determinant of Glycaemic Index in Rice. *Rice, 4*, 66-74. https://doi.org/10.1007/s12284-011-9073-z

Gaborieau, M., & Castignolles, P. (2009). Caractérisation de l'amidon et de ses matériaux composites. [Characterisation of starch and of its composite materials]. *Les Annales des falsifications de l'expertise chimique et toxicologique (Société des Experts Chimistes de France) 9710*, 23-32.

Gaborieau, M., De Bruyn, H., Mange, S., Castignolles, P., Brockmeyer, A., & Gilbert, R. G. (2009). Synthesis and characterization of synthetic polymer colloids colloidally stabilized by cationized starch oligomers. *Journal of Polymer Science A Polymer Chemistry, 47*, 1836-1852. https://doi.org/10.1002/pola.23287

Gartner, C., López, B. L., Sierra, L., Graf, R., Spiess, H. W., & Gaborieau, M. (2011). Interplay between structure and dynamics in chitosan films investigated with solid-state NMR, dynamic mechanical analysis, and X-ray diffraction. *Biomacromolecules, 12*, 1380-1386. https://doi.org/10.1021/bm200193u

Gidley, M. J. (1985). Quantification of the structural features of starch polysaccharides by NMR spectroscopy. *Carbohydrate Research, 139*, 85-93. https://doi.org/10.1016/0008-6215(85)90009-6

Hermann, T. S., & Harvey, S. R. (1969). Infrared spectroscopy at sub-ambient temperatures: I. Literature review. *Applied Spectroscopy, 23*, 435-450. https://doi.org/10.1366/000370269774380563

Hernández, J. M., Gaborieau, M., Castignolles, P., Gidley, M. J., Myers, A. M., & Gilbert, R. G. (2008). Mechanistic investigation of a starch-branching enzyme using hydrodynamic volume SEC analysis. *Biomacromolecules, 9*, 954-965. https://doi.org/10.1021/bm701213p

Herrero-Martínez, J. M., Schoenmakers, P. J., & Kok, W. T. (2004). Determination of the amylose–amylopectin ratio of starches by iodine-affinity capillary electrophoresis. *Journal of Chromatography A, 1053*, 227-234. https://doi.org/10.1016/j.chroma.2004.06.048

Hirano, H. Y., Eiguchi, M., & Sano, Y. (1998). A single base change altered the regulation of the Waxy gene at the posttranscriptional level during the domestication of rice. *Molecular Biology and Evolution, 15*, 978-987. https://doi.org/10.1093/oxfordjournals.molbev.a026013

Hoang, N.-L., Landolfi, A., Kravchuk, A., Girard, E., Peate, J., Hernandez, J. M., Gaborieau, M., Kravchuk, O., Gilbert, R. G., Guillaneuf, Y., & Castignolles, P. (2008). Toward a full characterization of native starch: Separation and detection by size-exclusion chromatography. *Journal of Chromatography A, 1205*, 60-70. https://doi.org/10.1016/j.chroma.2008.07.090

Hoffman, R. E. (2006). Standardization of chemical shifts of TMS and solvent signals in NMR solvents. *Magnetic Resonance in Chemistry, 44*, 606-616. https://doi.org/10.1002/mrc.1801

Jiang, H., Dian, W., & Wu, P. (2003). Effect of high temperature on fine structure of amylopectin in rice endosperm by reducing the activity of the starch branching enzyme. *Phytochemistry, 63*, 53-59. https://doi.org/10.1016/s0031-9422(03)00005-0

Juliano, B. O. (2016). Rice: Overview. In J. Faubion, K. Seetharaman, C. Wrigley & H. Corke (Eds.), *Encyclopedia of Food Grains (Second Edition)* (pp. 125-129). Oxford (UK): Academic Press.

Kazarian, A. A., Smith, J. A., Hilder, E. F., Breadmore, M. C., Quirino, J. P., & Suttil, J. (2010). Development of a novel fluorescent tag O-2- aminoethyl fluorescein for the electrophoretic separation of oligosaccharides. *Analytica Chimica Acta, 662*, 206-213. https://doi.org/10.1016/j.aca.2010.01.011

Kline, S. (2006). Reduction and analysis of SANS and USANS data using IGOR Pro. *Journal of Applied Crystallography, 39*, 895-900. https://doi.org/doi:10.1107/S0021889806035059

Knutson, C. A. (1999). Evaluation of variations in amylose-iodine absorbance spectra. *Carbohydrate Polymers, 42*, 65-72. https://doi.org/10.1016/S0144-8617(99)00126-5

Koch, K., Andersson, R., & Aman, P. (1998). Quantitative analysis of amylopectin unit chains by means of high-performance anion-exchange chromatography with pulsed amperometric detection. *Journal of Chromatography A, 800*, 199-206. https://doi.org/10.1016/S0021-9673(97)01151-5

Krishnan, P., Ramakrishnan, B., Reddy, K. R., & Reddy, V. R. (2011). Chapter three - High-temperature effects on rice growth, yield, and grain quality. In D. L. Sparks (Ed.), *Advances in Agronomy* (Vol. 111, pp. 87-206). Oxford (UK): Academic Press.

Larkin, P. D., & Park, W. D. (1999). Transcript accumulation and utilization of alternate and non-consensus splice sites in rice granule-bound starch synthase are temperature-sensitive and controlled by a single-nucleotide polymorphism. *Plant Molecular Biology, 40*, 719-727. https://doi.org/10.1023/a:1006298608408

Liu, F., Romanova, N., Lee, Elizabeth A., Ahmed, R., Evans, M., Gilbert, Elliot P., Morell, Matthew K., Emes, Michael J., & Tetlow, Ian J. (2012). Glucan affinity of starch synthase IIa determines binding of starch synthase I and starch-branching enzyme IIb to starch granules. *Biochemical Journal, 448*, 373-387. https://doi.org/10.1042/BJ20120573

Lopez-Rubio, A., Flanagan, B. M., Gilbert, E. P., & Gidley, M. J. (2008). A novel approach for calculating starch crystallinity and its correlation with double helix content: A combined XRD and NMR study. *Biopolymers, 89*, 761-768. https://doi.org/10.1002/bip.21005

Manelius, R., Maaheimo, H., Nurmi, K., & Bertoft, E. (2002). Characterisation of fractions obtained by isoamylolysis and ion-exchange chromatography of cationic waxy maize starch. *Starch - Stärke, 54*, 58-65. https://doi.org/10.1002/1521-379x(200202)54:2<58::aid-star58>3.0.co;2-1

Maniego, A. R., Sutton, A. T., Gaborieau, M., & Castignolles, P. (2017). Assessment of the branching quantification in poly(acrylic acid): Is it as easy as it seems? *Macromolecules, 50*, 9032-9041. https://doi.org/10.1021/acs.macromol.7b01411

Misra, G., Cuevas, R. P., Anacleto, R., Butardo, V. M., Jr, Sreenivasulu, N., & Kavi Kishor, P. B. (2015). Designing climate-resilient rice with ideal grain quality suited for high-temperature stress. *Journal of Experimental Botany, 66*, 1737-1748. https://doi.org/10.1093/jxb/eru544

Nilsson, G. S., Gorton, L., Bergquist, K.-E., & Nilsson, U. (1996). Determination of the degree of branching in normal and amylopectin type potato starch with 1H-NMR spectroscopy improved resolution and two-dimensional spectroscopy. *Starch - Stärke, 48*, 352-357. https://doi.org/10.1002/star.19960481003

Pallas, L. (2016). Rice processing: Beyond the farm gate. In G. Smithers & V. Trinetta (Eds.), *Reference Module in Food Science*. Cambridge (MA, USA): Elsevier Inc.

Pérez, S., & Bertoft, E. (2010). The molecular structures of starch components and their contribution to the architecture of starch granules: A comprehensive review. *Starch - Stärke, 62*, 389-420. https://doi.org/10.1002/star.201000013

Petoukhov, M. V., Franke, D., Shkumatov, A. V., Tria, G., Kikhney, A. G., Gajda, M., Gorba, C., Mertens, H. D. T., Konarev, P. V., & Svergun, D. I. (2012). New developments in the ATSAS program package for small-angle scattering data analysis. *Journal of Applied Crystallography, 45*, 342-350. https://doi.org/doi:10.1107/S0021889812007662

Salman, H., Blazek, J., Lopez-Rubio, A., Gilbert, E. P., Hanley, T., & Copeland, L. (2009). Structure–function relationships in A and B granules from wheat starches of similar amylose content. *Carbohydrate Polymers, 75*, 420-427. https://doi.org/10.1016/j.carbpol.2008.08.001

Sano, Y., Hirano, H. Y., & Nishimura, M. (1991). Evolutionary significance of differential regulation at the *wx* locus of rice. In S. J. Banta & G. S. Argosino (Eds.), *Rice Genetics II Proceedings of the Second International Rice Genetics Symposium 14-18 May 1990* (pp. 11-20). Manila (Philipines): International Rice Research Institute.

Schmitz, S., Dona, A. C., Castignolles, P., Gilbert, R. G., & Gaborieau, M. (2009). Assessment of the extent of starch dissolution in dimethyl sulfoxide by 1H NMR spectroscopy. *Macromolecular Bioscience, 9*, 506-514. https://doi.org/10.1002/mabi.200800244

Shrestha, A. K., Blazek, J., Flanagan, B. M., Dhital, S., Larroque, O., Morell, M. K., Gilbert, E. P., & Gidley, M. J. (2012). Molecular, mesoscopic and microscopic structure evolution during amylase digestion

of maize starch granules. *Carbohydrate Polymers, 90*, 23-33. https://doi.org/10.1016/j.carbpol.2012.04.041

Singh, J., McCarthy, O. J., & Singh, H. (2006). Physico-chemical and morphological characteristics of New Zealand Taewa (Maori potato) starches. *Carbohydrate Polymers, 64*, 569-581. https://doi.org/10.1016/j.carbpol.2005.11.013

Striegel, A. (2003). Advances in the understanding of the dissolution mechanism of cellulose in DMAc/LiCl. *Journal of the Chilean Chemical Society, 48*, 73-77. https://doi.org/10.4067/S0717-97072003000100013

The International Organization for Standardization. (2015). Rice - Determination of amylose content - Part 1: Reference method (ISO 6647-1:2015).

Thevarajah, J. J., Bulanadi, J. C., Wagner, M., Gaborieau, M., & Castignolles, P. (2016). Towards a less biased dissolution of chitosan. *Analytica Chimica Acta, 935*, 258-268. https://doi.org/10.1016/j.aca.2016.06.021

Thevarajah, J. J., Sutton, A. T., Maniego, A. R., Whitty, E. G., Cottet, H., Castignolles, P., & Gaborieau, M. (2016). Quantifying the heterogeneity of chemical structures in complex charged polymers through the dispersity of their distributions of electrophoretic mobilities or of compositions. *Analytical Chemistry 88*, 1674-1681.

Usui, T., Yokoyama, M., Yamaoka, N., Matsuda, K., Tuzimura, K., Sugiyama, H., & Seto, S. (1974). Proton magnetic-resonance spectra of d-gluco-oligosaccharides and d-glucans. *Carbohydrate Research, 33*, 105-116. https://doi.org/10.1016/s0008-6215(00)82944-4

van Soest, J. J. G., Tournois, H., de Wit, D., & Vliegenthart, J. F. G. (1995). Short-range structure in (partially) crystalline potato starch determined with attenuated total reflectance Fourier-transform IR spectroscopy. *Carbohydrate Research, 279*, 201-214. https://doi.org/10.1016/0008-6215(95)00270-7

Vermeylen, R., Goderis, B., & Delcour, J. A. (2006). An X-ray study of hydrothermally treated potato starch. *Carbohydrate Polymers, 64*, 364-375. https://doi.org/10.1016/j.carbpol.2005.12.024

Vermeylen, R., Goderis, B., Reynaers, H., & Delcour, J. A. (2005). Gelatinisation related structural aspects of small and large wheat starch granules. *Carbohydrate Polymers, 62*, 170-181. https://doi.org/10.1016/j.carbpol.2005.07.021

Wang, H., Liu, Y., Chen, L., Li, X., Wang, J., & Xie, F. (2018). Insights into the multi-scale structure and digestibility of heat-moisture treated rice starch. *Food Chemistry, 242*, 323-329. https://doi.org/10.1016/j.foodchem.2017.09.014

Wang, T. L., Bogracheva, T. Y., & Hedley, C. L. (1998). Starch: as simple as A, B, C? *Journal of Experimental Botany, 49*, 481-502. https://doi.org/10.1093/jexbot/49.320.481

Ward, R. (2017). Quality parameters and testing methods in rice cultivation. In T. Sasaki (Ed.), *Achieving sustainable cultivation of rice* (pp. 237-252). Cambridge (UK): Burleigh Dodds Science Publishing Limited.

Warren, F. J., Gidley, M. J., & Flanagan, B. M. (2016). Infrared spectroscopy as a tool to characterise starch ordered structure--a joint FTIR-ATR, NMR, XRD and DSC study. *Carbohydrate Polymers, 139*, 35-42. https://doi.org/10.1016/j.carbpol.2015.11.066

Waters, D. L. E., Henry, R. J., Reinke, R. F., & Fitzgerald, M. A. (2006). Gelatinization temperature of rice explained by polymorphisms in starch synthase. *Plant Biotechnology Journal, 4*, 115-122. https://doi.org/10.1111/j.1467-7652.2005.00162.x

WaveMetrics Inc. Igor Pro 6.37 (Version 6.3.7.2). Lake Oswego, OR, USA.

Witt, T., Doutch, J., Gilbert, E. P., & Gilbert, R. G. (2012). Relations between molecular, crystalline, and lamellar structures of amylopectin. *Biomacromolecules, 13*, 4273-4282. https://doi.org/10.1021/bm301586x

Highlights

- Starch structure was characterised in rice flours by spectroscopy and scattering
- The ability of starch structure to distinguish rices, growing conditions was explored
- The link between average branching degree and apparent amylose content was assessed
- Starch structure was affected by growing temperature, but not at all levels
- The methods suitability for inclusion in rice quality analysis was assessed

Graphical abstract

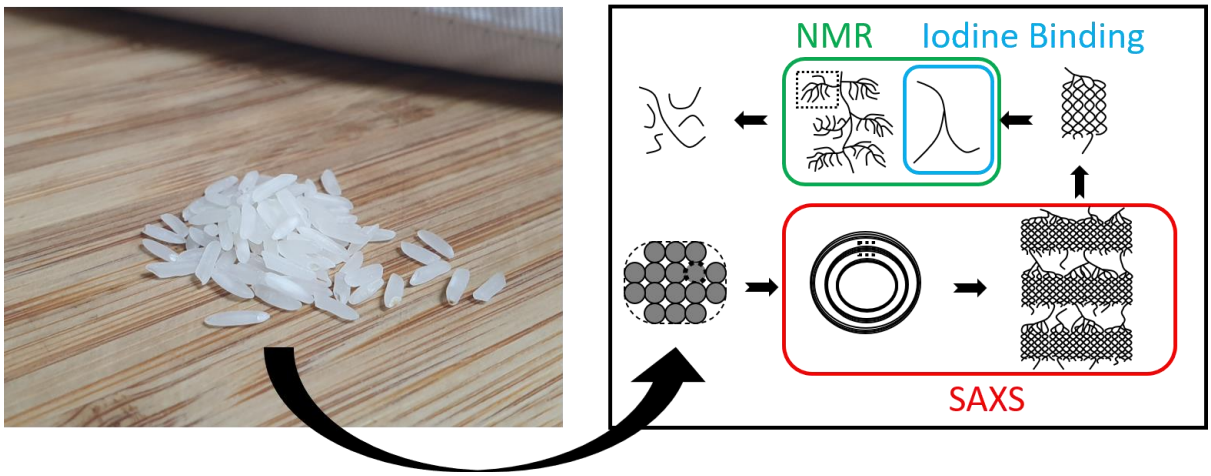

Supporting Information for

Assessment of starch branching and lamellar structure in rice flours

Matthew Paul Van Leeuwen, Michelle Rosemarie Toutounji, Jitendra Mata, Rachelle Ward, Elliot Paul Gilbert, Patrice Castignolles, Marianne Gaborieau

S1 Materials

S1.1 Rice flour samples

Seven varieties of rice were grown in glasshouses using a two-phase randomised design. The first phase was from sowing to five days after anthesis whereby 24 pots per variety were grown in the same glasshouse. In the second phase, between five days after anthesis and harvest, pots (6 per variety) were placed into replicated growth rooms with temperatures of 26/17 °C and 36/27 °C day/night temperatures. All other growth input and conditions were consistent. Grain was harvested at physiological maturity, dehulled (THU35A 250V 50Hz Test Husker, Satake, Australia), milled (brush mill) and ground (Cyclotec 1093 Sample Mill, Tecator AB, Sweden) to pass through a 50 µm sieve.

S1.2 Non-rice materials

Milli-Q® quality (Millipore, Bedford, MA, USA) water was used where specified, otherwise distilled water was used. Analytical grade sodium hydroxide pellets (NaOH), citric acid, potassium iodide and iodine were from Thermo Fisher Scientific (Scoresby, Victoria, Australia).

Deuterium oxide (D_2O) ≥99% (100 g bottles) and dimethyl sulfoxide-d6 (DMSO-d_6) ≥99% were obtained from Cambridge Isotope Laboratories, Inc. (Andowver, MA, USA). Ethanol ≥99% and lithium bromide (LiBr) ≥99% were purchased from Sigma-Aldrich (Castle Hill, NSW, Australia). Ethylene glycol in DMSO-d_6 (80 %) standard was obtained in a sealed 5 mm NMR tube from Bruker (Bruker Biospin Ltd, Sydney). Quartz glass tubes: 80 mm length, 2 mm outer diameter, and 0.01 mm wall thickness were purchased from Hilgenberg GmbH (Malsfeld, Germany).

S2 Determination of average DB

S2.1 Calibration of probe temperature

The probe temperature was calibrated using ethylene glycol (80 % in DMSO-d_6) and equation S1 (Tyburn, 1998):

$$T = \frac{(4.218 - \Delta\delta)}{0.009132} \qquad \text{Equation S1}$$

where T is the sample temperature in Kelvin and $\Delta\delta$ is the difference in ppm between the CH_2 and OH singlets.

S2.2 NMR measurement of waxy flour fractions

The protocol detailed in the main manuscript for rice flours was slightly modified as follows for the waxy rice flour fractions. The quantities were multiplied by 1.5 for the suspension in D_2O. DMSO-d_6 with 0.05 wt% LiBr was used for dissolution, as it yields complete dissolution of waxy rice flours (Schmitz et al., 2009). NMR spectra were measured on a Bruker Avance NMR spectrometer operating at a Larmor frequency of 500.13 MHz for ^1H, equipped with a TXI5z probe (Bruker Biospin); the temperature calibration was carried out with a pure ethylene glycol standard (distilled, in a sealed tube) (Schmitz et al., 2009). Quantitative ^1H NMR spectra were recorded at 90 °C using a 90° flip angle, and a repetition delay of 20 s. The signals of α and β reducing ends were negligible in the waxy rice flour fractions and not taken into account in the average *DB* calculation.

S2.3 Estimation of T_1 for quantitative determination of average DB

Longitudinal relaxation times (T_1) of the signals of interest (in the range of 5.4 to 4.2 ppm) were estimated using the one-dimensional inversion recovery pulse sequence. In this experiment, a signal is negative if the inversion recovery delay is shorter than T_1 *ln2, and positive if the inversion recovery delay is longer than T_1 *ln2. Signals in this range exhibited similar T_1, with T_1 determined to be between 0.5 and 1.5 s (Figure S1).

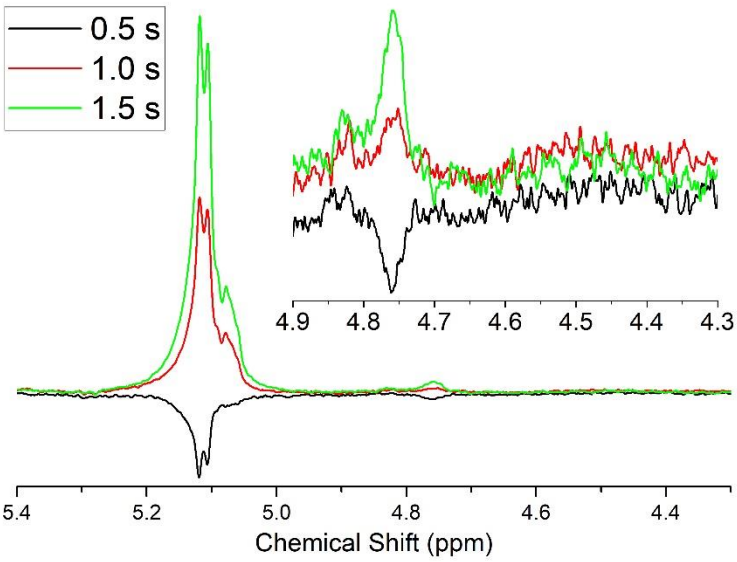

Figure S1 Partial spectra of rice starch in DMSO-d_6 at 80 °C displaying measurements to assess whether T_1 values are shorter than 0.5 s (black), 1.0 s (red) and 1.5 s (green), with inversion recovery delays of 347 ms (black), 694 ms (red) , and 1.042 s (green).

S2.4 Effect of probe temperature on average DB measurement

The work of Gidley employed high probe temperatures in order to maintain favourable conditions for a stable starch dissolution (Gidley, 1985). The effect of temperature was tested to ensure optimal resolution and sample dissolution stability. With a dissolution temperature of 80 °C, probe temperatures of 70 °C and 90 °C were compared on rice samples to determine if there were any dramatic effects on the resulting spectra. The results indicate that similar spectra are obtained, with a slightly improved resolution of the reducing ends afforded by the 90 °C probe temperature (Figure S2). This improved resolution was also noted in starch standard samples, leading to a lower calculated average *DB* (Figure S3).

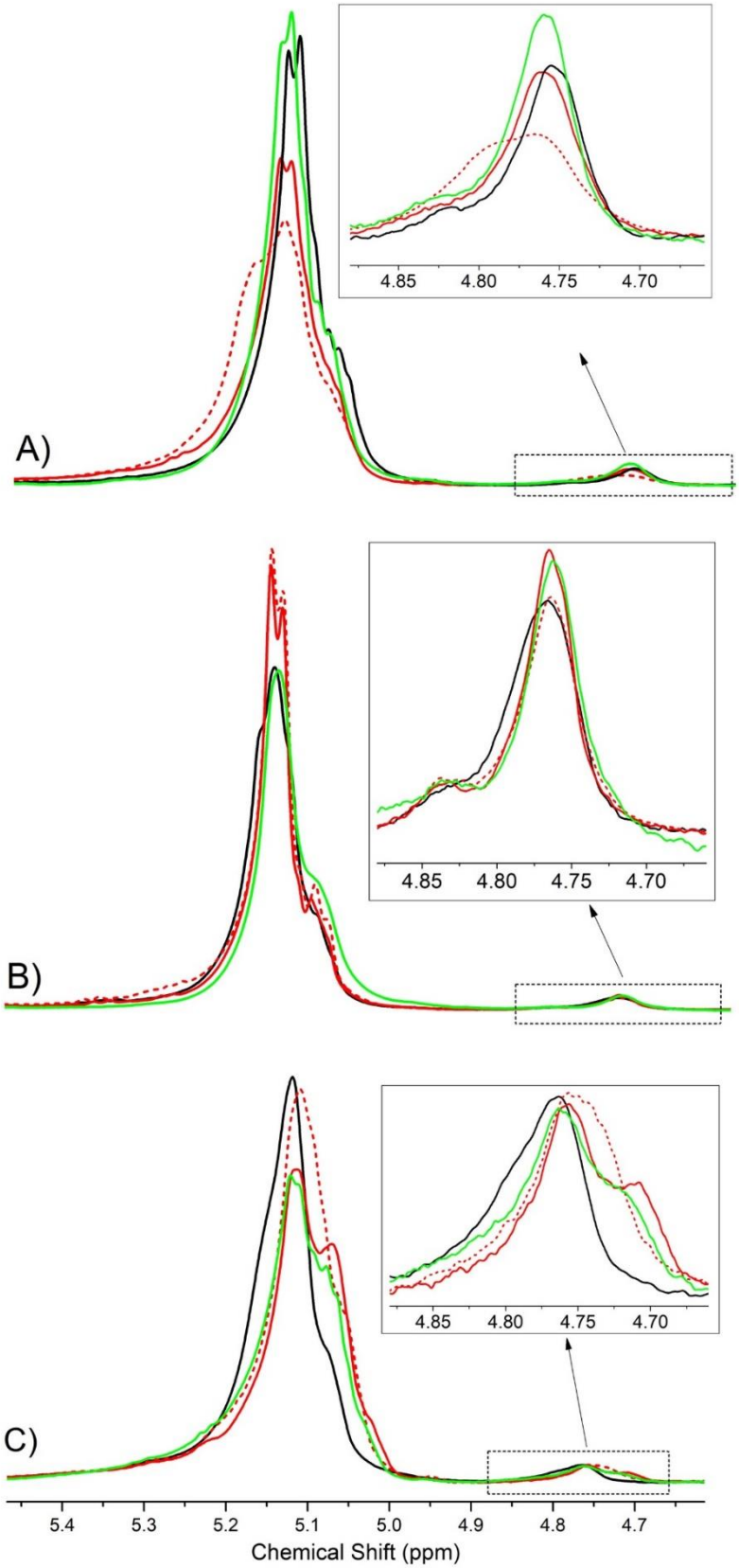

Figure S2 Partial spectra of I-Geo-Tze (a), Doongara (b) and Quest (c) rice samples grown at lower (black) and higher temperatures (red and green). ^{1}H NMR spectroscopy measurement temperatures were 70 °C (dashed line) and 90 °C (solid line).

S2.5 Solvent choice

The solvent was changed from pure D_2O (Gidley, 1985) to DMSO-d_6 with the addition of LiBr for improved sample dissolution (Schmitz et al., 2009). D_2O was also added. The amount of LiBr was tested on waxy maize, with 5 wt% found to give a more consistent average *DB* value regardless of probe temperature (Figure S3). This likely arises from a more stable dissolution.

In terms of absolute value, the average *DB* in waxy maize (3.96 ± 0.1 %) was lower compared to earlier measurements of another waxy maize (4.76 %) (Gidley, 1985).

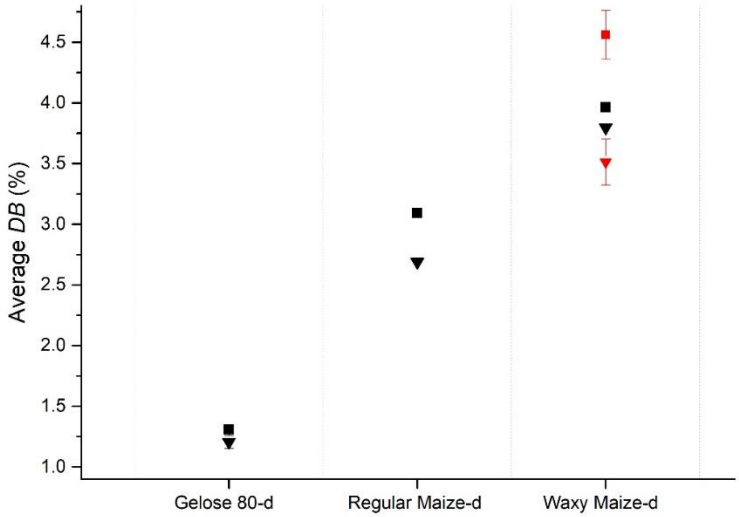

Figure S3 Average degree of branching in standard starch samples, measured at 70 °C (square) and 90 °C (triangle) in 3:1 DMSO-d_6:D_2O with 5 wt% LiBr (black) or 0.05 wt% LiBr (red). Error bars were estimated from the signal-to-noise ratio of the α(1, 6) signal (Castignolles et al., 2009).

S2.6 Repeatability of sample preparation

The error arising from the preparation of samples in the measurement of average *DB* was assessed using 5 repeat preparations of a single rice sample, from a single glass house (Table S1). This was done to minimise the influence of sampling error arising from differences between samples grown in separate glass houses but at the same temperature. The first measurement was found to be significantly higher than later measurements. This has been attributed to the difference in freeze drying protocol, longer time in D_2O and shorter drying time, as well as the uncontrolled timing of measurement in regard to short term aging that was observed later (S1.7). For this reason, the first experiment is considered to be an outlier and is not included in the assessment of repeatability. Given these results, the sample preparation was determined to contribute a relative standard deviation (*RSD*) of 2.6 %.

Table S1 Average *DB* of Doongara rice flour for 5 repeat sample preparations, with freeze drying protocol timing and date of measurement of each preparation. The corresponding partial ^{1}H NMR spectra are shown on Figure S21.

Date	Average *DB (%)*	*SNR* of α(1,6) signal	Shaking time in D_2O (h)	Freeze-drying (h)	Shaking time in D_2O (h)	Freeze-drying (h)
9/04/2019	4.49	61.9	16.75	7	16.75	5.5
30/04/2019	3.79	77.6	6	16	8	65
4/06/2019	3.72	76.8	8.5	19	6.5	17.5
4/06/2019	3.95	78.3	8.5	19	6.5	17.5
4/09/2019	3.87	75.8	8.5	19	6.5	17.5

S2.7 Assessing reliability of average DB through long- and short-term sample aging

The reliability and reproducibility of the *DB* measurement were assessed to determine the robustness. A set of samples were prepared and measured 4 years apart by two different operators, in two separate laboratories due to the relocation of the spectrometer to a new campus, and the average degree of branching calculated from the resulting spectra (Figure S4). The repeated experiments were in good agreement, indicating a high level of reproducibility, as well as a lack of any aging effect on the rice samples in the observed branching structure.

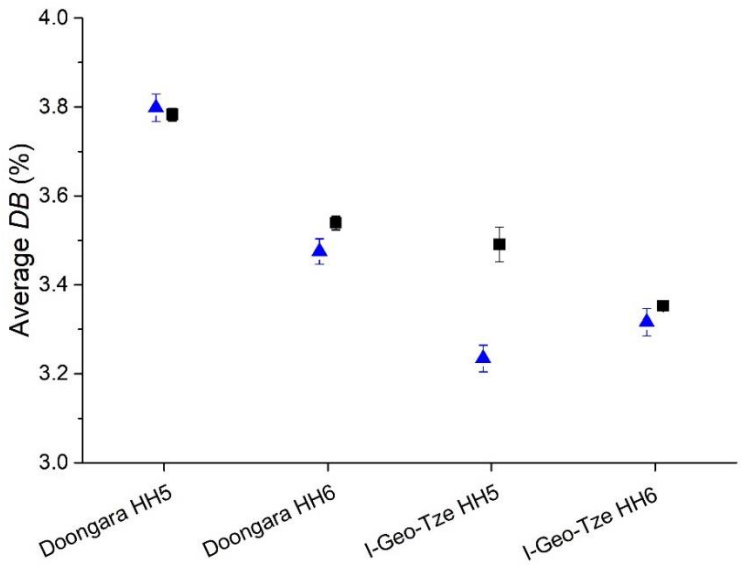

Figure S4 Average degree of branching (%) of rice measured in 2015 (blue triangles) and 2019 (black squares). Error bars were estimated from the signal-to-noise ratio of the α(1, 6) signal (Castignolles et al., 2009). Data points are offset along the x-axis for greater clarity. HHx refers to glasshouse x listed in table S4.

Typically, this type of measurement is only performed on pure or modified starches while, in the current case, rice flours contain lipids and proteins. Thus, the potential for other components to interfere with analysis is an issue. Neither lipids nor proteins yield signals in the same regions as the starch signals used for *DB* quantification; however, other polysaccharides could. Rice flour displayed typical starch signals in the 6.0 to 4.0 ppm range indicating no additional components from other polysaccharides. However, any convoluted signals arising from other polysaccharides would be difficult to isolate and would result in a bias in average *DB* values. Despite this, direct analysis of rice flours is possible for comparative purposes.

S2.8 Example spectrum of rice flour and integration regions for calculation of average DB

Figure S6 shows partial spectra of the signals of interest for the calculation of average *DB*. Figure S6A shows the spectrum with baseline correction for integration of α(1, 4) and α(1, 6) signals while Figure S6B shows the zoomed and baseline corrected spectrum for integration of α and β reducing end signals. The full ^{1}H NMR spectrum is shown in Figure S5 for information.

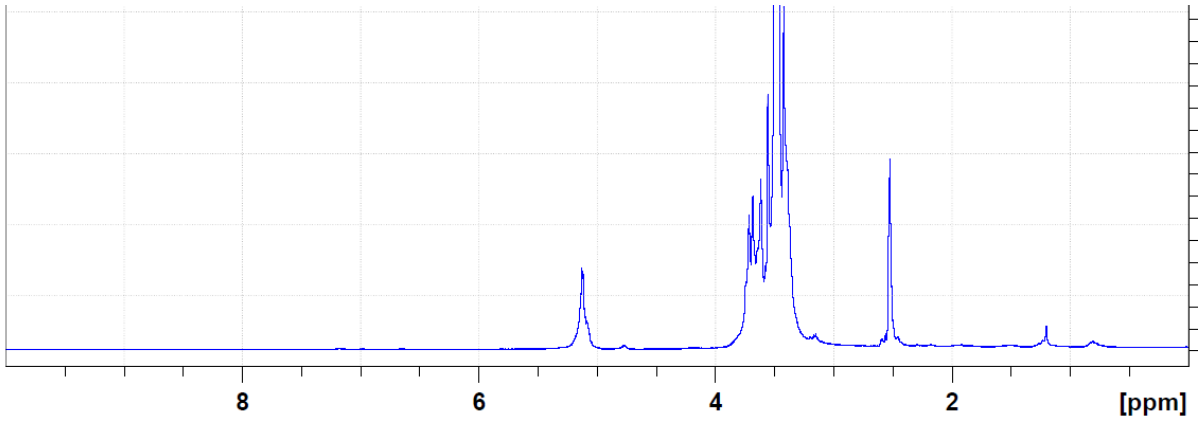

Figure S5 Typical full ^{1}H NMR spectrum obtained for Kyeema rice flour grown at lower temperature (large signals at 2.5 and 3.3 ppm are from residual DMSO-d_5 and residual water, respectively)

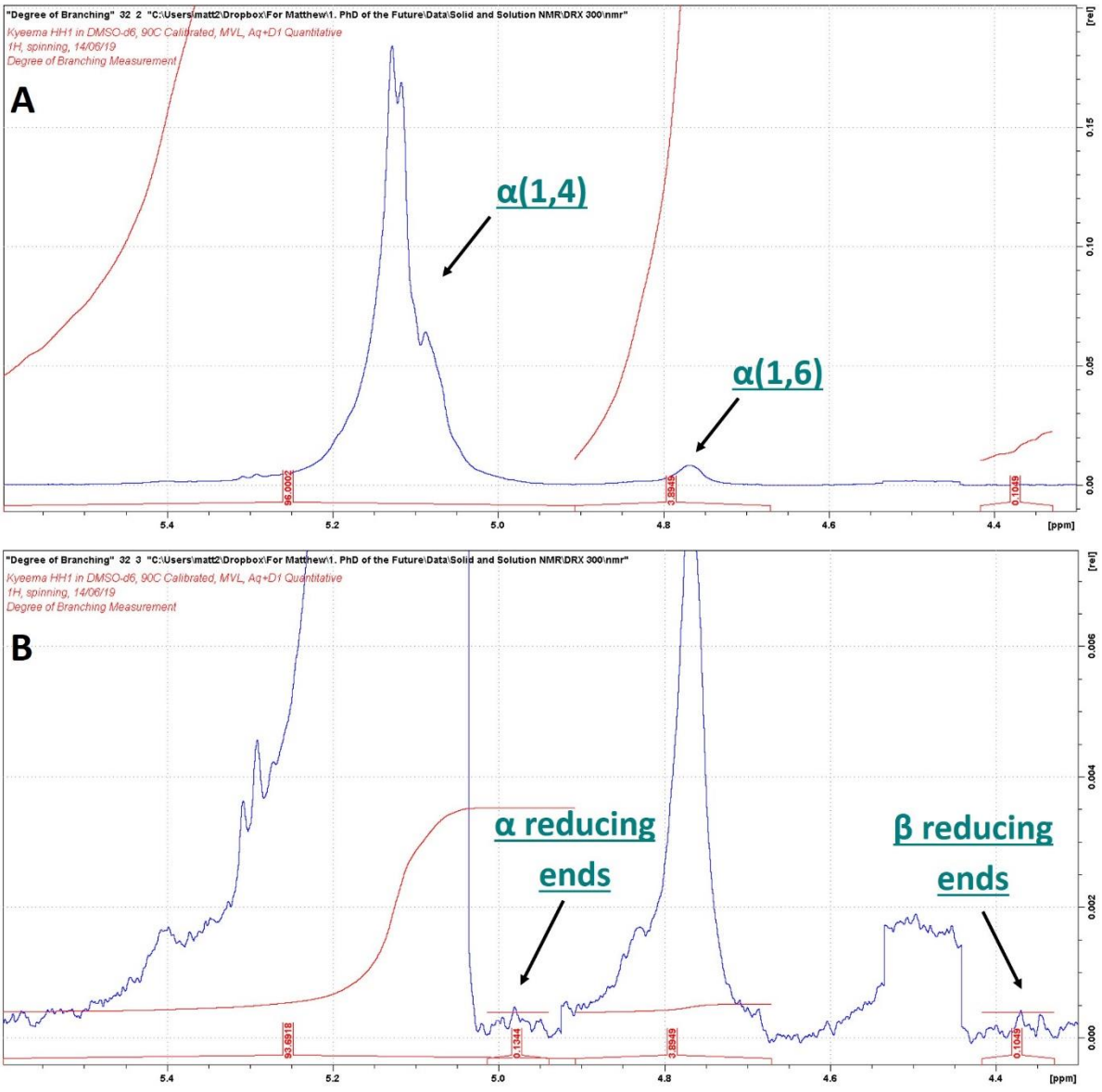

Figure S6 Typical partial ^{1}H NMR spectrum of rice flour with integration regions required for determination of average *DB* annotated with: A) baseline corrected for integration of α(1, 4) and α(1, 6) signals, and B) baseline corrected for integration of α and β reducing end signals

S2.9 Partial ^{1}H NMR spectra for all rice flours measured in this work

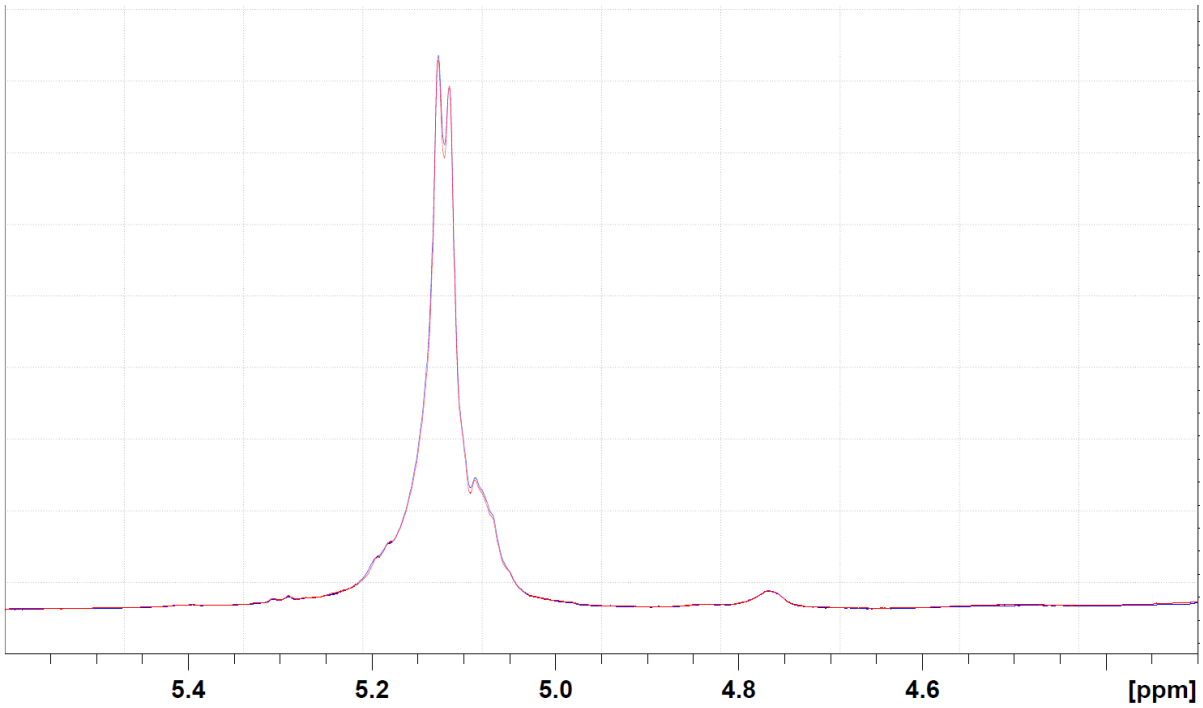

Figure S7 Partial ^{1}H NMR spectra of rice flours of Cocodrie grown at higher temperature. Different spectra correspond to different glasshouses at the same temperature.

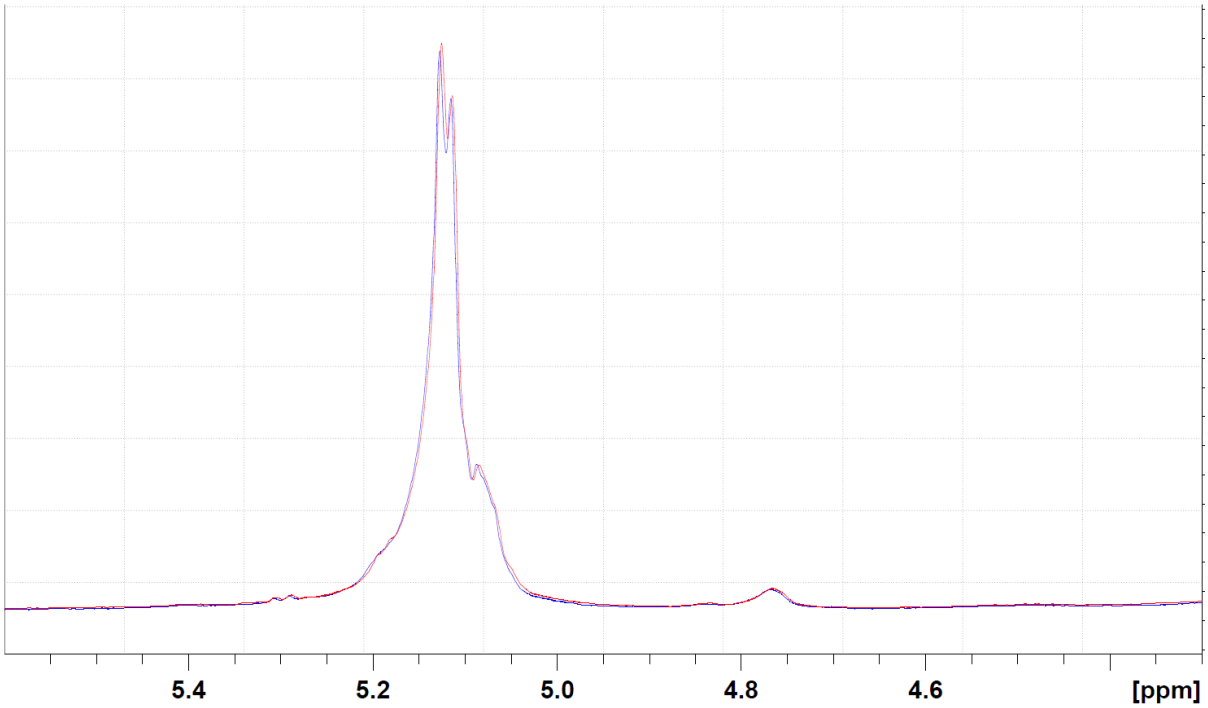

Figure S8 Partial ^{1}H NMR spectra of rice flours of Cocodrie grown at lower temperature. Different spectra correspond to different glasshouses at the same temperature.

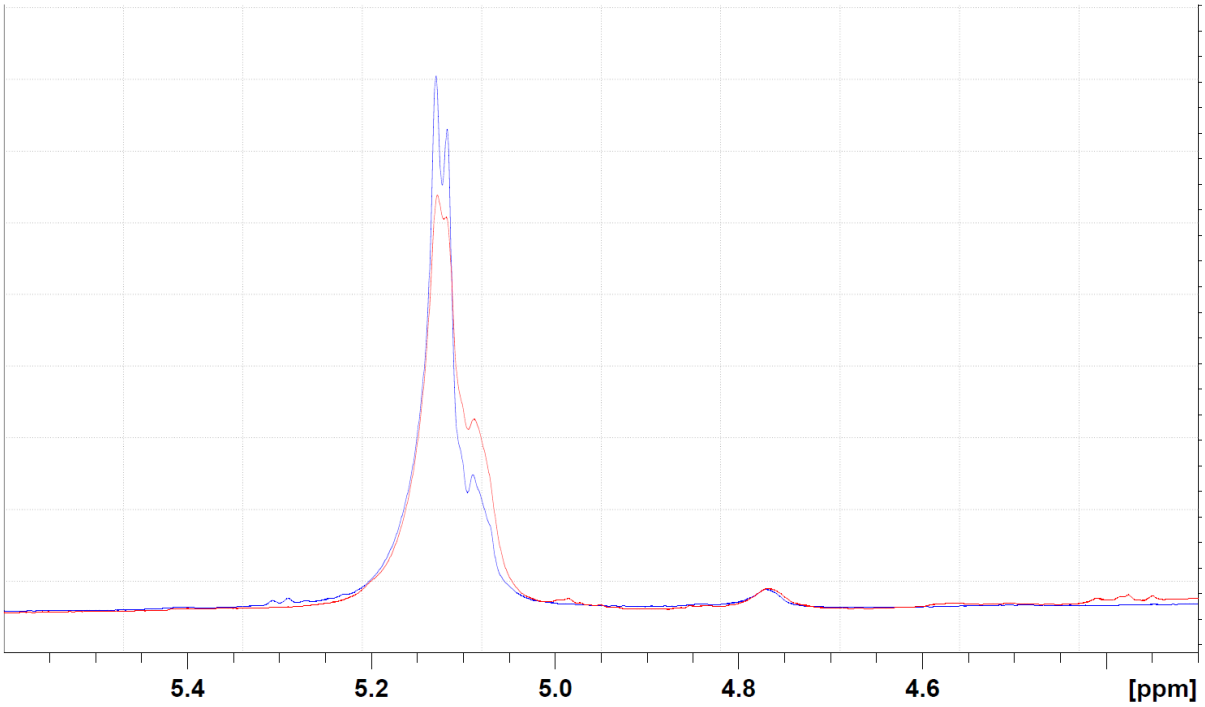

Figure S9 Partial ^{1}H NMR spectra of rice flours of I-Geo-Tze grown at higher temperature. Different spectra correspond to different glasshouses at the same temperature.

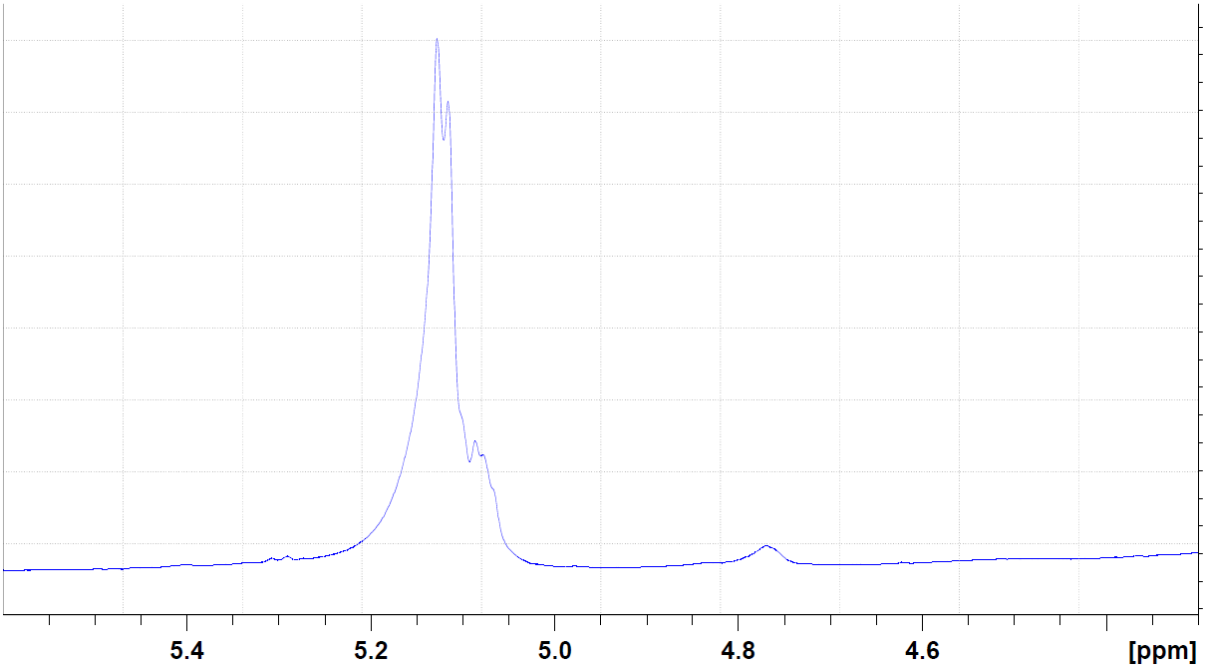

Figure S10 Partial ^{1}H NMR spectrum of rice flours of I-Geo-Tze grown at lower temperature.

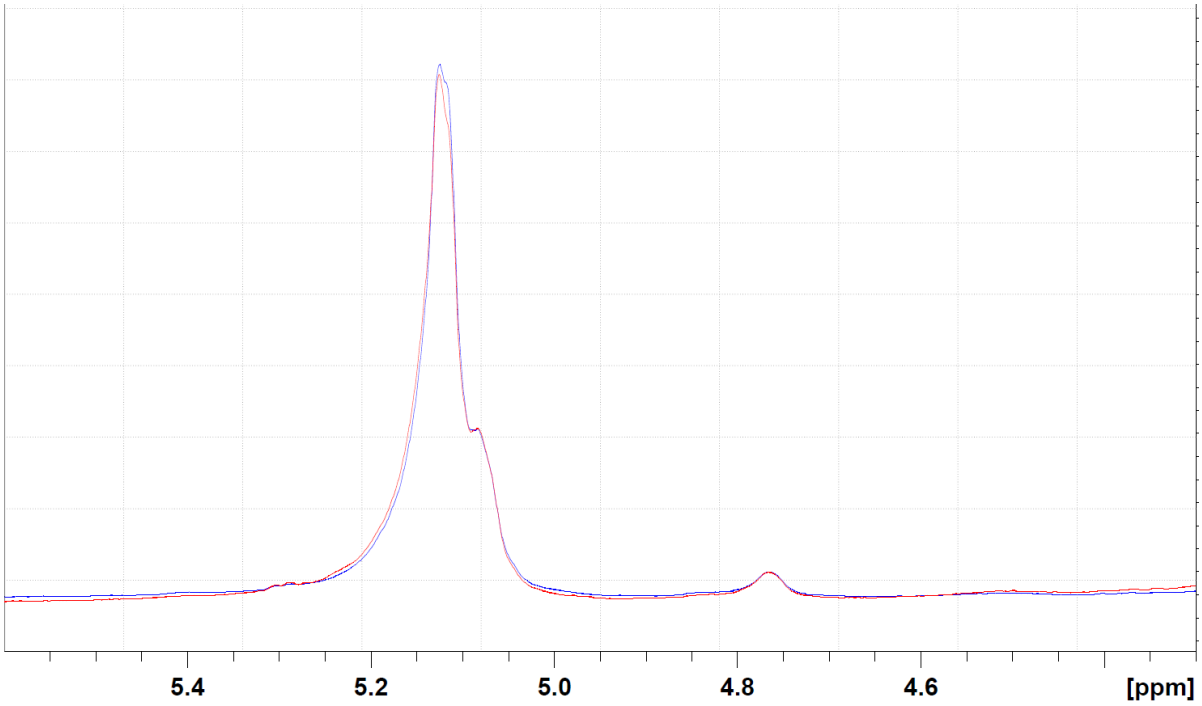

Figure S11 Partial ^{1}H NMR spectra of rice flours of IR64 grown at higher temperature. Different spectra correspond to different glasshouses at the same temperature.

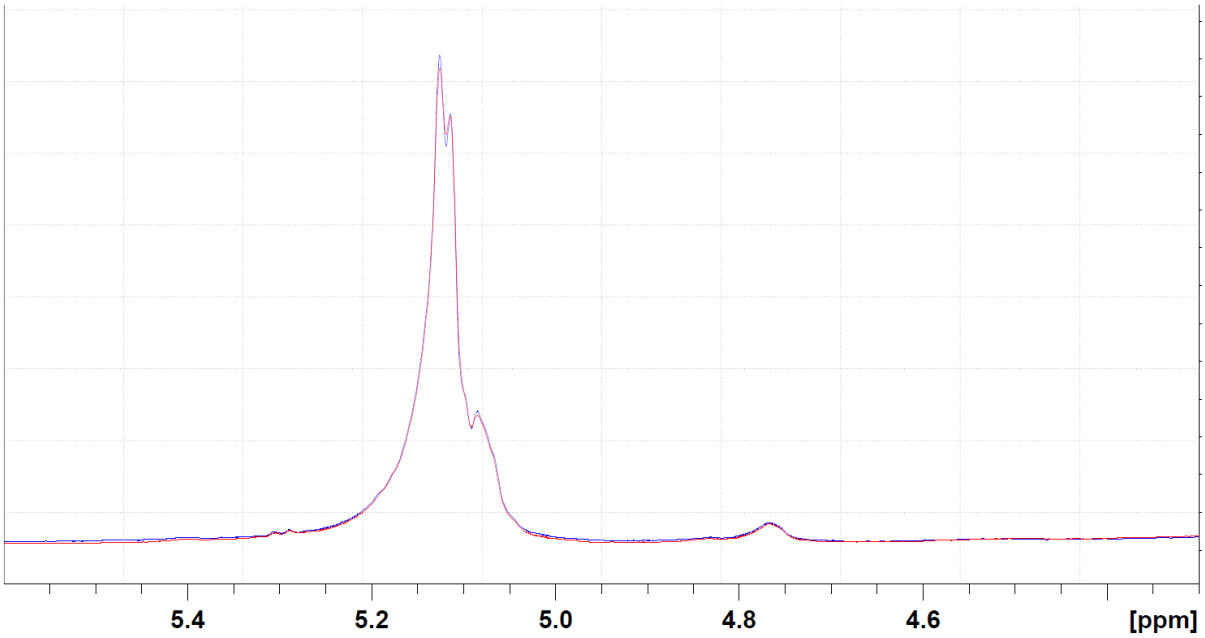

Figure S12 Partial ^{1}H NMR spectra of rice flours of IR64 grown at lower temperature. Different spectra correspond to different glasshouses at the same temperature.

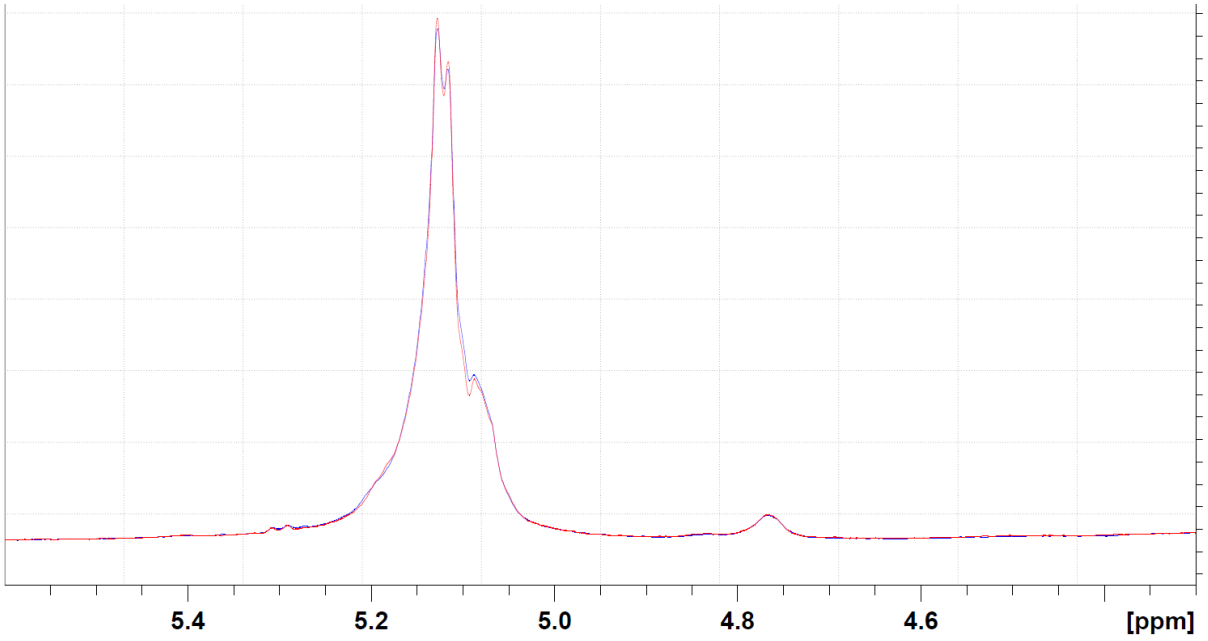

Figure S13 Partial ^{1}H NMR spectra of rice flours of IR55419-04 grown at higher temperature. Different spectra correspond to different glasshouses at the same temperature.

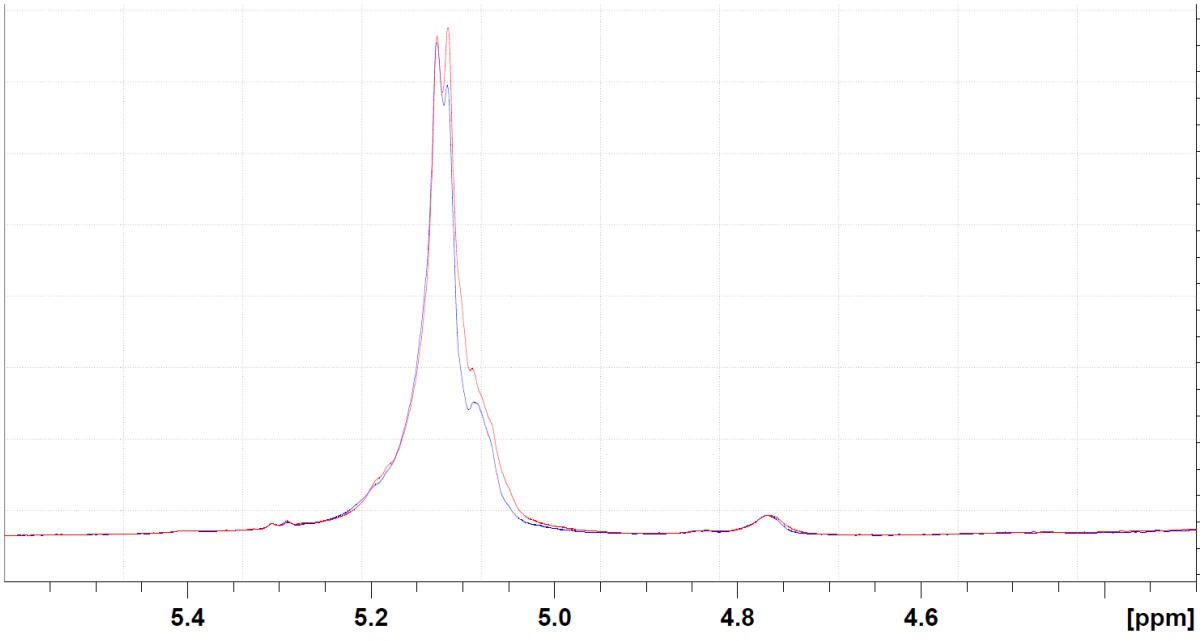

Figure S14 Partial ^{1}H NMR spectra of rice flours of IR55419-04 grown at lower temperature. Different spectra correspond to different glasshouses at the same temperature.

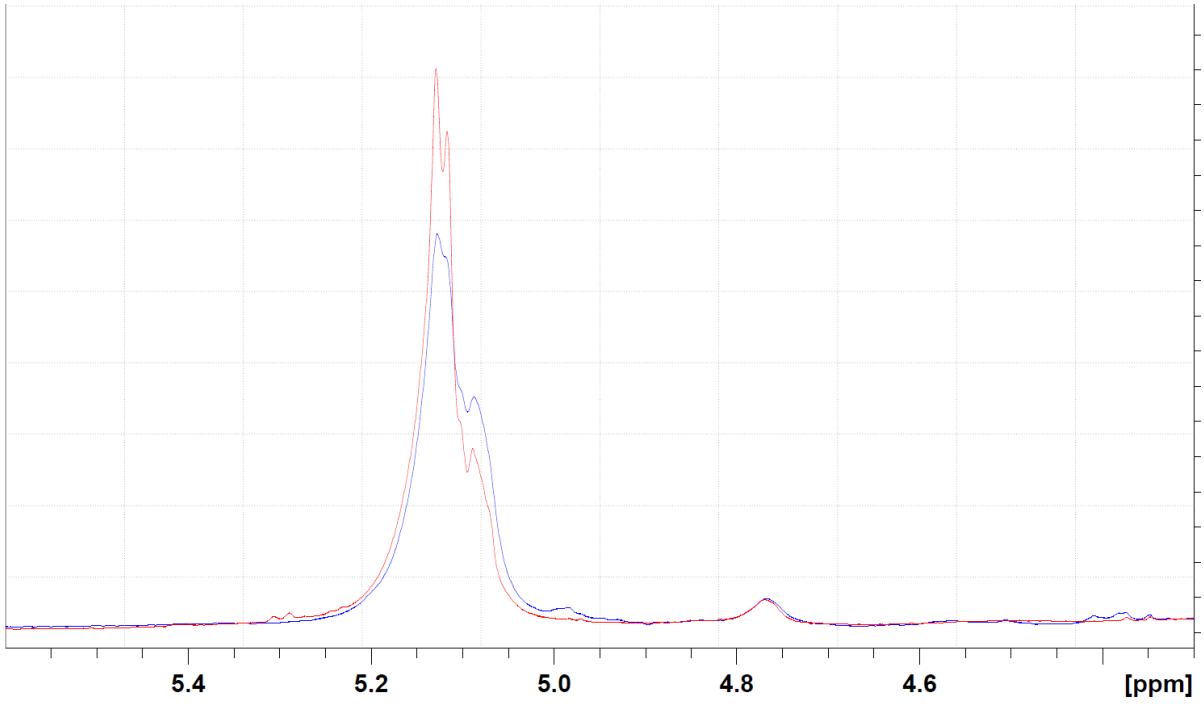

Figure S15 Partial ^{1}H NMR spectra of rice flours of Doongara grown at higher temperature. Different spectra correspond to different glasshouses at the same temperature.

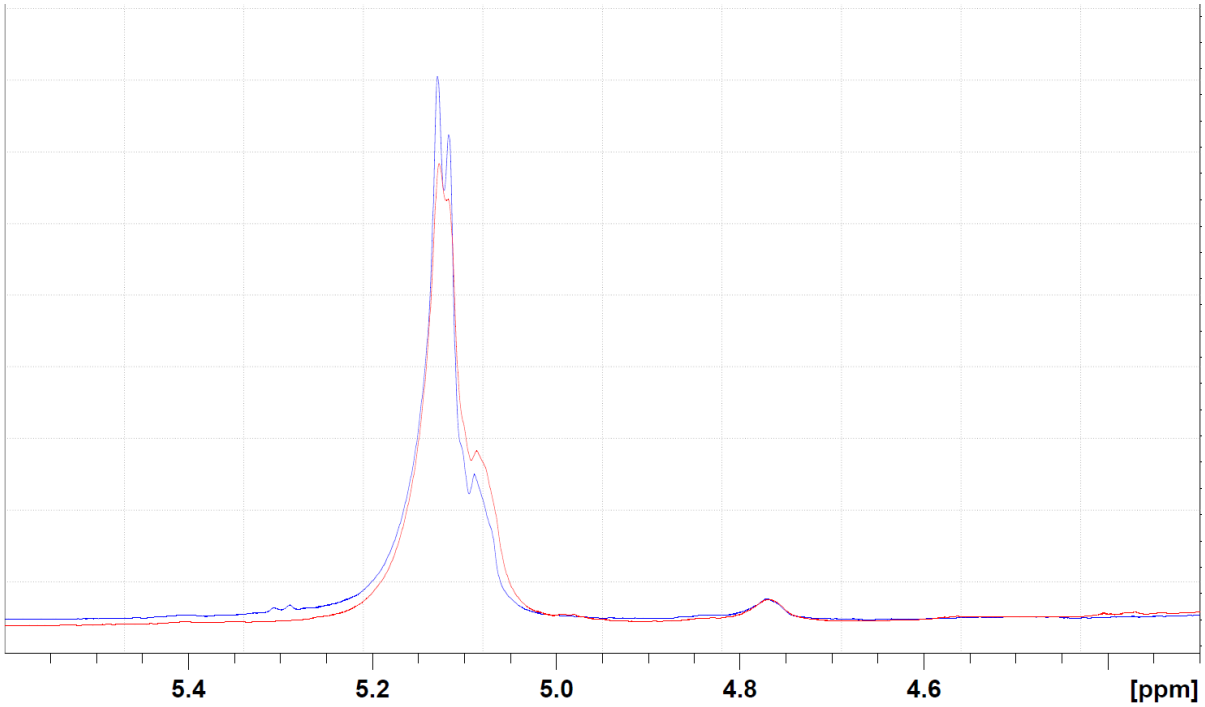

Figure S16 Partial ^{1}H NMR spectra of rice flours of Doongara grown at lower temperature. Different spectra correspond to different glasshouses at the same temperature.

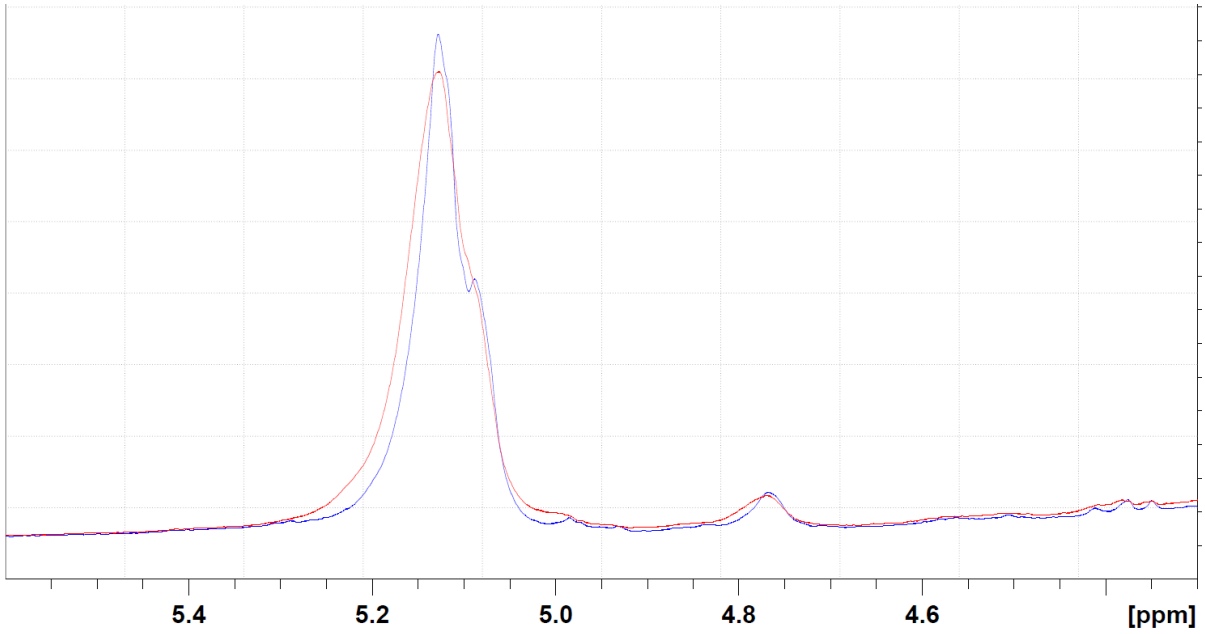

Figure S17 Partial ^{1}H NMR spectra of rice flours of Quest grown at higher temperature. Different spectra correspond to different glasshouses at the same temperature.

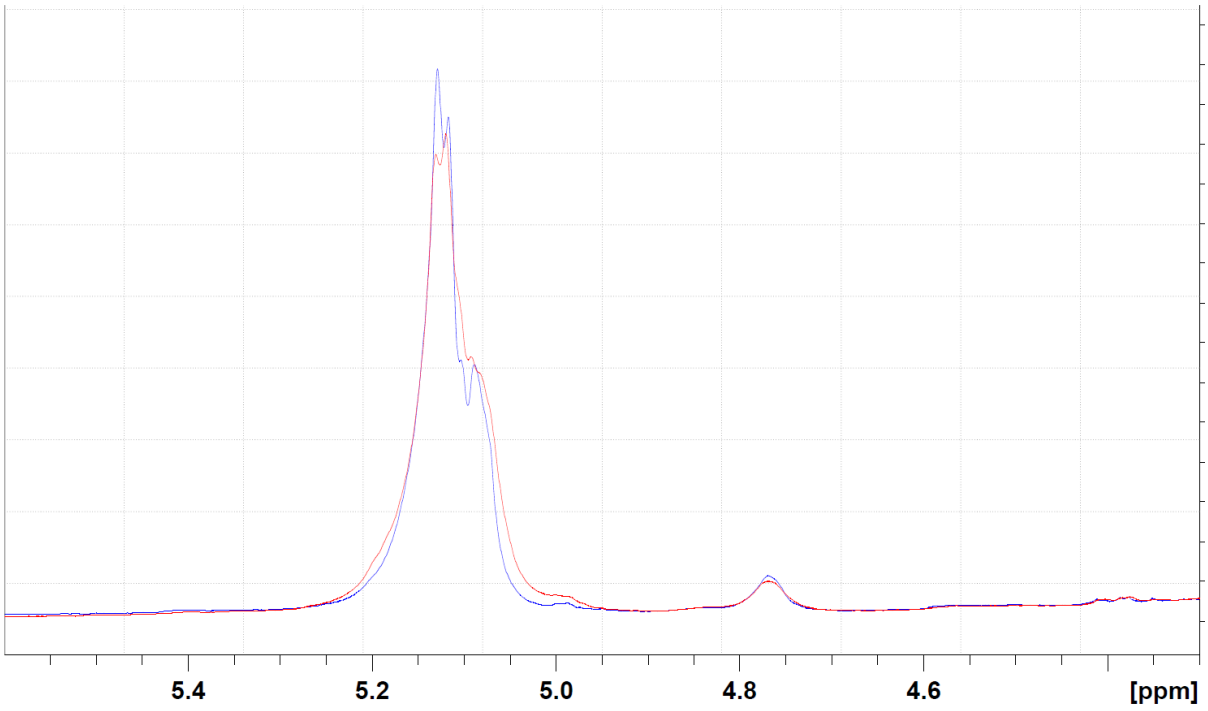

Figure S18 Partial ^{1}H NMR spectra of rice flours of Quest grown at lower temperature. Different spectra correspond to different glasshouses at the same temperature.

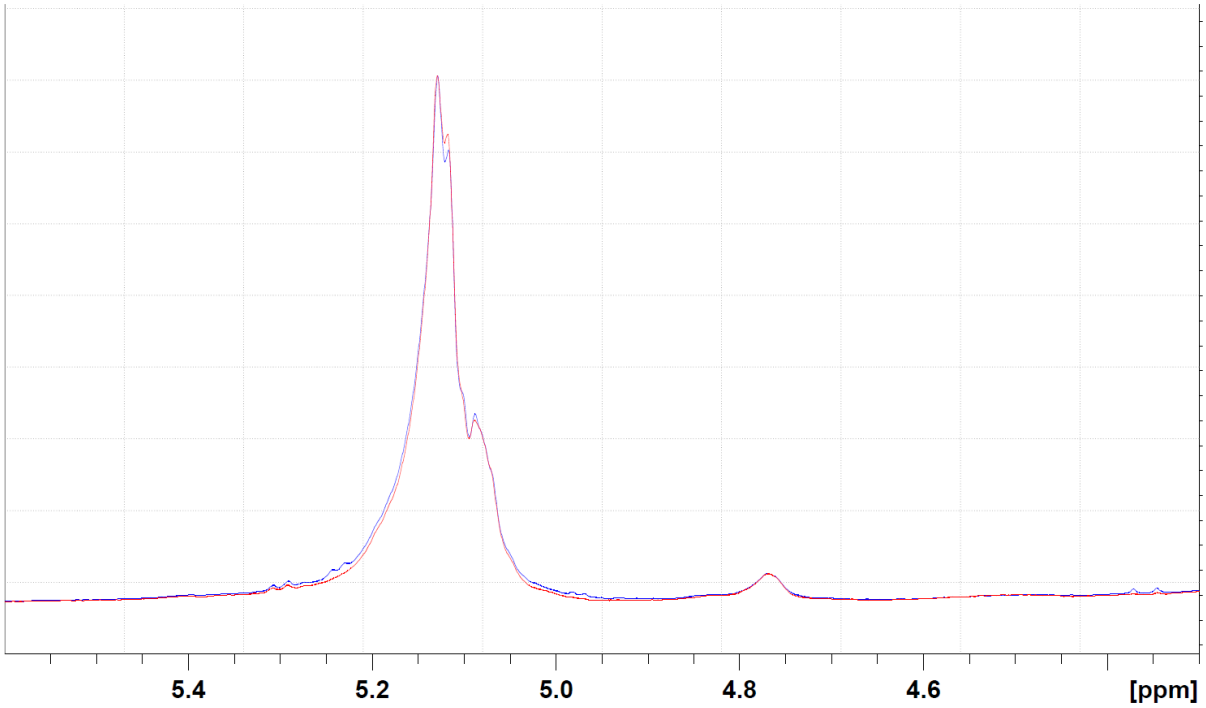

Figure S19 Partial ^{1}H NMR spectra of rice flours of Kyeema grown at higher temperature. Different spectra correspond to different glasshouses at the same temperature.

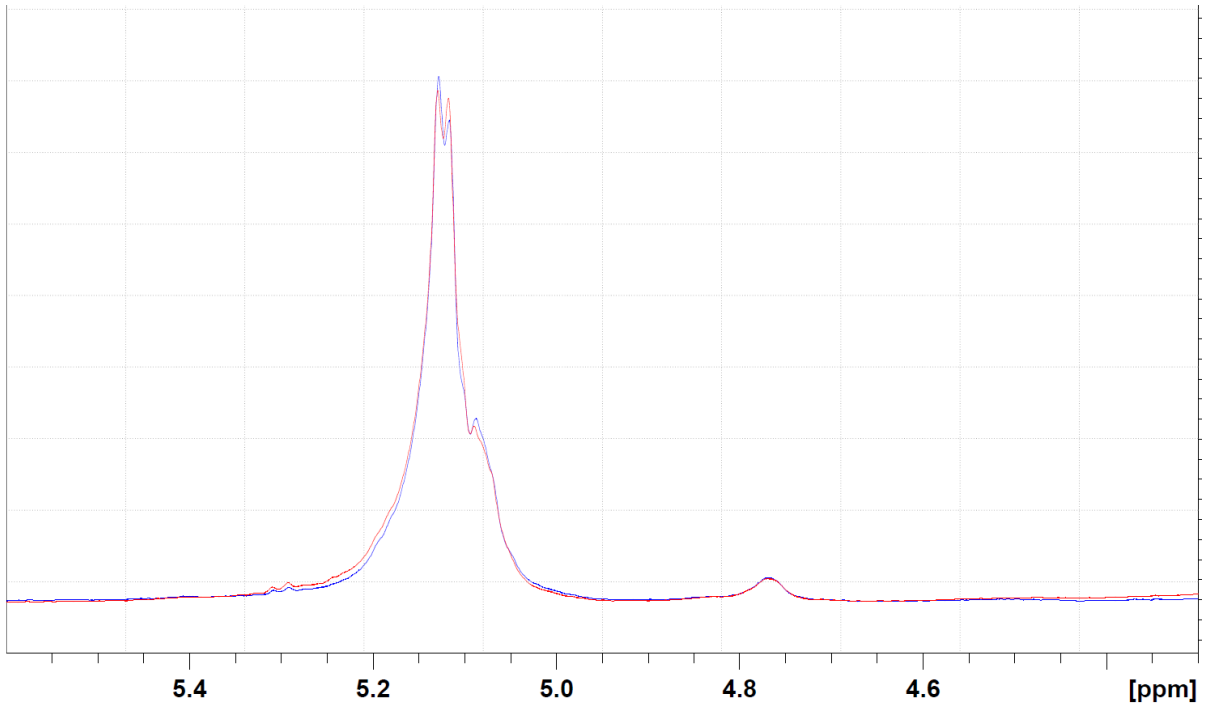

Figure S20 Partial ^{1}H NMR spectra of rice flours of Kyeema grown at lower temperature. Different spectra correspond to different glasshouses at the same temperature.

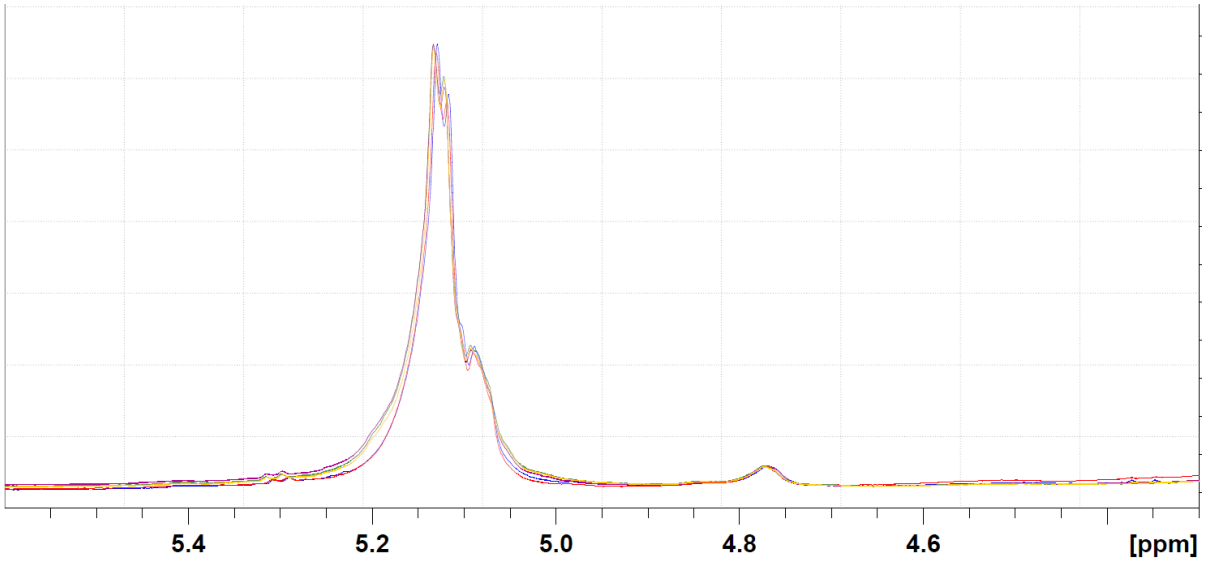

Figure S21 Partial ^{1}H NMR spectra of rice flours of Doongara grown at higher temperature. Different spectra correspond to repeat experiments on different parts of the same sample.

S2.10 Assessing short-term aging contribution of reducing ends

The average *DB* was also monitored over a 24 h period after addition of D_2O and initial measurement (Figure S22A). An immediate increase in the average *DB* was observed after the first hour, subsequently plateauing at ~0.3 % above the initial measurement. Further analysis of the α and β reducing ends revealed a proportional increase with time (Figure S22B). This indicates that the average *DB* increase is likely not a result of chain aggregation, but rather of some degradation process. All data indicate that for measurements taken immediately after addition of D_2O, as done here, the effects of degradation are insignificant.

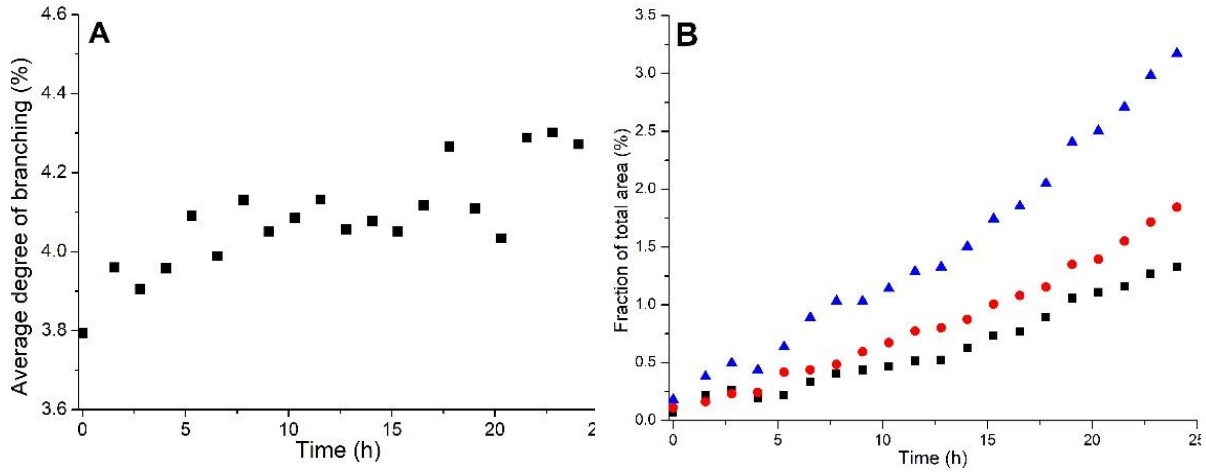

Figure S22 Evolution with time spent in the spectrometer at 90 °C after D_2O addition of a) average *DB* (%) and b) percentage contribution to the total starch signal of α reducing ends (red circles), β reducing ends (black squares) and both α and β reducing ends (blue triangles).

S2.11 Values of average DB for waxy flours

Table S2 Values of average *DB* for waxy rice flours. Individual NMR measurements of the hot-water insoluble fraction (HWI) and hot-water soluble fraction (HWS) are reported; HWx-1 and HWx-2 refer to repeat fractionation of the flour. n.d. refers to 'not determined'.

Variety	*Average DB (%), HWI-1*	*Average DB (%), HWI-2*	*Average DB (%), HWS-1*	*Average DB (%), HWS-2*
Phae Savan	4.80	4.93	4.75	5.10
Laboun	4.61	4.35	5.20	5.03, 4.98, 5.07, 4.98, 4.95
Med Gnay	4.40	4.42	n.d.	5.00
Makfay	4.59	4.44, 4.54, 4.52, 4.35, 4.52	4.83 (for mixed sample of HWS-1+HWS-2)	
Hom	4.42	4.43	n.d.	4.92, 4.94

Table S3 Values of average *DB* by ^{1}H NMR for different types of waxy starch samples

Type of waxy starch	*Average DB (%)*
Waxy maize starch	5.00 (Gidley, 1985), 3.80 (Elfstrand et al., 2004), 5.26 (Dunn & Krueger, 1999)
Potato amylopectin	4.35 (Gidley, 1985), 3.6 (McIntyre et al., 1990), 4.07 (Nilsson et al., 1996)
Tapioca amylopectin	5.71 (Gidley, 1985)
Corn amylopectin	4.77 (Nilsson et al., 1996)

S3 Apparent amylose content by iodine binding – Consistency over time

The *AAC* of the samples in this work was originally measured in 2015 in the conditions cited in the methods section 2.2.1. To confirm samples had not aged at the molecular level, the *AAC* was remeasured 3 years later on 3 varieties, including four glasshouses each. Due to changes in instrument, methodology and operators, the 2018 measurements also give an indication of the reproducibility of the *AAC*. The original values (2015) and remeasured values (2018) are shown in Table S4. One apparent outlier was the I-Geo-Tze variety in glasshouse 5, with a 19.1 % relative difference in *AAC*, the remaining samples had an average relative difference of 6.8 %.

Table S4 *AAC* for different varieties grown in difference glasshouses initially measured in 2015 then remeasured in 2018

Variety	Glasshouse	*AAC* (%) (2015)	*AAC* (%) (2018)	Relative difference (%)
Kyeema	Glasshouse 1 - Low Temp	19.63	20.61	4.9
Doongara	Glasshouse 1 - Low Temp	25.39	27.53	8.1
I-Geo-Tze	Glasshouse 1 - Low Temp	27.48	29.36	6.6
Kyeema	Glasshouse 3 - High Temp	14.58	15.70	7.4
Doongara	Glasshouse 3 - High Temp	16.76	17.79	6.0
I-Geo-Tze	Glasshouse 3 - High Temp	28.27	29.60	4.6
Kyeema	Glasshouse 5 - High Temp	14.89	15.92	6.7
Doongara	Glasshouse 5 - High Temp	18.64	19.87	6.4
I-Geo-Tze	Glasshouse 5 - High Temp	26.72	32.38	19.1
Kyeema	Glasshouse 6 - Low Temp	19.22	20.37	5.8
Doongara	Glasshouse 6 - Low Temp	24.38	26.31	7.6
I-Geo-Tze	Glasshouse 6 - Low Temp	26.01	28.96	10.7

S4 Characterisation of lamellar structure by small angle X-ray scattering

S4.1 SAXS curves for all samples measured in this work

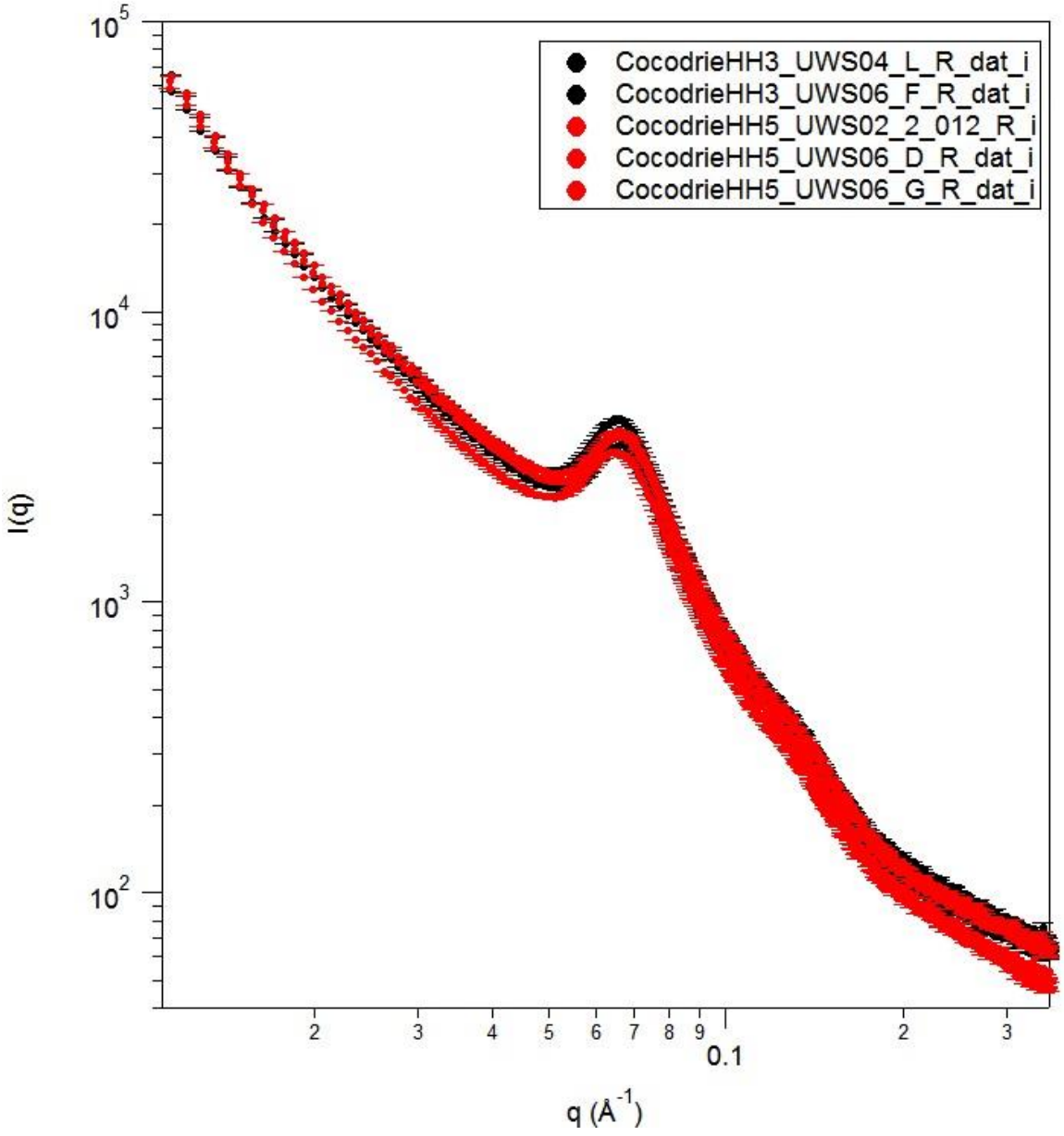

Figure S23 Small angle X-ray scattering curves of rice flours of Cocodrie grown at higher temperature. Red and black curves correspond to different glasshouses at the same temperature. Separate curves of same colour correspond to repeat experiments on different parts of the same sample.

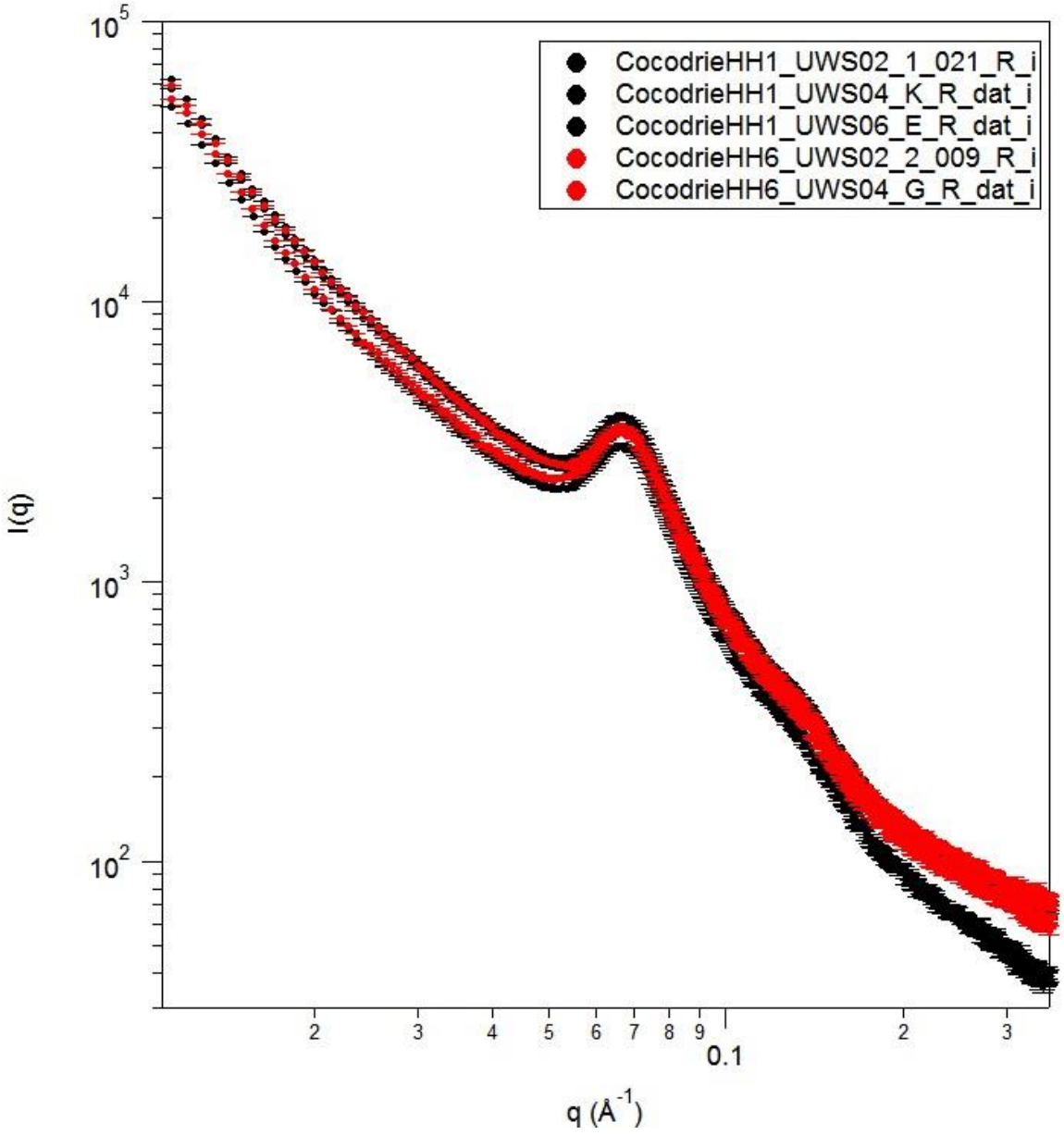

Figure S24 Small angle X-ray scattering curves of rice flours of Cocodrie grown at lower temperature. Red and black curves correspond to different glasshouses at the same temperature. Separate curves of same colour correspond to repeat experiments on different parts of the same sample.

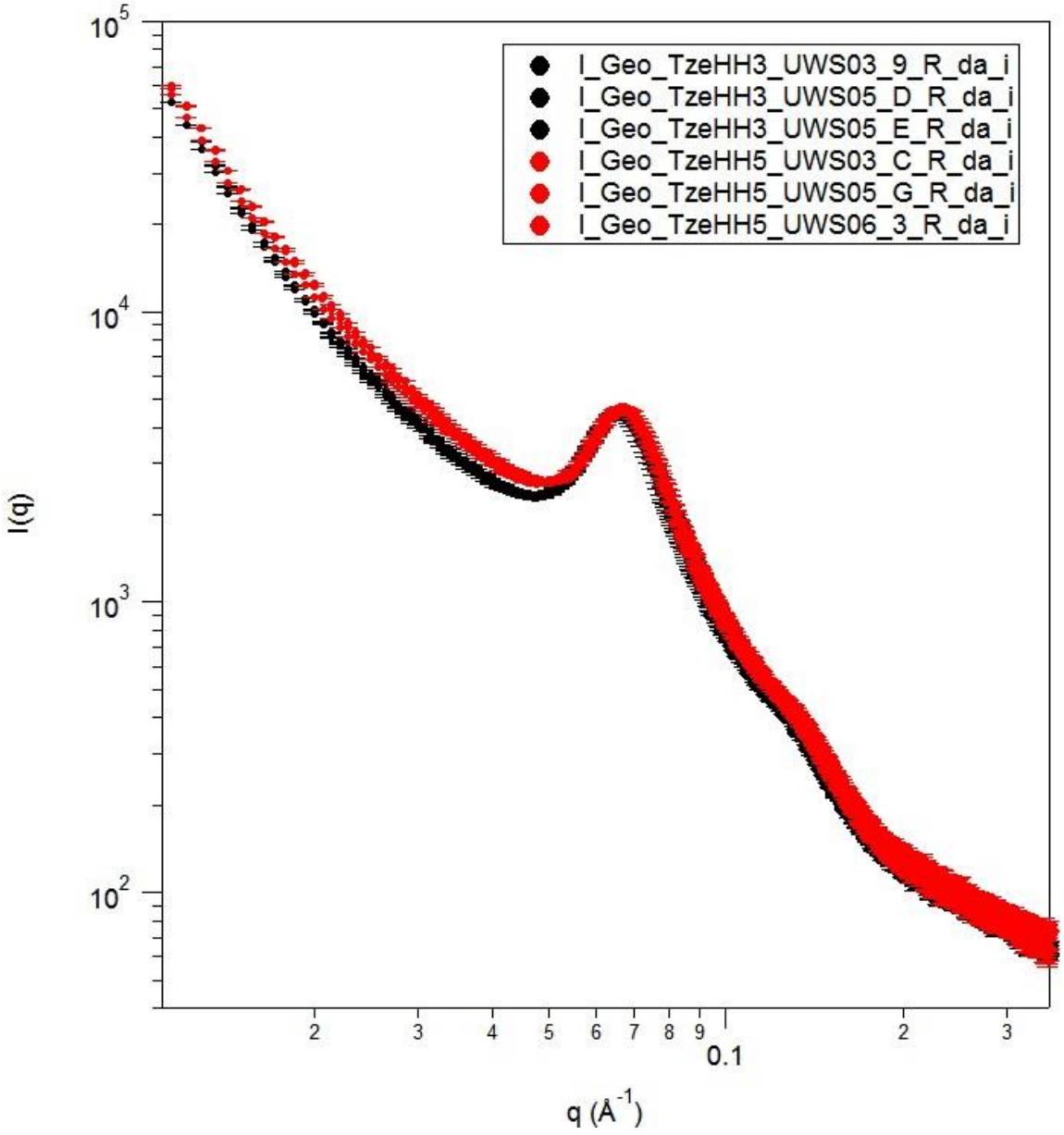

Figure S25 Small angle X-ray scattering curves of rice flours of I-Geo-Tze grown at higher temperature. Red and black curves correspond to different glasshouses at the same temperature. Separate curves of same colour correspond to repeat experiments on different parts of the same sample.

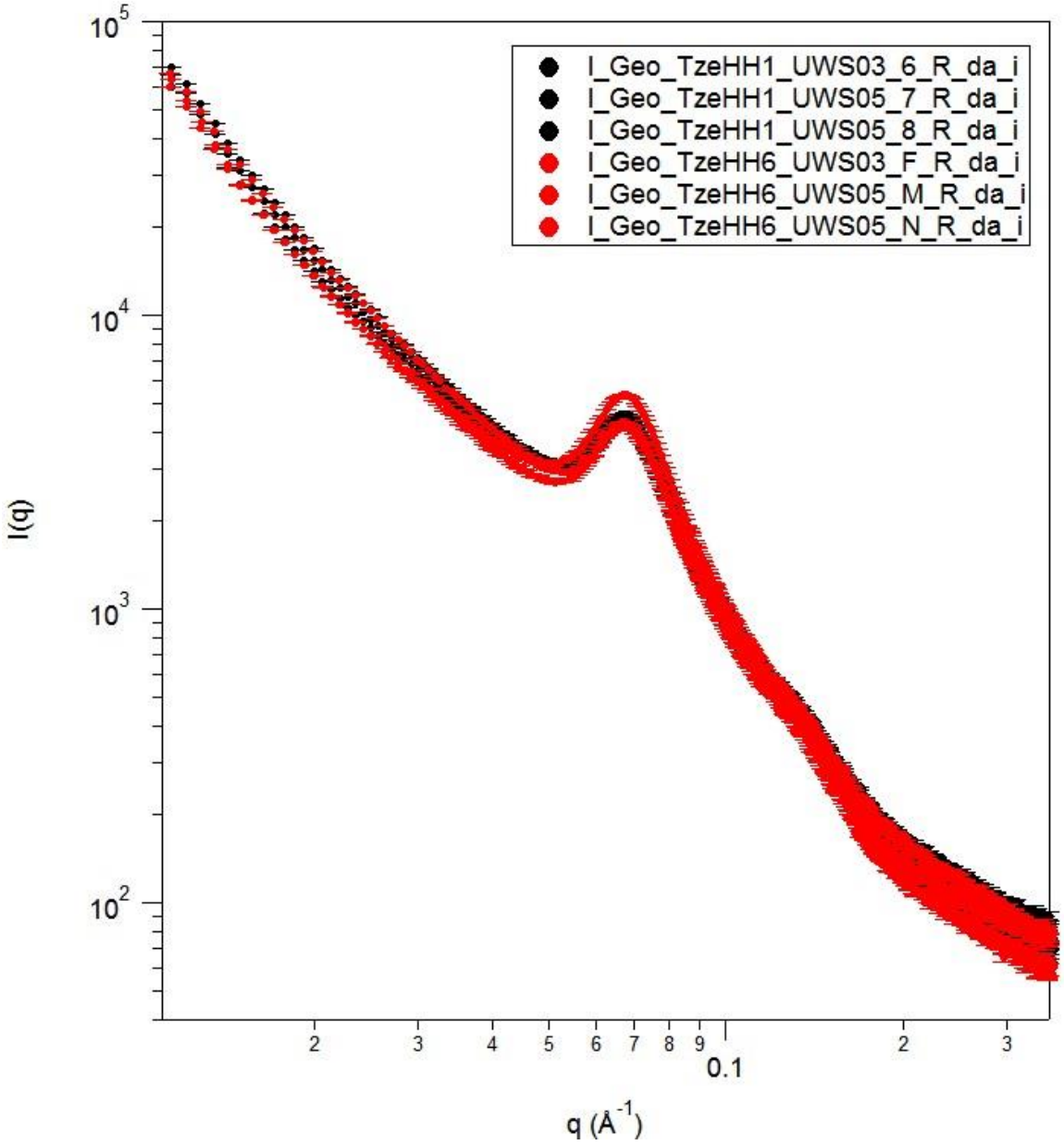

Figure S26 Small angle X-ray scattering curves of rice flours of I-Geo-Tze grown at lower temperature. Red and black curves correspond to different glasshouses at the same temperature. Separate curves of same colour correspond to repeat experiments on different parts of the same sample.

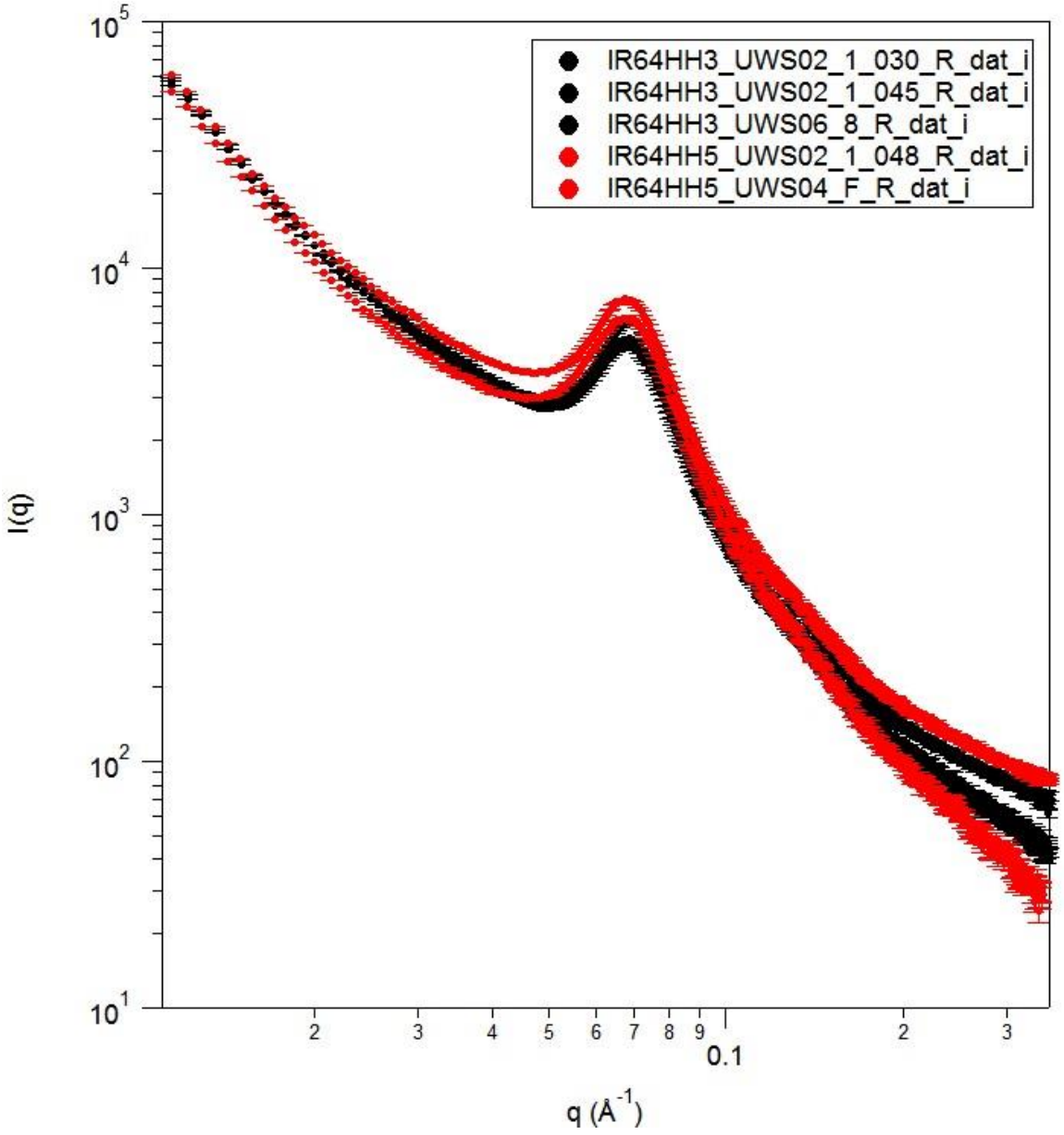

Figure S27 Small angle X-ray scattering curves of rice flours of IR64 grown at higher temperature. Red and black curves correspond to different glasshouses at the same temperature. Separate curves of same colour correspond to repeat experiments on different parts of the same sample.

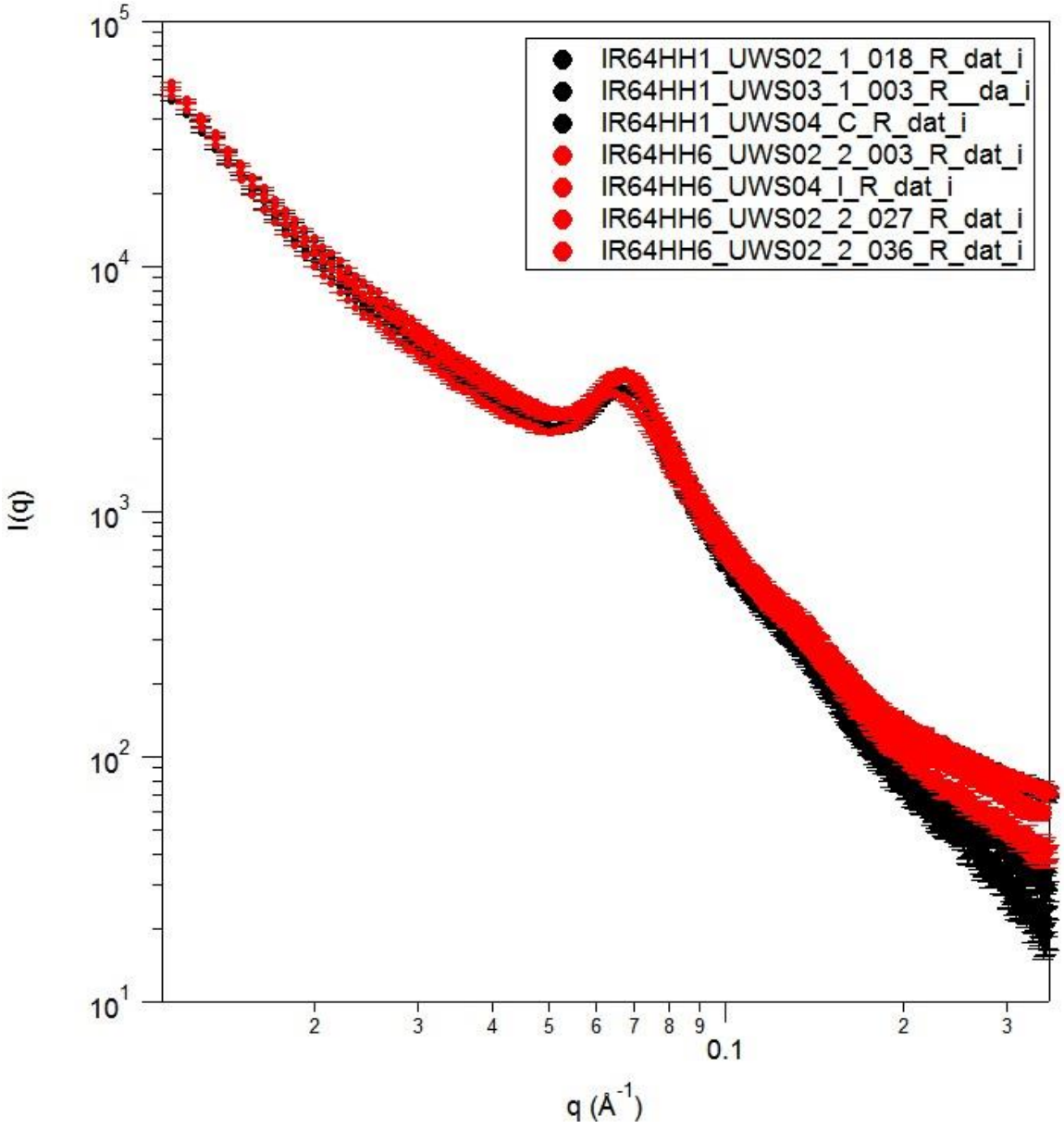

Figure S28 Small angle X-ray scattering curves of rice flours of IR64 grown at lower temperature. Red and black curves correspond to different glasshouses at the same temperature. Separate curves of same colour correspond to repeat experiments on different parts of the same sample.

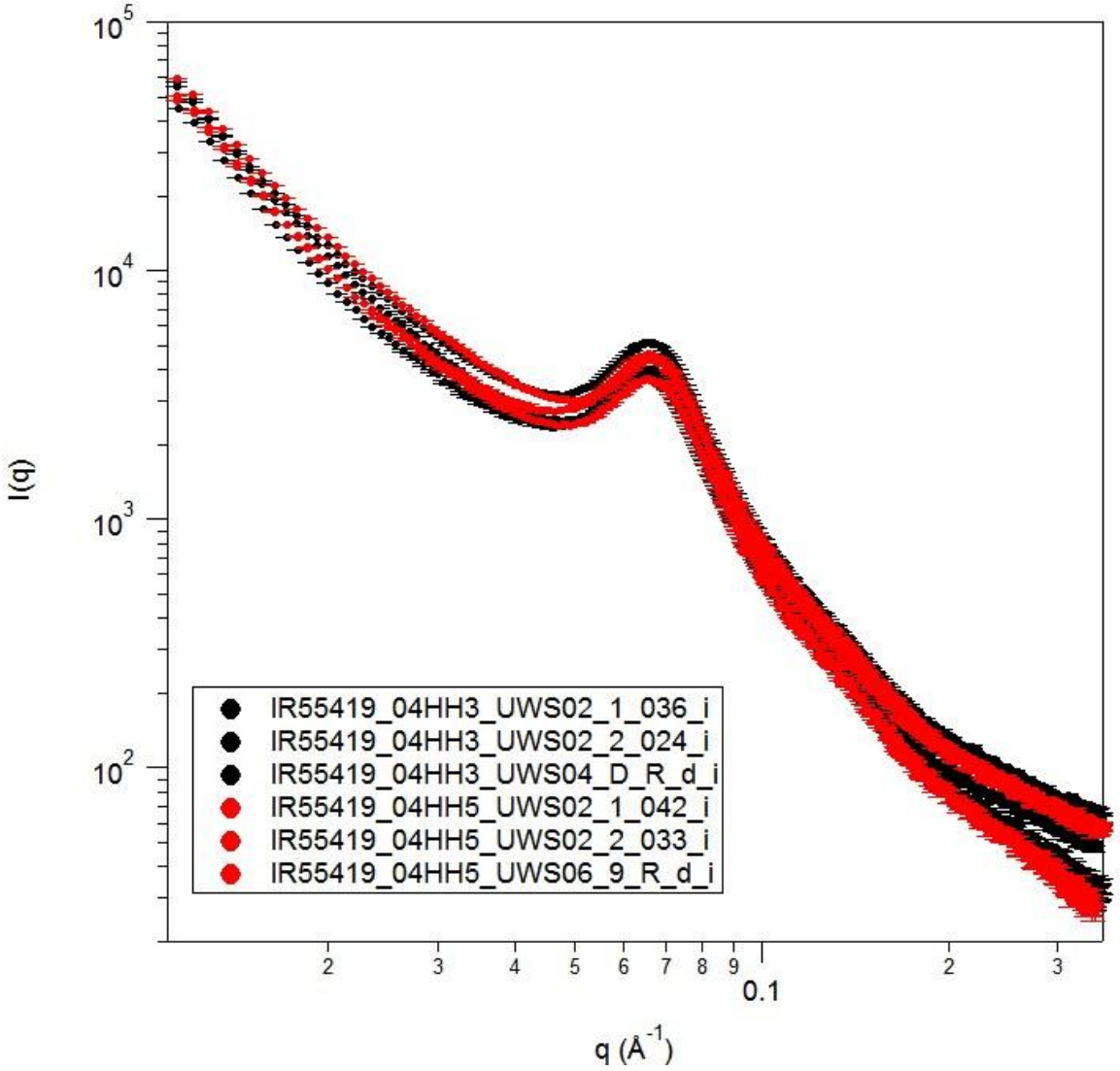

Figure S29 Small angle X-ray scattering curves of rice flours of IR55419-04 grown at higher temperature. Red and black curves correspond to different glasshouses at the same temperature. Separate curves of same colour correspond to repeat experiments on different parts of the same sample.

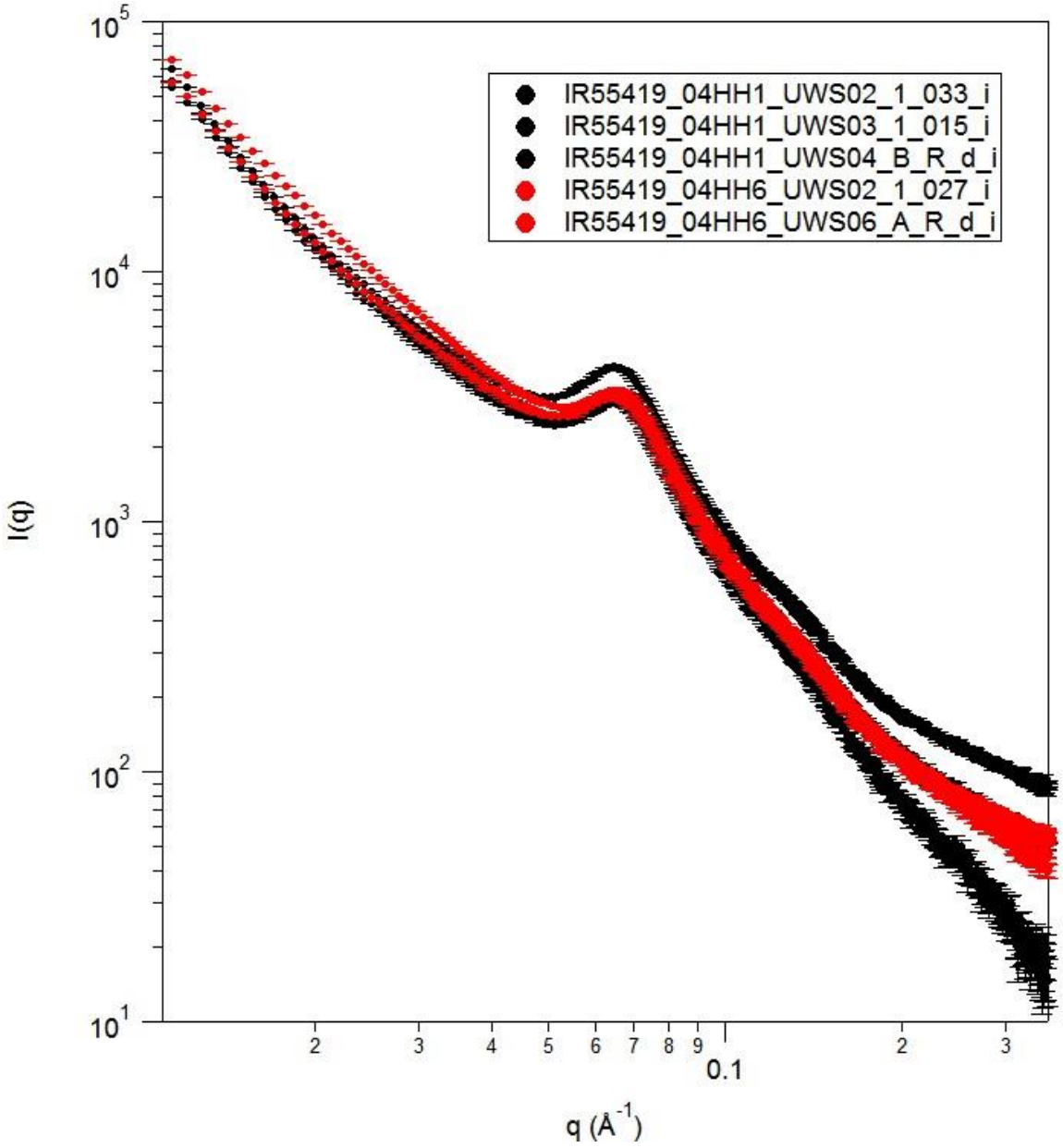

Figure S30 Small angle X-ray scattering curves of rice flours of IR55419-04 grown at lower temperature. Red and black curves correspond to different glasshouses at the same temperature. Separate curves of same colour correspond to repeat experiments on different parts of the same sample.

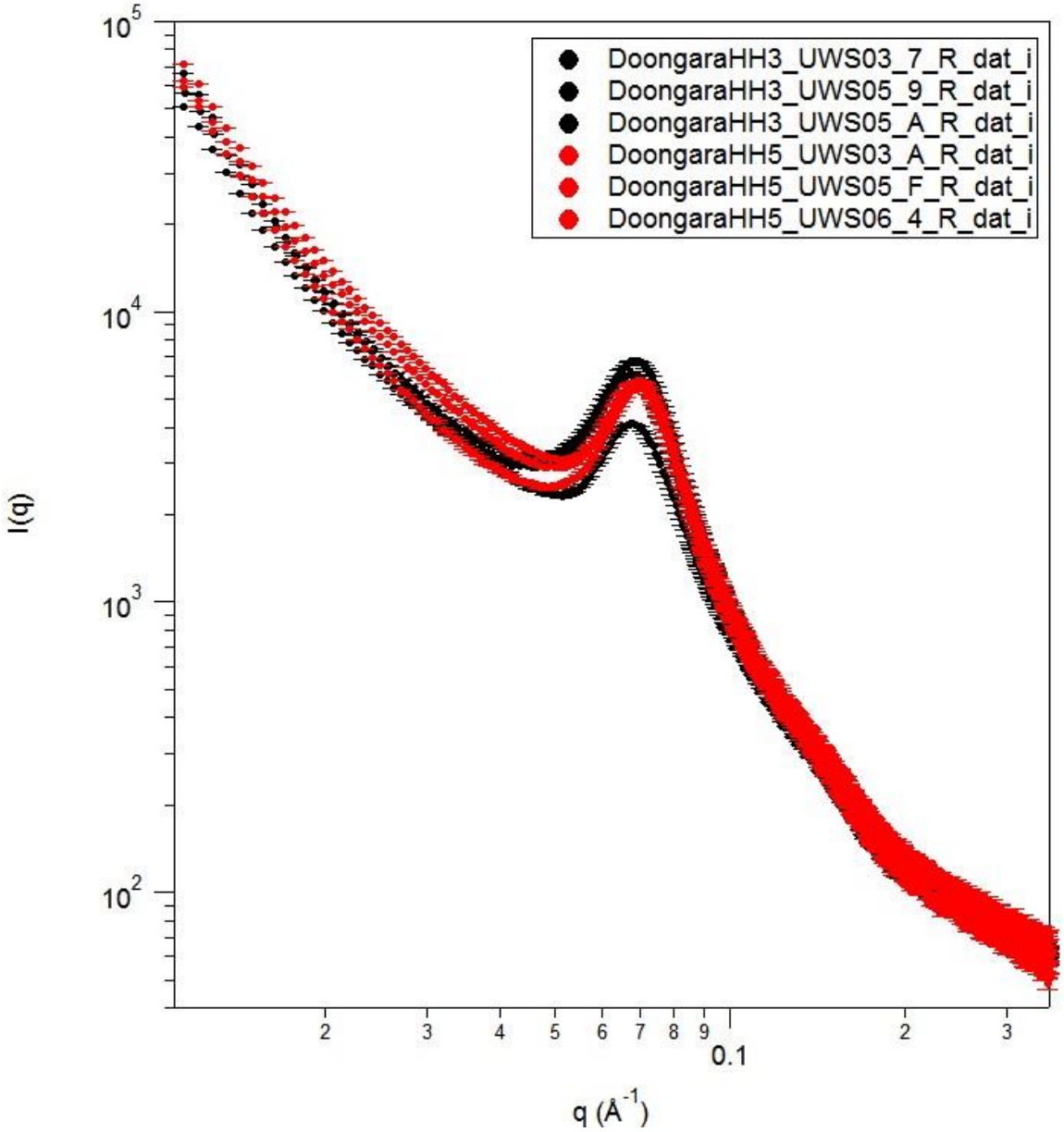

Figure S31 Small angle X-ray scattering curves of rice flours of Doongara grown at higher temperature. Red and black curves correspond to different glasshouses at the same temperature. Separate curves of same colour correspond to repeat experiments on different parts of the same sample.

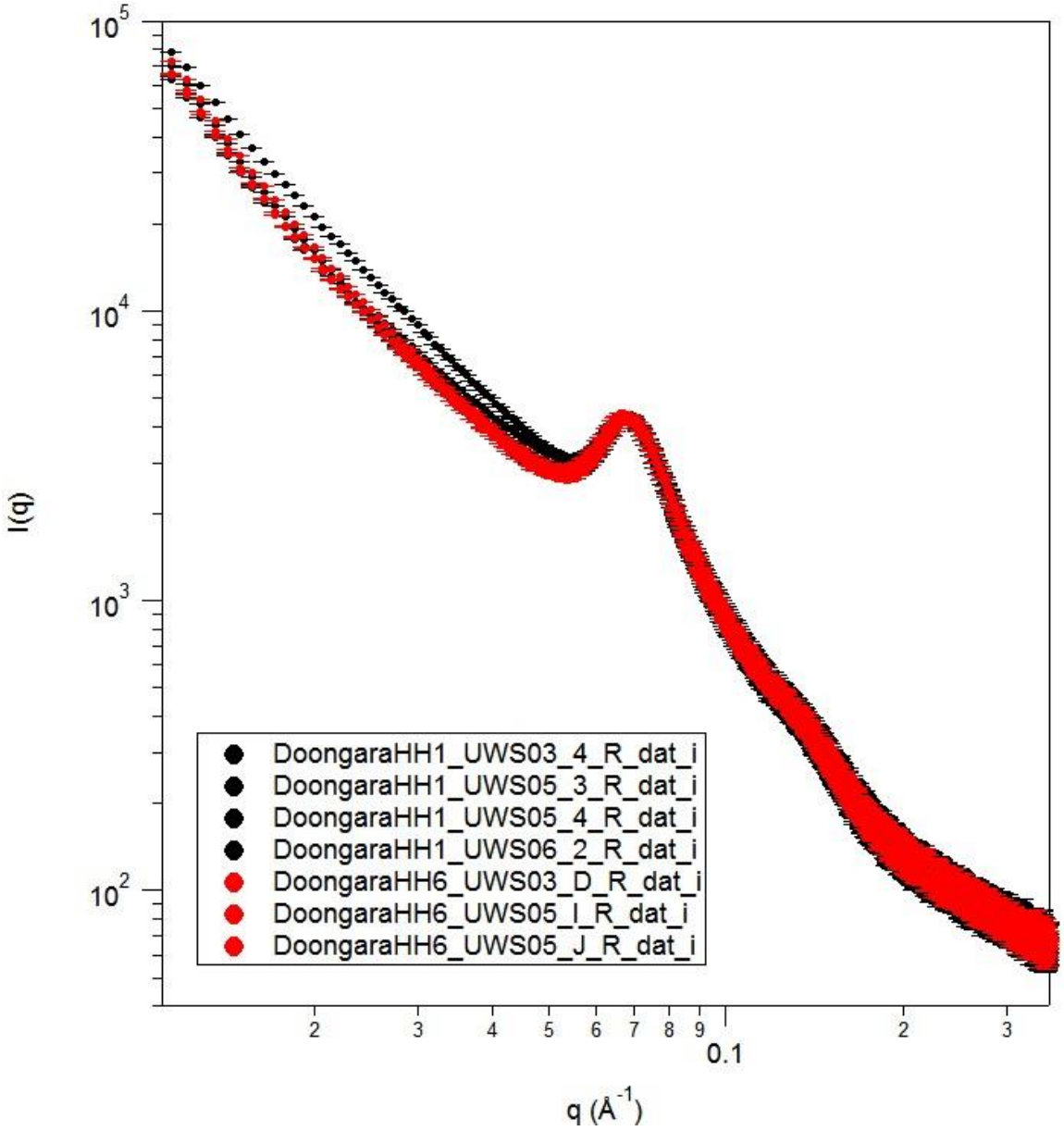

Figure S32 Small angle X-ray scattering curves of rice flours of Doongara grown at lower temperature. Red and black curves correspond to different glasshouses at the same temperature. Separate curves of same colour correspond to repeat experiments on different parts of the same sample.

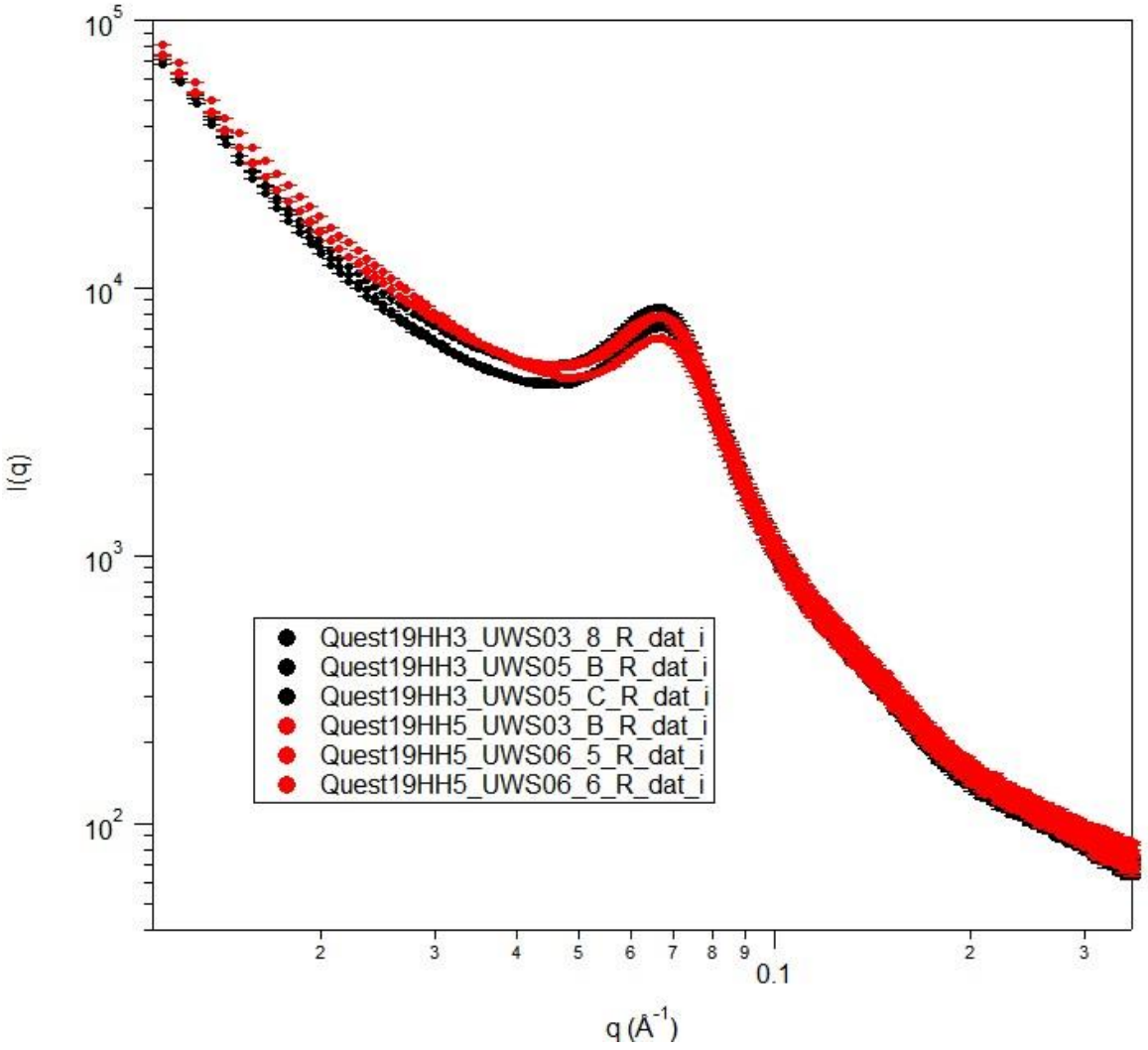

Figure S33 Small angle X-ray scattering curves of rice flours of Quest grown at higher temperature. Red and black curves correspond to different glasshouses at the same temperature. Separate curves of same colour correspond to repeat experiments on different parts of the same sample.

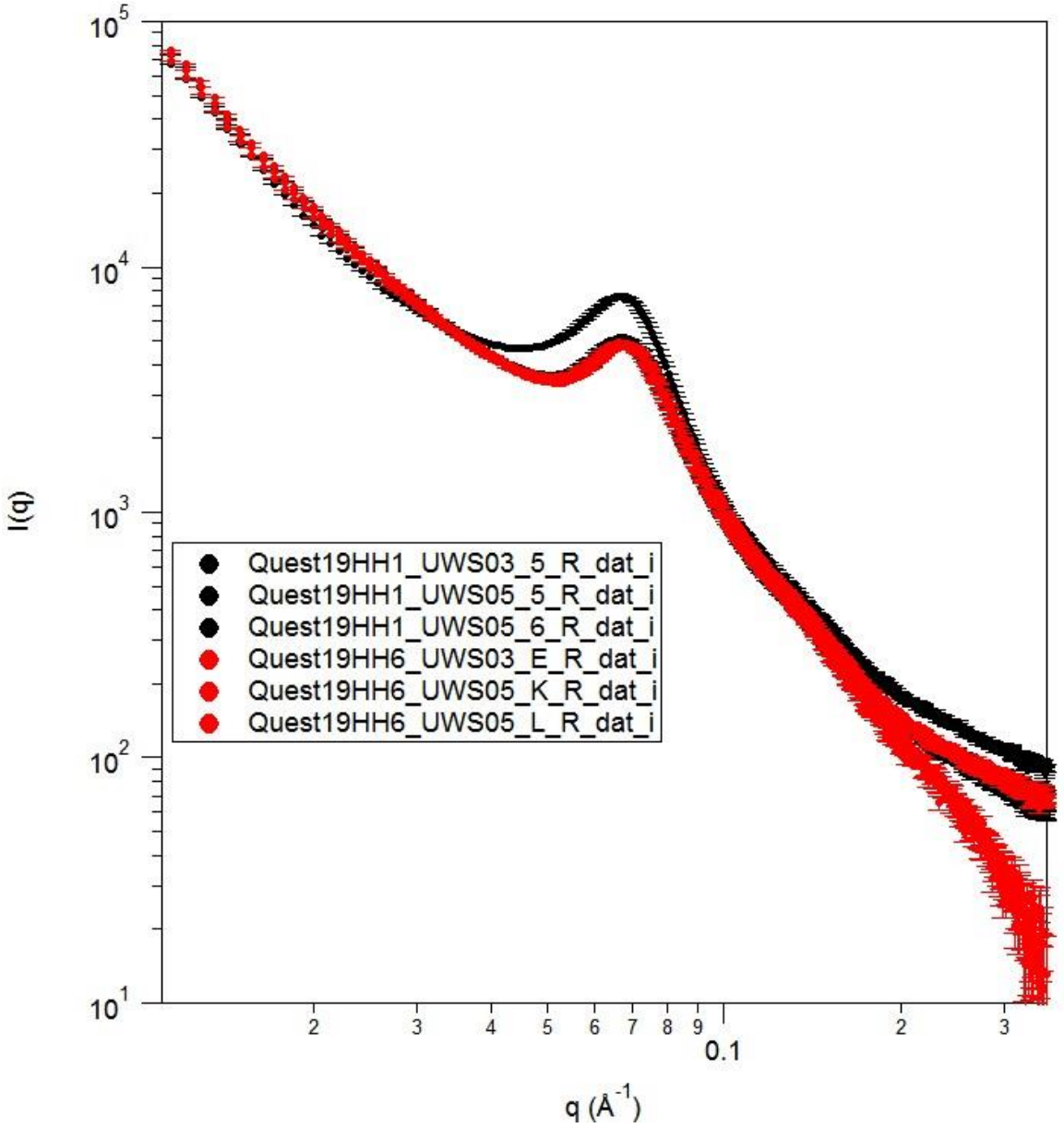

Figure S34 Small angle X-ray scattering curves of rice flours of Quest grown at lower temperature. Red and black curves correspond to different glasshouses at the same temperature. Separate curves of same colour correspond to repeat experiments on different parts of the same sample.

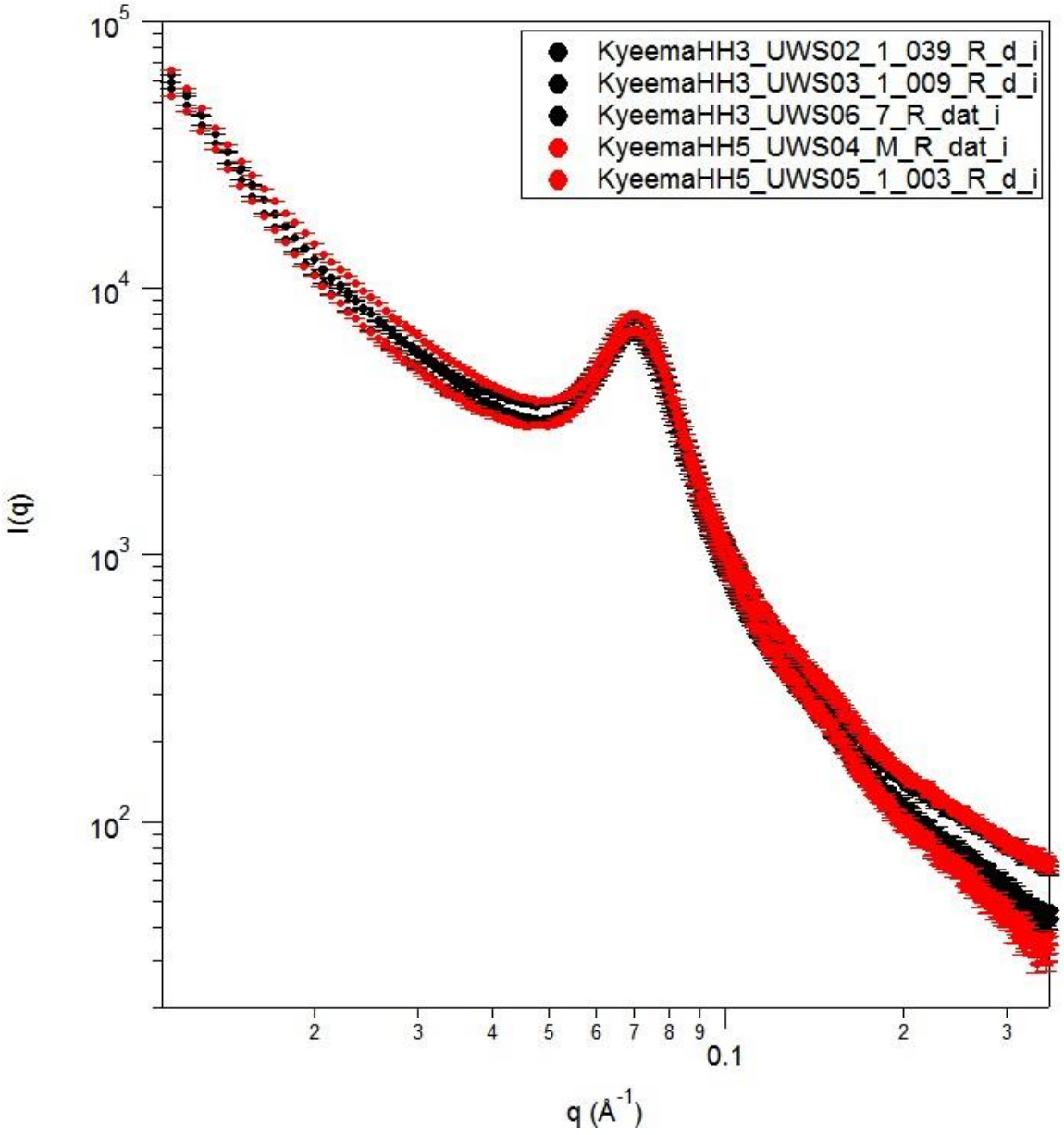

Figure S35 Small angle X-ray scattering curves of rice flours of Kyeema grown at higher temperature. Red and black curves correspond to different glasshouses at the same temperature. Separate curves of same colour correspond to repeat experiments on different parts of the same sample.

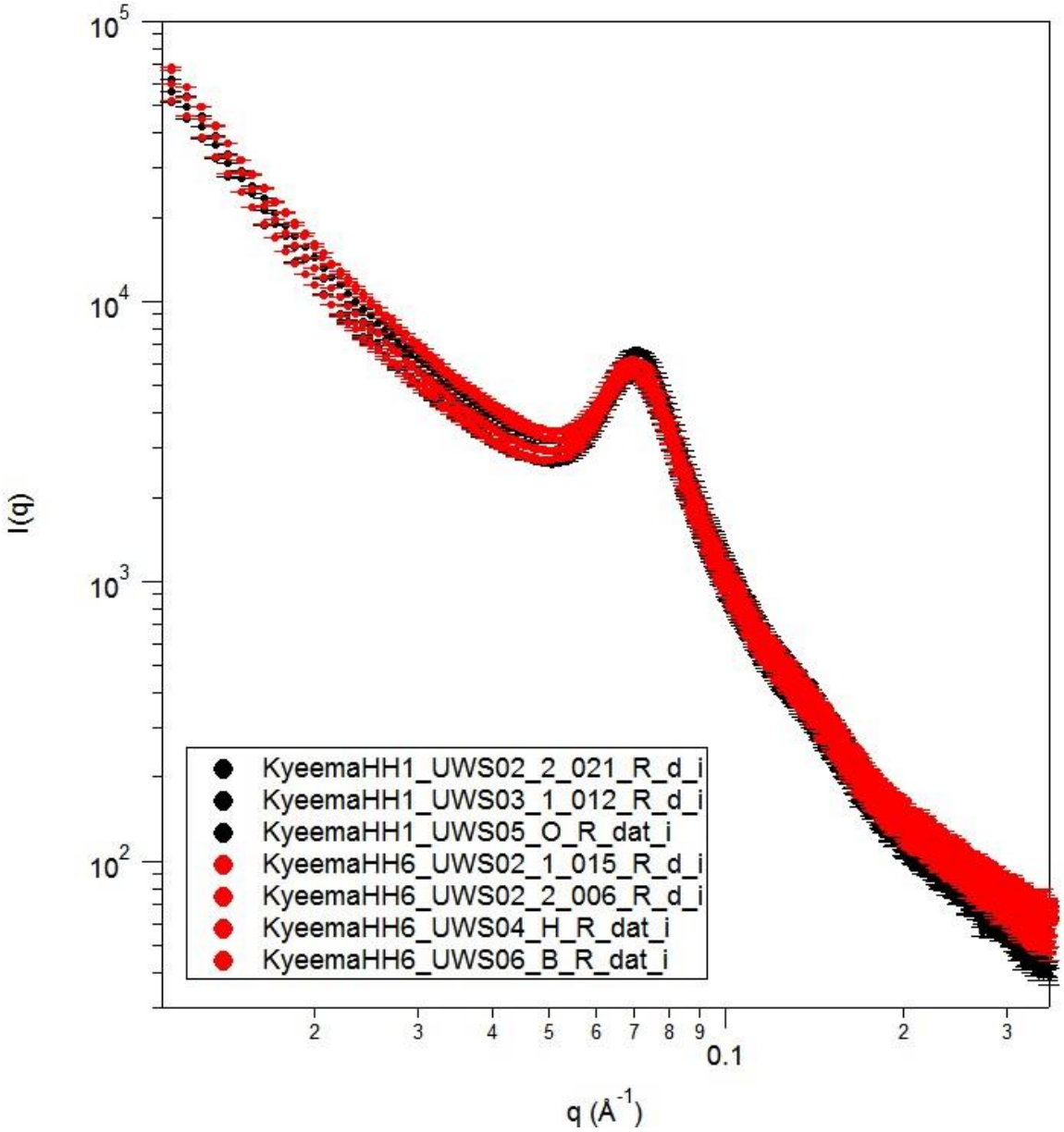

Figure S36 Small angle X-ray scattering curves of rice flours of Kyeema grown at lower temperature. Red and black curves correspond to different glasshouses at the same temperature. Separate curves of same colour correspond to repeat experiments on different parts of the same sample.

S4.2 Fitting of small angle X-ray scattering data

Scattering curves of rice flour samples were iteratively fitted with a power law function to describe the underlying small angle scattering (where β is the power law prefactor and α is the power law exponent) plus a Gaussian/Lorentzian function and a second Gaussian function to describe both the starch primary lamellar and secondary peaks (position, $q_{\max}$; Intensity, $I_{\max}$; full width at half maximum, Δq).

$$I(q) = (r(I_{\max 1}(1 + A_1)^{-1}) + (1 - r)I_{\max 1}A_2) + I_{\max 2}A_3 + (\beta q^{-\alpha}) \quad \text{Equation S2}$$

$$A_1 = \left[\frac{2(q - q_{\max 1})}{\Delta q_1}\right]^2 \quad \text{Equation S3}$$

$$A_2 = \left[e^{-\left(\frac{q - q_{\max 1}}{\Delta q_1}\right)^2}\right] \quad \text{Equation S4}$$

$$A_3 = \left[e^{-\left(\frac{q - q_{\max 2}}{\Delta q_2}\right)^2}\right] \quad \text{Equation S5}$$

where q is the modulus of the scattering vector equal to $(4\pi/\lambda)\sin\theta$ where λ is the X-ray wavelength (0.1542 nm) and 2ϑ is the scattering angle. r is the ratio of Lorentzian to Gaussian characteristics to the primary peak.

Figure S37 shows an example scattering curve of a rice flour and its fit overlaid after iterative calculation to minimise chi-squared.

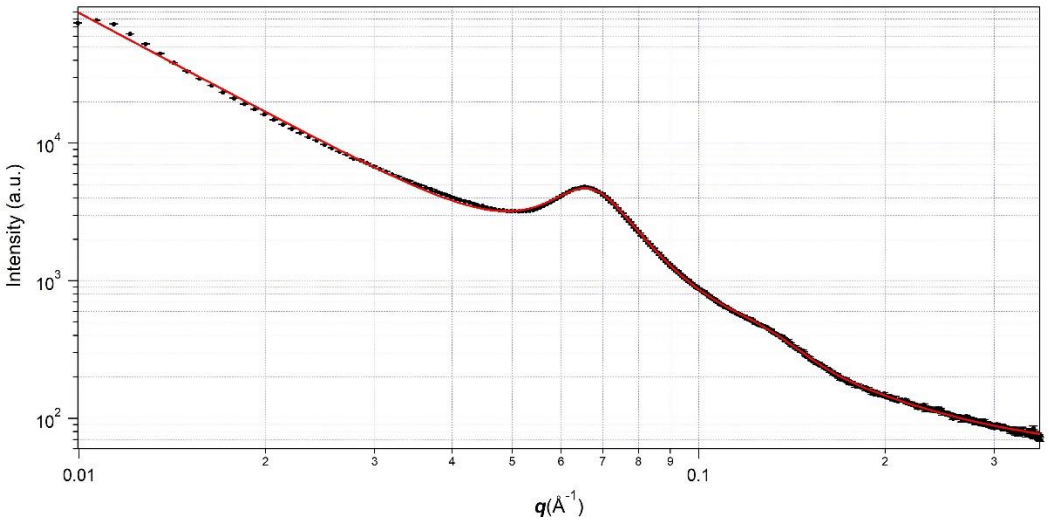

Figure S37 Small angle X-ray scattering curve of Cocodrie rice flour grown at a higher temperature (black crosses) with an iteratively calculated fit with equation S1 (red line)

The real space lamellar repeat thickness was calculated from the peak position with equation S6. HWHM in real space was determined with equation S7.

$$\text{Lamellar repeat thickness (real space)} = \frac{2\pi}{q_{\max}} \quad \text{Equation S6}$$

$$\text{HWHM} = \frac{2\pi}{{q_{\max}}^2} \times \frac{\Delta q}{2} \quad \text{Equation S7}$$

S4.3 Relationship of peak intensity with AAC and average DB

A general trend of decreasing lamellar peak intensity with increasing amylose content has been reported in the literature (Blazek & Gilbert, 2011). This has been explained by the accumulation of defects within the lamellar structure. A similar trend was observed in the rice samples in this study, with the data shown in Figure S38.

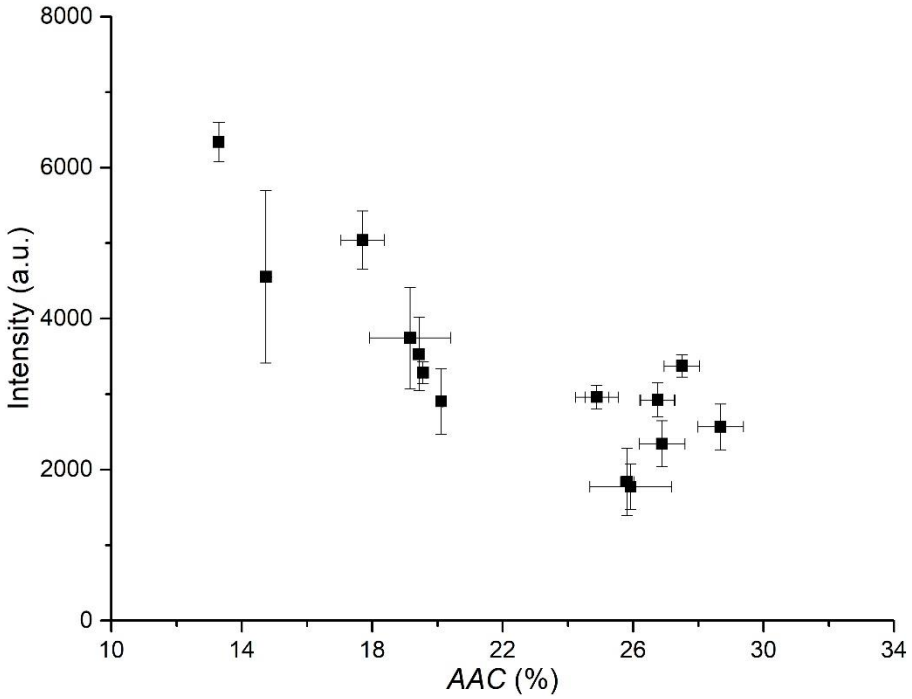

Figure S38 Relation between SAXS peak intensity and *AAC* for rice flours of different varieties grown at lower or higher temperatures. SAXS peak intensity error bars represent the standard error of 6 values (2 independent replicates of temperature, 3 preparations for each replicate). *AAC* error bars represent the standard error of 4 values (2 independent replicates of temperature, 2 instrument readings for each). See Table S5 for individual *AAC* and average *DB* values.

The peak intensity and average *DB* were loosely correlated, indicating an increased extent of semi-crystalline order with increasing average *DB* (Figure S39). However, given the poor correlation, it is unlikely that the branching frequency is the primary driver for changes in the extent of semi-crystalline order. It is possible that other aspects of the branching structure such as chain length distribution play a larger role, thus peak intensity and average *DB* are both relevant in reporting on different aspects in the overall starch structure.

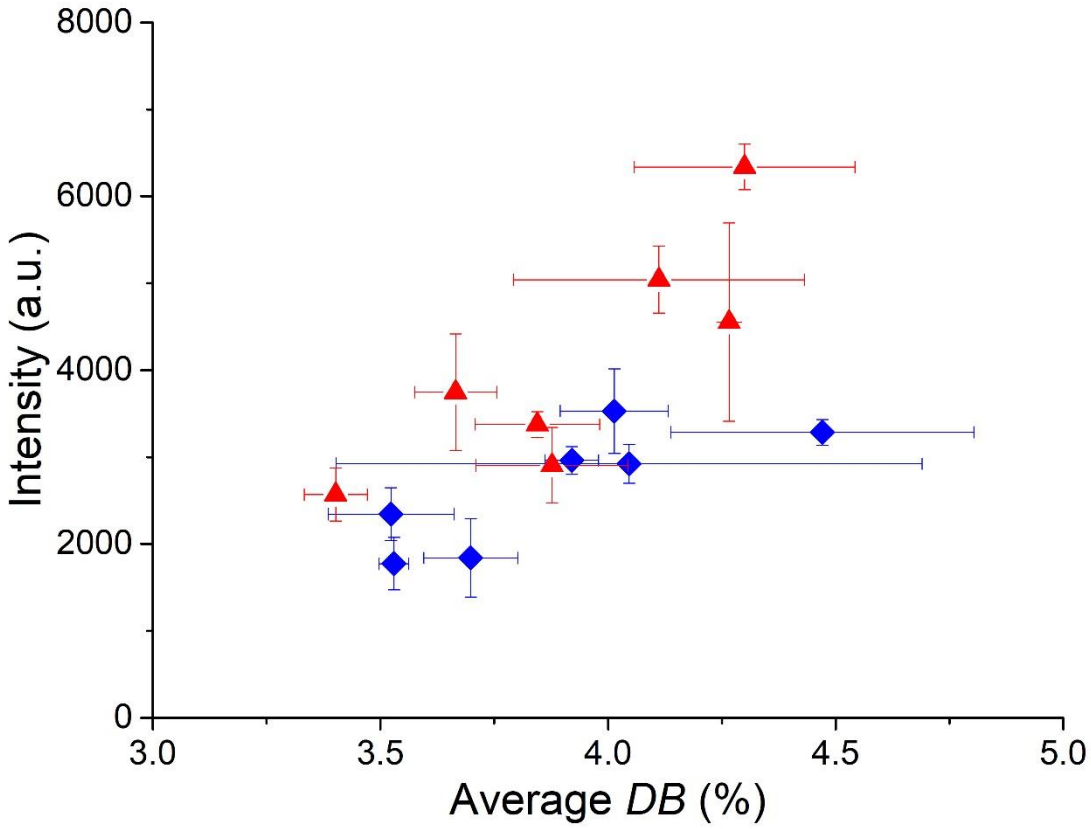

Figure S39 Relation between SAXS peak intensity and average *DB* for rice flours of different varieties grown at lower (blue diamonds) or higher (red triangles) temperatures. SAXS peak intensity error bars represent the standard error of 6 values (2 independent replicates of temperature, 3 preparations for each replicate). Average *DB* error bars represent the standard error of 2 values (2 independent replicates of temperature). See Table S5 for individual *AAC* and average *DB* values.

S4.4 Relationship of repeat unit thickness with HWHM

The HWHM and lamellar repeat thickness are positively correlated (Figure S40). This was previously observed on extracted starches of various botanical origin and thought to be due to a conserved distribution of lamellar sizes limited by the minimum number of glucose units (degree of polymerisation of 10-12) required to form a helix (Witt et al., 2012).

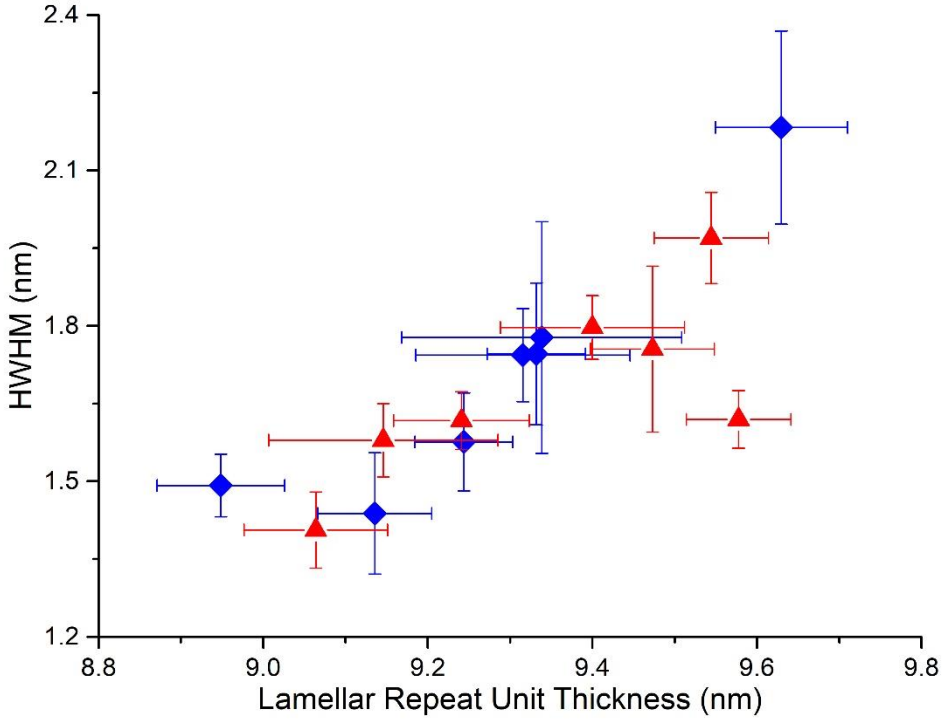

Figure S40 Relation between HWHM and lamellar repeat unit thickness for rice flours of different varieties grown at lower (blue diamonds) or higher (red triangles) temperatures. Error bars represent the standard error of 6 values (2 independent replicates of temperature, 3 preparations for each replicate).

S5 Mean and standard error values for AAC, average DB, SAXS intensity of main lamellar peak, SAXS lamellar repeat unit thickness, SAXS half-width half-maximum (HWHM) of main lamellar peak

Table S5 Individual values of *AAC*, average *DB,* SAXS intensity of main lamellar peak, SAXS lamellar repeat unit thickness, SAXS half-width half-maximum (HWHM) of main lamellar peak. Mean values are reported for samples grown at lower and higher temperatures, with their standard error (Std error) for 4 measurements for *AAC* (2 independent replicates of temperature, 2 instrument readings for each), 2 measurements for average *DB* (2 independent replicates of temperature), 6 measurements for SAXS (2 independent replicates of temperature, 3 preparations for each).

Variety	*AAC (%)*		*Average DB (%)*		*SAXS peak intensity (a.u.)*		*SAXS thickness (nm)*		*SAXS HWHM (nm)*	
	Mean	*Std error*	*Mean*	*Std error*	*Mean*	*Std error*	*Mean*	*Std error*	*Mean*	*Std error*
Cocodrie, lower T	26.88	0.01	3.52	0.14	2344	305	9.33	0.02	1.75	0.06
Cocodrie, higher T	28.68	0.70	3.40	0.07	2568	302	9.47	0.03	1.70	0.06
I-Geo-Tze, lower T	26.75	0.52	4.05	0.64	2924	226	9.24	0.02	1.58	0.04
I-Geo-Tze, higher T	27.50	0.54	3.84	0.14	3376	148	9.40	0.05	1.74	0.02
IR64, lower T	25.92	0.06	3.53	0.03	1773	302	9.34	0.07	1.78	0.09
IR64, higher T	19.16	1.25	3.67	0.09	3746	671	9.24	0.03	1.65	0.02
IR55419-04, lower T	25.81	0.20	3.70	0.1	1840	449	9.63	0.03	2.18	0.08
IR55419-04, higher T	20.11	0.05	3.88	0.17	2904	436	9.54	0.03	2.01	0.04
Doongara, lower T	24.88	0.36	3.92	0.06	2961	160	9.14	0.03	1.44	0.05
Doongara, higher T	17.70	0.67	4.11	0.32	5041	382	9.15	0.06	1.58	0.03
Quest, lower T	19.56	0.13	4.47	0.33	3284	147	9.32	0.05	1.74	0.04
Quest, higher T	13.29	0.09	4.30	0.24	6338	262	9.58	0.03	1.53	0.02
Kyeema, lower T	19.43	0.14	4.01	0.12	3529	486	8.95	0.03	1.49	0.02
Kyeema, higher T	14.74	0.11	4.27	0	4552	1141	9.06	0.04	1.37	0.03

S6 Fourier transform infrared spectroscopy at cryogenic temperatures

S6.1 Materials and Methods

FTIR spectroscopy was performed on a Bruker Vertex 70 spectrometer. All spectra were acquired with 64 scans, at a resolution of 1 cm^{-1} in a transmission mode arrangement using a Specac variable temperature cell holder under vacuum. Samples were pressed into KBr pellets with a sample concentration of 2 wt% (200 mg total mass). Powder for pressing was prepared by combining sample and KBr powder and grinding together into a fine powder using an agate mortar and pestle. The powder was then transferred to the die and spread with light tapping. Pellets were pressed using a PIKE Technologies CrushIR digital hydraulic press. The pressure sequence was: 3 tonnes followed by immediate release, 7 tonnes for 30 s, then ramp from 7 to 10 tonnes and hold for 2 min. Pressed pellets were analysed on the day of pressing and stored in a desiccator until analysis.

Three types of commercial maize starches with different amylose contents: waxy maize (3.4 % amylose), regular maize (24 % amylose) and Gelose 80 (83 % amylose) (Tan et al., 2007) were from Penford Australia Limited (Lane Cove, NSE, 2066, Australia). All starch samples were conditioned to 44 % relative humidity for at least 1 week prior to analysis. Sample environments at 44 % relative humidity was created by placing a saturated solution of potassium carbonate (K_2CO_3) in a desiccator (Greenspan, 1977).

All spectra were processed with Bruker OPUS 7.5 (Bruker Optik GmbH). All FTIR spectra were baseline corrected by 1 step (minimum amount) in the software's interactive mode using a rubber band based correction algorithm. All FTIR spectra were then normalised to an absorbance range of 0 to 2.0 based on min-max calculations.

S6.2 Effects of cryogenic temperatures on FTIR spectra

Cryogenic temperatures have been used widely over the life of infrared technology, across an extremely broad range of applications, and leading to data exhibiting reduced peak width and improved resolution (Caspary, 1968; Hermann & Harvey, 1969). This has been explained by weaker intermolecular interactions and lower intensity of bands corresponding to excited-state energy levels (Hermann et al., 1969; Holland-Moritz & Siesler, 1976; Stuart, 2004).

Figure S41 displays the FTIR spectra of the three model starches at both 25 °C and -170 °C. Slight improvements in resolution were noted for all three starch samples; however, these improvements were minimal and still did not result in clearly resolved signals. As a result, the investigation of crystalline order by FTIR spectroscopy was not explored in this work.

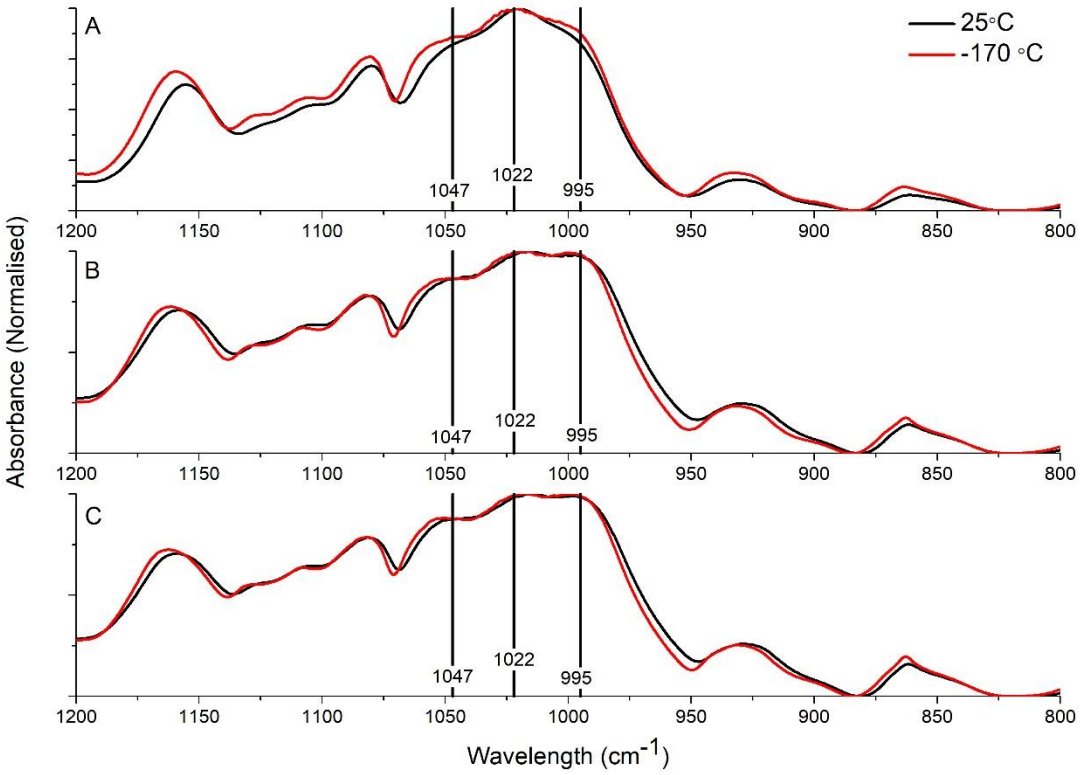

Figure S41 Transmission mode FTIR spectra of A) Gelose 80, B) Regular maize and C) Waxy maize, conditioned at 44 % relative humidity and measured at different temperatures. Bands of interest are noted by vertical black lines and labelled with the wavelength.

References

Blazek, J., & Gilbert, E. P. (2011). Application of small-angle X-ray and neutron scattering techniques to the characterisation of starch structure: A review. *Carbohydrate Polymers, 85*, 281-293. https://doi.org/10.1016/j.carbpol.2011.02.041

Bruker Optik GmbH. Opus 7.5 (Version 7.5). Rudolf-Plank-Straße, Ettlingen, Germany.

Caspary, R. (1968). Infrared spectroscopy at low temperature for the improved resolution of spectra. *Applied Spectroscopy, 22*, 694-696. https://doi.org/10.1366/000370268774383994

Castignolles, P., Graf, R., Parkinson, M., Wilhelm, M., & Gaborieau, M. (2009). Detection and quantification of branching in polyacrylates by size-exclusion chromatography (SEC) and melt-state 13C NMR spectroscopy. *Polymer, 50*, 2373-2383. https://doi.org/10.1016/j.polymer.2009.03.021

Dunn, L. B. J., & Krueger, W. J. (1999). Branching ratios of starch via proton nuclear magnetic resonance and their use in determining amylose/amylopectin content: Evidence for three types of amylopectin. *Macromolecular Symposia, 140*, 179-186. https://doi.org/10.1002/masy.19991400119

Elfstrand, L., Frigård, T., Andersson, R., Eliasson, A.-C., Jönsson, M., Reslow, M., & Wahlgren, M. (2004). Recrystallisation behaviour of native and processed waxy maize starch in relation to the molecular characteristics. *Carbohydrate Polymers, 57*, 389-400. https://doi.org/10.1016/j.carbpol.2004.05.018

Gidley, M. J. (1985). Quantification of the structural features of starch polysaccharides by NMR spectroscopy. *Carbohydrate Research, 139*, 85-93. https://doi.org/10.1016/0008-6215(85)90009-6

Greenspan, L. (1977). Humidity fixed points of binary saturated aqueous solutions. *Journal of Research of the National Bureau of Standards - A. Physics and Chemistry, 81A*, 89-96. https://doi.org/10.6028/jres.081a.011

Hermann, T. S., & Harvey, S. R. (1969). Infrared spectroscopy at sub-ambient temperatures: I. Literature review. *Applied Spectroscopy, 23*, 435-450. https://doi.org/10.1366/000370269774380563

Hermann, T. S., Harvey, S. R., & Honts, C. N. (1969). Infrared spectroscopy at sub-ambient temperatures: II. Pure molecules. *Applied Spectroscopy, 23*, 451-460. https://doi.org/10.1366/000370269774380437

Holland-Moritz, K., & Siesler, H. W. (1976). Infrared spectroscopy of polymers. *Applied Spectroscopy Reviews, 11*, 1-55. https://doi.org/10.1080/05704927608081704

McIntyre, D. D., Ho, C., & Vogel, H. J. (1990). One-dimensional nuclear magnetic resonance studies of starch and starch products. *Starch - Stärke, 42*, 260-267. https://doi.org/10.1002/star.19900420705

Nilsson, G. S., Gorton, L., Bergquist, K.-E., & Nilsson, U. (1996). Determination of the degree of branching in normal and amylopectin type potato starch with 1H-NMR spectroscopy improved resolution and two-dimensional spectroscopy. *Starch - Stärke, 48*, 352-357. https://doi.org/10.1002/star.19960481003

Schmitz, S., Dona, A. C., Castignolles, P., Gilbert, R. G., & Gaborieau, M. (2009). Assessment of the extent of starch dissolution in dimethyl sulfoxide by 1H NMR spectroscopy. *Macromolecular Bioscience, 9*, 506-514. https://doi.org/10.1002/mabi.200800244

Stuart, B. (2004). *Infrared spectroscopy: Fundamentals and applications*. Hoboken (NJ, USA): Wiley.

Tan, I., Flanagan, B. M., Halley, P. J., Whittaker, A. K., & Gidley, M. J. (2007). A method for estimating the nature and relative proportions of amorphous, single, and double-helical components in starch granules by 13C CP/MAS NMR. *Biomacromolecules, 8*, 885-891. https://doi.org/10.1021/bm060988a

Tyburn, J.-M. (1998). *Variable temperature unit user manual version 001*. Wissembourg (France): Bruker.

Witt, T., Doutch, J., Gilbert, E. P., & Gilbert, R. G. (2012). Relations between molecular, crystalline, and lamellar structures of amylopectin. *Biomacromolecules, 13*, 4273-4282. https://doi.org/10.1021/bm301586x